Construction of optimally directed localized basis for arbitrary bond-angles, and correlated real time dynamics in the proposed directed basis for accurate estimation of optical properties of large systems

By

Joydev De

Enrolment No: PHYS11201504003

National Institute of Science Education and Research, Bhubaneswar

A thesis submitted to the

Board of Studies in Physical Sciences

In partial fulfillment of requirements

for the Degree of

DOCTOR OF PHILOSOPHY

of

HOMI BHABHA NATIONAL INSTITUTE
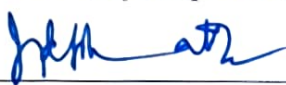
Homi Bhabha National Institute

Recommendations of the Viva Voce Committee

As members of the Viva Voce Committee, we certify that we have read the dissertation prepared by **Joydev De** entitled **"Construction of optimally directed localized basis for arbitrary bond-angles, and correlated real time dynamics in the proposed directed basis for accurate estimation of optical properties of large systems.**

Chairman - Prof. Bedangadas Mohanty _____ Date

Bmohanty 28/12/2023

Guide/Convener - Dr. Joydeep Bhattacharjee _____ Date

28/12/23

Examiner - Prof. Nisanth N. Nair _____ Date

28.12.2023

Member 1- Prof. Saroj Kumar Nayak _____ Date

Member 2- Dr. Prasanjit Samal _____ Date

28.12.2023

Member 3- Dr. A. V. Anil Kumar _____ Date

28/12/23

Final approval and acceptance of this thesis is contingent upon the candidate's submission of the final copies of the thesis to HBNI.

I/We hereby certify that I/we have read this thesis prepared under my/our direction and recommend that it may be accepted as fulfilling the thesis requirement.

Date:

Place: NISER
BBSR.

Signature
Co-guide(if applicable)

Signature   28/12/23
Guide

STATEMENT BY AUTHOR

This dissertation has been submitted in partial fulfillment of requirements for an advanced degree at Homi Bhabha National Institute (HBNI) and is deposited in the Library to be made available to borrowers under rules of the HBNI.

Brief quotations from this dissertation are allowable without special permission, provided that accurate acknowledgement of source is made. Requests for permission for extended quotation from or reproduction of this manuscript in whole or in part may be granted by the Competent Authority of HBNI when in his or her judgment the proposed use of the material is in the interests of scholarship. In all other instances, however, permission must be obtained from the author.

<div align="right">Joydev De</div>

DECLARATION

I, hereby declare that the investigation presented in the thesis has been carried out by me. The work is original and has not been submitted earlier as a whole or in part for a degree / diploma at this or any other Institution / University.

Joydev De

List of Publications arising from the thesis

Journal

- **Published**

  1. "Hybrid atomic orbital basis from first principles: Bottom-up mapping of self-energy correction to large covalent systems", Manoar Hossain, **Joydev De**, and Joydeep Bhattacharjee, The Journal of Physical Chemistry A, 125 6805–6817, **2021**. *https://doi.org/10.1021/acs.jpca.1c00320*

  2. "Maximally valent orbitals in systems with non-ideal bond-angles: Atomic Wannier orbitals guided by Mayer bond order",**Joydev De**, Sujith N S, Manoar Hossain, and Joydeep Bhattacharjee, Physical Chemistry Chemical Physics, **2022**, DOI: 10.1039/d2cp04259b

- **Submitted to arXiv**

  1. "Optical excitation from anti-causally corrected real-time dynamics in a minimal basis",**Joydev De**, Manoar Hossain, and Joydeep Bhattacharjee, *https://arxiv.org/abs/2306.06701*
  (submitted to Journal of Chemical Theory and Computation)

- **Manuscript under preparation**

  1. "Optical excitation as a signature of chemical activation",**Joydev De**, Rita Maji, and Joydeep Bhattacharjee

Conferences

1. **Joydev De**. Current Trends in Condensed Matter Physics (CTCMP), 19th -22nd February, 2015, National Institute of Science Education and Research (NISER), Bhubaneswar

2. **Joydev De**. International conference on nanoscience and technology, March 21-23, 2018.Indian Institute of Science, Bengaluru.

3. **Joydev De**. Annual Condensed Matter Physics Meeting 2018, National Institute of Science Education and Research (NISER), Bhubaneswar

4. **Joydev De**. "Ab-initio Many-Body Methods and Simulations with the Yambo Code" 04 April 2022 to 08 April 2022.The Abdus Salam International Centre for Theoretical Physics.

Joydev De

DEDICATIONS

Dedicated to

.....

My Grandmother

Tufan Rani Paul

.....

ACKNOWLEDGEMENTS

First of all, I would like to thank Prof. Joydeep Bhattacharjee for his unwavering support and guidance throughout my PhD journey, I am fortunate to have him as my PhD advisor. I am thankful to him for introducing the research problem(s) to me. His expertise and patience have been invaluable to me and have played a crucial role in the success of my thesis. His vision and ambition towards doing something new not only taught me how to handle pressure and keep going but also forced me to think out of the box and push the boundary of my comfort zone. He is my primary resource to get all my doubts and research questions answered. His constant support help me to crank out this thesis, all in one month.

I would like to thank my family for their unconditional love and support as always.

I would like to express my sincere gratitude to my doctoral committee members Prof. Bedangadas Mohanty, Prof. Saroj Kumar Nayak, Prof. Prasanjit Samal and Prof. A. V. Anil Kumar for their valuable feedback and comments towards improvement of my research work.

I would also like to thanks the NISER for providing me with the opportunity of my research and for all of the computational resources and support they provided.

I would also like to thank the Computational Materials Science Group members and all the members of theoretical condensed matter physics at NISER. I also thank my friends here at NISER for providing support and friendship that I needed.

Contents

SUMMARY

The aim of my Ph.D was to study the optical signatures of chemical and physical functionalization of nano structures, primarily the experimentally realizable nano structures made of $2p$ block elements which are known for their versatile electronic and magnetic properties, as a guide for experimentalists. These nano structures are typically made of hundreds to thousands of atoms which makes them difficult to study computationally using the standard methodologies like the time dependent density functional theory (TDDFT) based on approximations of the exchange correlation interaction among electrons in the valence and conduction bands, and almost impossible for the more accurate framework based on many body perturbation theory and Bethe-Salpeter equation. This motivated us to explore methodological strategies to cut-down the computational cost of accurate estimation of optical excitation within the tight-binding (TB) framework, leading us to develop a minimal multi orbital basis.

In my thesis,first I described the construction of directed hybrid atomic Wannier orbital (HAWO) basis constructed from Kohn-Sham (KS) states of a given system. By construction , the degenerate HAWOs being oriented to directions of coordination in systems with ideal bond angle , they render predominantly single TB parameters for each nearest neighbor bond irrespective of their orientation and also facilitates an easy route for the transfer of such TB parameters across iso-structural systems exclusively through mapping of neighborhoods and projection of orbital charge centers. However in a host of molecules and low dimensional systems bond-angles are non-ideal, which makes degenerate HAWOs unusable. For such systems we have proposed construction of the optimally oriented maximally valent orbitals (MVO),which maximally incorporate covalent interactions prevalent in the system

estimated in terms of the Mayer's bond order, also known as the Wiberg's bond index.

We calculate TB parameters in the proposed directed basis at the level of KS DFT and further also include self-energy corrections of single particle levels computed using GW approximation. Self energy corrected TB parameters are computed in small reference systems and transferred to larger isomorphic systems to reproduce quasi-particle band gap with workable accuracy ($>90\%$) in systems with hundreds of atoms where an explicit DFT+G_0W_0 computation would be prohibitively expensive.

In the second part of my thesis work, we have developed a computationally inexpensive anti-causally corrected real time dynamics(ACC-RTD) approach to study the optical absorption spectra beyond the independent particle level, for experimentally realizable systems in the directed basis proposed in the first part of my thesis works. ln ACC-RTD, Hamiltonian is updated at every time step using the dielectric susceptibility , leading to good agreement of, primarily the absorption threshold, with reported experimental spectra, as well as those computed using GW-BSE, for systems ranging from small molecules to nano diamonds made of carbon and silicon atoms we have tested in so far. I hope the methodological efforts reported in my thesis will pave the way for inexpensive computation of optical excitation in experimentally realizable nano structures leading to refinement of computational proposals of optically active device configurations.

List of Figures

Chapter 1

Preface

The aim of my Ph.D when I started, was to study the optical signatures of chemical and physical functionalization of nano-structures as a guide for experimentalists. My primary goal was to investigate experimentally realizable nano-structures made of $2p$ block elements which are known for their versatile electronic and magnetic properties. These nano-structures are typically made of few hundreds to thousands of atoms which makes them difficult to study computationally.

Time dependent density functional theory (TDDFT)[1] is an exact frame work for study the optical properties but accurate computation of the same based on TDDFT requires realistic approximations of the exchange correlation interaction among electrons in the valence as well as conduction bands. The key inadequacy stems from the local and static nature of the primarily jellium based exchange-correlation kernel[2,3] primarily in use. Overcoming these inadequacies a more accurate frame work based on many body perturbation theory[4,5] and Bethe-Salpeter[6] equation, known popularly as GW-BSE approach,[7] has been shown to render optical gap comparable with experimentally observed optical excitation. However GW-BSE computation of optical excitation, which explicitly considers an electron-hole quasi particle interaction kernel is computationally prohibitively expensive and practically impossible for the kind of systems I planned to investigate with the standard configuration of stand-alone computational infrastructure available in general with exception of large scale

super-computing facilities. This limitation motivated us to evolve methodological strategies to cut-down the computational cost. As a feasible direction we started exploring possibilities within the tight-binding (TB) framework, which led us to develop a localized orbital basis which will not only maximally incorporate the electronic structure of a given system in a minimal set of basis but will also facilitate easy transfer of parameters across systems. Then I returned to the original goal of my Ph.D to compute optical properties of realizable nano-structure. We took recourse of the real time dynamics (RTD) approach with the Hamiltonian describe in our proposed directed basis. We have introduced an easily parameterizable anti-causally corrected RTD approach for accurate estimation of primarily the optical absorption threshold beyond the independent particle level. Hopefully the methodological efforts reported in my thesis will pave the way for inexpensive computation of optical excitation in experimentally realizable nano-structures leading to refinement of computational proposals of optically active device configurations.

1.1   This Thesis

In the first part of my thesis, I described the construction of optimally directed localized atomic Wannier orbital[8] basis constructed from Kohn-Sham (KS)[9] states of a given system. In this direction we first proposed construction of localized degenerate hybrid atomic orbitals (HAO)[10] as approximate eigenstates, which maximally joint diagonalize the non-commuting first moment matrices. Relative orientation of HAOs by construction are as per the direction of nearest neighbor co-ordinations in systems with ideal bond angle. Wannierization of HAOs in the basis of Kohn - Sham (KS) single particle states lead to the hybrid atomic Wannier orbitals (HAWO) which constitute an orthonormal multi-orbital tight binding (TB) basis.[10] By construction HAWOs being locked to directions of coordination, they render predominantly single TB parameters for each nearest neighbor bond involving no more than two orbitals irrespective of their orientation and also facilitates an easy route for the transfer of such TB parameters across iso-structural systems exclusively through mapping of

neighborhoods and projection of orbital charge centers.

However in a host of atoms and low dimensional systems bond-angles are non-ideal, which makes degenerate HAOs unusable. For many such systems a possible bent nature of covalent bonding has also been reported.[11] Accordingly, we have proposed construction of maximally valent orbitals (MVO), which are non-degenerate HAOs with customizable hybridization as per their orientations, chosen such that they maximally incorporate covalent interactions prevalent in the system, which we estimated in terms of the Mayer's bond order,[12,13] also known as the Wiberg's bond index.[14]

We calculate TB parameters in the Wannierized HAO or MVO basis as per the orientation of nearest neighbor co-ordinations in the given system. TB parameters are computed based on energetics of single particle states not only at the level of KS DFT but also including their self-energy corrections computed using GW approximation[15] of many body perturbation theory. TB parameters are computed in small reference systems and transferred to larger isomorphic systems through mapping of neighborhoods. We have shown[10] that such transferred self-energy corrected TB parameters can reproduce quasi-particle band gap with workable accuracy ($> 90\%$) in systems with hundreds of atoms where an explicit DFT+G_0W_0 computation of self-energy correction would be prohibitively expensive.

In the second part of my thesis work, we have developed a computationally inexpensive anti-causally corrected real time dynamics (ACC-RTD) approach to study the optical properties of experimentally realizable systems as per the original aim of my Ph.D., in the directed basis (HAO/MVO) proposed in the first part of my thesis work. In our RTD[16,17] calculation, we apply a delta like pulse to the system at the initial time step and allow the system to evolve in time using the Cranck-Nicolson scheme.[16,17] The absorption spectra calculated from the polarization profile matches with the same calculated at the independent particle (IP) level with the KS single particle states. To compute optical excitation beyond the IP level we resort to ACC-RTD where the self-energy corrected TB Hamiltonian is updated at every time step in order to ensure minimal evolution of the density with the rationale being that the

true Hamiltonian corresponding to the evolving states should naturally incorporate excitonic interactions which are minimized by the evolving states. We find that the resultant absorption spectra are in good agreement with reported experimental spectra as well as those computed using GW-BSE, for systems ranging from small molecules to nano-diamonds made of four co-ordinated carbon and silicon atoms that we have tested for so far.

I hope the methodological efforts reported in my thesis will pave the way for inexpensive computation of optical excitation in experimentally realizable nano-structures leading to refinement of computational proposals of optically active device configurations.
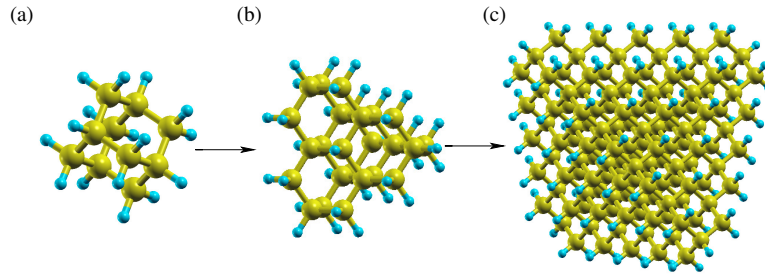
Figure 1.1: (a) Adamantane ($C_{10}H_{16}$), (b) Pentamantane ($C_{26}H_{32}$), (c) large nano-diamond with sp^3 hybridization. The arrow denotes the transfer of TB parameters from smaller reference to larger isomorphic systems, which is procedurally central to computation of electronic structure and optical excitation of realizably large systems reported in this thesis.

The construction of Wannierized directed hybrid orbitals has been demonstrated in a wide variety of molecules and clusters with non-ideal as well as ideal bond angles, for example water, ammonia, diborane, cyclo propane and to others cyclic molecules like C_3H_3, C_4H_4, C_5H_5, benzine. I have demonstrated the propose ACC-RTD scheme for estimation of absorption cross-section in carbon and silicon based nano diamond [Fig.1.1] in good agreement with the corresponding experimental or GW-BSE based spectra.[18,19,20,21] Self-energy corrected TB parameters have been transferred from pentamantane to larger nano-diamonds. As an application, I have tried to correlate chemical activation and presence of local magnetic moments with the absorption spectra in carbon doped h-BN segments of realizable length scales.

Chapter 2

Theoretical background

2.1 Introduction

The exact description of the electronic structure of atoms, molecules and solids is important to understand the properties in the significant portion of condensed matter physics, quantum chemistry and material science. However, this is a daunting task mainly because of two reasons. Firstly, electrons in matter must be described by the laws of quantum mechanics rather than classical ones. This is because the de Broglie wavelength ($\lambda = h/p$) of an electron in a many-electron environment is comparable to the average inter-particle separation, h being the Planck's constant and p the momentum of the electron. The second problem arises from the complex multi-particle interaction due to the overlapping of de Broglie wavelengths of different electrons. This causes the solution to be impossible for many-electron systems and the complexity grows drastically with the increasing number of electrons. For these reasons, computing electronic structure of matter is essentially a quantum many-body problem.

The quantum many-body problem is hard because the equations required for exact solution are known but computationally impossible to solve as is for more than one electron. Reasonably accurate approximate analytic solution exist only for systems with two confined electrons. In principle any static quantum system can be

described from the solution of the time independent Schrödinger equation :

$$\hat{H}\psi(\mathbf{r}_i) = E\psi(\mathbf{r}_i) \tag{2.1}$$

where $\hat{H}$, $\psi(\mathbf{r}_i)$ and E are the static Hamiltonian, many-body wavefunction and total energy of the system respectively. Here, $\mathbf{r}_i$ for $i = 1, 2, 3, \cdots, N$ denote the position of N electrons. For a system of M atoms the Hamiltonian of Eqn.(2.1) consists of the following terms

$$
\begin{aligned}
\hat{H} &= \hat{T}_{\mathrm{n}}(\mathbf{R}) + \hat{T}_{\mathrm{e}}(\mathbf{r}) + \hat{V}_{\mathrm{nn}}(\mathbf{R}) + \hat{V}_{\mathrm{ee}}(\mathbf{r}) + \hat{V}_{\mathrm{ne}}(\mathbf{r}, \mathbf{R}) \\
&= -\sum_{I=1}^{M} \frac{\hbar^2}{2M_I} \nabla_I^2 - \sum_{i=1}^{N} \frac{\hbar^2}{2m_e} \nabla_i^2 + \frac{e^2}{4\pi\epsilon_0} \sum_{I}^{M} \sum_{J>I}^{M} \frac{Z_I Z_J}{|\mathbf{R}_I - \mathbf{R}_J|} \\
&+ \frac{e^2}{4\pi\epsilon_0} \sum_{i}^{N} \sum_{j>i}^{N} \frac{1}{|\mathbf{r}_i - \mathbf{r}_j|} - \frac{e^2}{4\pi\epsilon_0} \sum_{I}^{M} \sum_{i}^{N} \frac{Z_I}{|\mathbf{R}_I - \mathbf{r}_i|}
\end{aligned} \tag{2.2}
$$

where Z_I, M_I and m_e are the atomic numbers, nuclear masses and electron mass, respectively. The first two terms of the above equation represent the kinetic energies of the nuclei and electrons. The last three terms represent the interaction energy operators between nuclei-nuclei ($\hat{V}_{\mathrm{nn}}$), electron-electron ($\hat{V}_{\mathrm{ee}}$) and electron-nuclei ($\hat{V}_{\mathrm{ne}}$) respectively. In practice, the partial differential Eqn.(2.1) is impossible to solve within a full quantum mechanical framework. There are various features that contribute to this difficulty, but the most important one is that the two-body nature of the Coulomb interaction which makes the above Schrödinger equation not separable.

As the first approximation, known as the Born Oppenheimer approximation,[22] we can decouple the motion of electrons from the nuclear motion owing to the fact that the time scale associated with the motion of nuclei is much larger than that of electrons. Within this approximation, we can factorize the total wavefunction ψ into a nuclear wavefunction ψ_n and electronic wavefunction ψ_e, as :

$$\psi(\{\mathbf{R}_I\}, \{\mathbf{r}_i\}) = \psi_{\mathrm{n}}(\{\mathbf{R}_I\})\psi_{\mathrm{e}}(\{\mathbf{x}_i\}). \tag{2.3}$$

The approximation allows us to fix nuclear configuration at some particular value $\mathbf{R}_I$ and solve for the electronic wavefunction $\psi_e(\{\mathbf{r}_i\})$ depending parametrically on R_I.

The electronic Hamiltonian is thus :

$$\hat{H}_e = -\sum_{i=1}^{N} \frac{1}{2}\nabla_i^2 + \sum_{i}^{N}\sum_{j>i}^{N} \frac{1}{|\mathbf{r}_i - \mathbf{r}_j|} - \sum_{I}^{M}\sum_{i}^{N} \frac{Z_I}{|\mathbf{R}_I - \mathbf{r}_i|}. \tag{2.4}$$

In the above equation, we use hartree atomic units, whereby $\hbar = e = m_e = 4\pi\epsilon_0 = 1$ unless otherwise stated, we will use this unit for the rest part of the thesis.

Although we simplified our many-body Schrödinger equation in Eqn.(2.4) by applying Born-Oppenheimer approximation, but still the solution of the electronic Schrödinger equation i.e. Eqn.(2.4) is too complex because of the many-electron wavefunction which depends on $3N$ variables and which for a solid of $N \sim 10^{26}$ electrons, is an unmanageable number of degrees of freedom. In the next section, we will briefly describe the wavefunction based approaches to obtain approximate solutions of Eqn.(2.4).

2.2   Hartree-Fock Method

The starting point of this method was introduced by D. R. Hartree in 1928, where each electron in a many-electron system is assumed to be moving in an effective potential which takes into account the effect of attraction to the nucleus and the average effect of the repulsive electron-electron interactions due to other electrons. Each electron in the system is described by its own wavefunction, which was written within the independent particle approximation as product of individual orbitals for each electrons.

$$\Phi(\mathbf{r}_1, \mathbf{r}_2, \mathbf{r}_3, \cdots, \mathbf{r}_N) = \phi(\mathbf{r}_1), \phi(\mathbf{r}_2), \phi(\mathbf{r}_3), \cdots, \phi(\mathbf{r}_N) \tag{2.5}$$

In 1930, V. A. Fock generalized Hartree's method which takes into account the antisymmetry requirement of the many-electron wavefunction. In the Hartree-Fock (HF) approximation, the wavefunction of a N electron system is taken as a Slater determinant[23]

$$\psi^{\mathrm{HF}} = \frac{1}{\sqrt{N!}} \begin{vmatrix} \alpha_1(\mathbf{X}_1) & \alpha_1(\mathbf{x}_2) & \ldots & \alpha_1(\mathbf{x}_N) \\ \alpha_2(\mathbf{x}_1) & \alpha_2(\mathbf{x}_2) & \ldots & \alpha_2(\mathbf{x}_N) \\ \vdots & \vdots & \ddots & \vdots \\ \alpha_N(\mathbf{x}_1) & \alpha_N(\mathbf{x}_2) & \ldots & \alpha_N(\mathbf{x}_N) \end{vmatrix}, \tag{2.6}$$

where $\alpha_i(\mathbf{X}_j) = \phi_i(\mathbf{r}_j)\sigma_i(j)$ are spin-orbitals which follow the orthonormality condition :

$$\langle \alpha_i | \alpha_j \rangle = \delta_{ij}. \tag{2.7}$$

Within the HF approximation, the expectation value of the Hamiltonian of Eqn.(2.4) is given by :

$$E_{\mathrm{HF}} = \langle \psi^{\mathrm{HF}} | \hat{H}_e | \psi^{\mathrm{HF}} \rangle = \sum_{i=1}^{N} h_i + \frac{1}{2} \sum_{i,j=1}^{N} (J_{ij} - K_{ij}), \tag{2.8}$$

where

$$h_i = \int \phi_i^*(\mathbf{r}) \left(-\frac{1}{2}\nabla_{\mathbf{r}}^2 + \mathbf{v}_{\mathrm{ext}}(\mathbf{r}) \right) \phi_i^*(\mathbf{r}) \mathbf{d^3r} \tag{2.9}$$

$$J_{ij} = \int \int \phi_i^*(\mathbf{r}_1)\phi_j^*(\mathbf{r}_2) \frac{1}{|\mathbf{r}_1 - \mathbf{r}_2|} \phi_i(\mathbf{r}_1)\phi_j(\mathbf{r}_2) d^3r_1 d^3r_2 \tag{2.10}$$

$$K_{ij} = \int \int \phi_i^*(\mathbf{r}_1)\phi_j^*(\mathbf{r}_2) \frac{1}{|\mathbf{r}_1 - \mathbf{r}_2|} \phi_i(\mathbf{r}_2)\phi_j(\mathbf{r}_1) d^3r_1 d^3r_2. \tag{2.11}$$

The term in Eqn.(2.10) is the Coulomb interaction energy between electrons and the Eqn.(2.11) represents the exchange energy between electrons arising due to Pauli exclusion. For $i = j$, we have $J_{ii} = K_{ii}$ leading to cancellation of the self-interaction of orbitals. Many-electron wavefunction ψ is the basic quantity for the wave function based methods. The variation principle states that for any guessed wave function the expectation value of the Hamiltonian ($\hat{H}_e$) always gives the upper bound to the

electronic ground state energy :

$$\langle\psi|\hat{H}_e|\psi\rangle \geq \langle\psi_0|\hat{H}_e|\psi_0\rangle, \tag{2.12}$$

where the equality sign holds only for the true ground state wave function ψ_0. Minimizing the above expression w.r.t. the orbital ϕ_i^* gives the canonical HF equation for the ith orbital

$$\left(-\frac{1}{2}\nabla_{\mathbf{r}}^2 + v_{\text{ext}}(\mathbf{r}) + \int \frac{\rho(\mathbf{r}')}{|\mathbf{r}-\mathbf{r}'|}d\mathbf{r}'\right)\phi_i(\mathbf{r}) - \sum_{\substack{i,j \\ (\sigma_i||\sigma_j)}} \int\int \frac{\phi_j^*(\mathbf{r}')\phi_j(\mathbf{r})\phi_i(\mathbf{r}')}{|\mathbf{r}-\mathbf{r}'|}d\mathbf{r}' = \varepsilon_i\phi_i(\mathbf{r}),$$
$$\tag{2.13}$$

where ε_i is the Lagrange multiplier to ensure the orthonormality of the orbitals and σ_i is the spin of the ith orbital. The Eqn.(2.13) is solved self-consistently and the solution results in a set of orthonormal orbitals which can be used in Eqn.(2.8) to calculate the total energy of a given system.

The inherent non-locality and multitude of orbitals make the HF approach computationally expensive. We recall at this point that omitting the exchange term in Eqn.(2.13) results into the Hartree Eqn. HF method renders total energy of diatomic molecules with high degree of accuracy. HF orbitals are often used as zero-order states for perturbation schemes.[24]

However, due to lack of dynamic correlation, the binding energy of molecules calculated using HF is large and also the dissociation limit of molecules is usually predicted incorrectly.

To account for dynamic correlation linear combination of Slater determinants made of different combination of orbitals are used, leading to the configuration interaction (CI) scheme which is very accurate but computationally prohibitively expensive. From the variational approach, accuracy of the quantum Montecarlo (QMC) based estimation of the ground state is comparable to CI but also computationally exorbitantly expensive. Both QMC and CI are used as benchmarking reference for various parametrizations in the construction of functional in DFT.

2.3   Density Functional Theory

Owing to the numerical complexity of dealing with many particle wave function in the HF approach alternate route to calculate the electronic structure evolved based on the one electron density. Efforts in this direction started with the Thomas Fermi approach[25,26] and matured in the Kohn-Sham[27] density functional theory which constitutes the primary methodology employed widely in deriving quantum mechanical description of materials with weak to modest correlation. The main advantage of using the density rather than wave function is that it always involves only three generalized coordinates regardless of the number of electrons in the system. This enables DFT to compute the properties of large systems containing hundreds to thousands of atoms. Electron density defined as :

$$\rho_{\sigma_1=\sigma'}(\mathbf{r}_1) = N_{\sigma'} \int \cdots \int |\psi(\mathbf{x}_1, \mathbf{x}_2, \cdots, \mathbf{x}_N)|^2 d\mathbf{x}_2 \cdots d\mathbf{x}_N \qquad (2.14)$$

determines the probability of finding an electrons with σ_1 spin at $\mathbf{r}_1$:

$$\sum_\sigma \int \rho_\sigma(\mathbf{r}) d\mathbf{r} = N \qquad (2.15)$$

where $\psi(x_1, x_2)$ is a normalized Slater wavefunction for a combination of them.

2.3.1   The Hohenberg-Kohn Theorem

Foundation of DFT is the fundamental correspondence of the ground state charge density and the external potential proved by Hohenberg-Kohn in 1964.[9]

Theorem I: There exists a one-to-one mapping between ground state charge density and the external potential up to a trivial constant.

Corollary Since the density $\rho(\mathbf{r})$ determines the external potential and the density can be obtained from the ground state wave function, the density therefore determines the complete Hamiltonian. Therefore, the ground state energy is expressed

as a functional of the density :

$$E[\rho] = \langle \psi | \hat{H}_{\mathrm{e}}[\rho] | \psi \rangle = F[\rho] + \int v_{\mathrm{ext}}(\mathbf{r}) \rho(\mathbf{r}) d\mathbf{r}, \qquad (2.16)$$

where

$$F[\rho] = \langle \psi | \hat{T}[\rho(\mathbf{r})] + \hat{V}_{\mathrm{ee}}[\rho(\mathbf{r})] | \psi \rangle. \qquad (2.17)$$

$F[\rho]$ is called the universal functional as it is independent of the external potential. Its form should thus remain unchanged irrespective of the system. Therefore, a particular system is completely determined by $v_{ext}(\mathbf{r})$ given which, the ground state charge density can be uniquely determined.

Theorem II: The ground-state energy can be determined using variational principle and the density which minimizes the total energy functional is the exact ground-state density.

Corollary This implies that the energy functional $E[\rho(\mathbf{r})]$ gives the true ground-state energy only for the exact ground-state density $\rho_0(\mathbf{r})$. For any other density, the predicted energy will be higher than the ground state energy.

$$E[\rho_0] = \min_{\rho(\mathbf{r})} \left\{ E[\rho(\mathbf{r})] \right\} \leq E[\rho(\mathbf{r})]. \qquad (2.18)$$

The ground-state energy can be therefore calculated using the variational principle with the constraint of conserving the number of electrons.

$$\delta \left\{ E[\rho(\mathbf{r})] - \mu \left(\int \rho(\mathbf{r}) d\mathbf{r} - N \right) \right\} = 0. \qquad (2.19)$$

This leads to the Euler-Lagrange equation,

$$\frac{\delta E[\rho(\mathbf{r})]}{\delta \rho(\mathbf{r})} = \mu = v_{\mathrm{ext}}(\mathbf{r}) + \frac{\delta F[\rho(\mathbf{r})]}{\delta \rho(\mathbf{r})}, \qquad (2.20)$$

where, μ is the Lagrange multiplier and also known as the chemical potential of the electrons. These two theorems form the mathematical basis of density-functional

theory.

2.4   Kohn-Sham Self-consistent Field Equation

The Eqn.(2.16) and Eqn.(2.18) in the previous subsection give a way of calculating the ground-state ρ if the form of $F[\rho]$ is known. However, for practical calculations, we have to rely on the approximate form of $F[\rho]$ and finding a good approximation beyond Jellium model remains a challenge. The universal density functional of Eqn.(2.17) can be rewritten as follows

$$F[\rho] = T_{\mathrm{s}}[\rho] + E_{\mathrm{H}}[\rho] + E_{\mathrm{xc}}[\rho], \tag{2.21}$$

where $E_{\mathrm{H}}[\rho] = \frac{1}{2} \int \int \frac{\rho(\mathbf{r})\rho(\mathbf{r}')}{|\mathbf{r}-\mathbf{r}'|} d\mathbf{r} d\mathbf{r}'$ is the part of the electron-electron coulomb repulsion or the Hartree energy and the term E_{xc} is the exchange correlation functional which is supposed to described electron-electron interactions rooted at exchange interaction as well as the Pauli, Coulomb and kinetic correlation. We finally obtain the Kohn-Sham total energy functional,

$$E_{\mathrm{KS}}[\rho] = T_{\mathrm{s}}[\rho] + \int \rho(\mathbf{r}) v_{\mathrm{ext}}(\mathbf{r}) d\mathbf{r} + E_{\mathrm{H}}[\rho] + E_{\mathrm{xc}}[\rho]. \tag{2.22}$$

The Kohn-Sham potential is determined by minimizing the KS energy functional w.r.t. density under the constraint of the density integrates to the N electrons,

$$\frac{\delta}{\delta\rho(\mathbf{r})} \left\{ E_{\mathrm{KS}}[\rho] - \mu \int \rho(\mathbf{r}) d\mathbf{r} \right\} = 0. \tag{2.23}$$

From the above equation, we obtain the following equation for the minimizing ground state density

$$\frac{\delta T_{\mathrm{s}}[\rho]}{\delta\rho(\mathbf{r})} + v_{\mathrm{ext}}(\mathbf{r}) + \int \frac{\rho(\mathbf{r}')}{|\mathbf{r}-\mathbf{r}'|} d\mathbf{r}' + \frac{\delta \mathrm{E}_{xc}}{\delta\rho(\mathbf{r})} = \mu. \tag{2.24}$$

The effective KS potential v_{KS} will be

$$v_{\text{KS}}(\mathbf{r}) = v_{\text{ext}}(\mathbf{r}) + v_{\text{H}}(\mathbf{r}) + v_{\text{xc}}(\mathbf{r}) \tag{2.25}$$

where $v_{\text{H}}(\mathbf{r}) = \int \frac{\rho(\mathbf{r}')}{|\mathbf{r}-\mathbf{r}'|} d\mathbf{r}'$ and $v_{\text{xc}}(\mathbf{r}) = \frac{\delta E_{\text{xc}}}{\delta \rho(\mathbf{r})}$ are the Hartree and exchange-correlation (XC) potential respectively.

In terms of one electron orbitals constituting the Slater determinant Φ Eqn.(2.6) density and kinetic energy expectation value expressed :

$$\rho(\mathbf{r}) = \sum_{i=1}^{N} |\phi_i(\mathbf{r})|^2 \quad \text{and} \quad T_{\text{s}}[\rho] = \langle \Phi | \hat{T}_s | \Phi \rangle = -\frac{1}{2} \int \phi^*(\mathbf{r}) \nabla^2 \phi(\mathbf{r}) d\mathbf{r}, \tag{2.26}$$

In view of the above expressions Eqn.(2.24) can be further simplified as:

$$\left[\frac{\delta T_{\text{s}}[\rho]}{\delta \phi_i^*(\mathbf{r})} \frac{\delta \phi_i^*(\mathbf{r})}{\delta \rho(\mathbf{r})} + v_{\text{ext}}(\mathbf{r}) + \int \frac{\rho(\mathbf{r}')}{|\mathbf{r}-\mathbf{r}'|} d\mathbf{r}' + \frac{\delta E_{xc}}{\delta \rho(\mathbf{r})} \right] \phi_i = \mu \phi_i \tag{2.27}$$

leading to

$$\left[-\frac{1}{2} \nabla_i^2 \phi_i + v_{\text{ext}}(\mathbf{r}) + \int \frac{\rho(\mathbf{r}')}{|\mathbf{r}-\mathbf{r}'|} d\mathbf{r}' + \frac{\delta E_{xc}}{\delta \rho(\mathbf{r})} \right] \phi_i = \mu \phi_i. \tag{2.28}$$

The Eqn.(2.28) can be written separately for all single particle orbital implying different values of μ for different orbitals. Each such μ can thus be interpreted as single particle energy levels:

$$\hat{H}_{\text{KS}} \phi_i(\mathbf{r}) = \varepsilon_i \phi_i(\mathbf{r}). \tag{2.29}$$

where

$$\hat{H}_{\text{KS}} = \sum_{i=1}^{N} \left[-\frac{1}{2} \nabla_i^2 + v_{\text{KS}}(\mathbf{r}_i) \right]. \tag{2.30}$$

Eqn.(2.25) and Eqn.(2.29) imply a self-consistent computation of single particle orbitals starting from a reasonable initial guess as summarized in the flowchart below.

$$\text{Choose } \phi_i^{in}(\mathbf{r})$$

$$\text{Construct } \rho^{in}(\mathbf{r}) \;=\; \sum_i |\phi_i^{in}(\mathbf{r})|^2, V_{\text{KS}}(\mathbf{r}, \rho^{in}(\mathbf{r}))$$

$$\left[-\frac{1}{2}\nabla_{\mathbf{r}}^2 + V_{\text{KS}}(\mathbf{r}, \rho^{in}(\mathbf{r})) \right] \phi_i^{out}(\mathbf{r}) \;=\; \epsilon_i^{out}\phi_i^{out}(\mathbf{r})$$

$$\text{Construct } \rho^{out}(\mathbf{r}) \;=\; \sum_i |\phi_i^{out}(\mathbf{r})|^2$$

$$\rho^{out}(\mathbf{r}) = \rho^{in}(\mathbf{r})$$

$$\text{if } |\rho^{in}(\mathbf{r}) - \rho^{out}(\mathbf{r})| \;<\; \delta_{tol}$$

no

yes

$$\text{Calculate the ground state property}$$
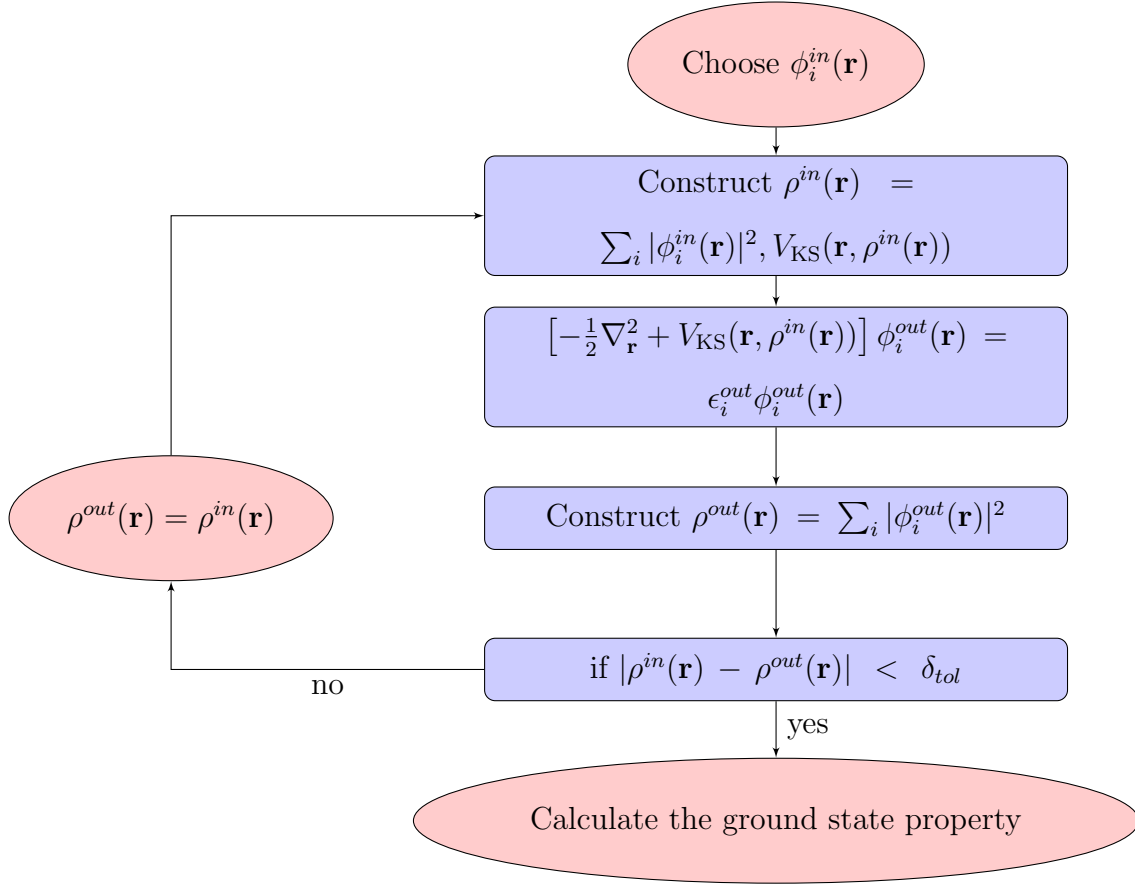
In the next section, we will discuss about various approximations to the XC energy term for practical calculations.

2.5 Exchange-Correlation Functionals

Since the advent of DFT various types of approximations for E_{xc} have been used for practical calculations. Proposed XC functionals are categorized as different rungs of a Jacob's ladder[28] depending upon the ingredients used as shown in Fig. 2.1. Furthermore, the XC functionals can be divided into non-empirical ones which are analytical in nature and empirical ones which are proposed by fitting to known atomic or molecular properties. Next, we briefly describe the rungs of the Jacob's ladder to introduce some of the most widely used XC functionals which also have been used later in this thesis for studying different properties of solid-state and molecular systems.
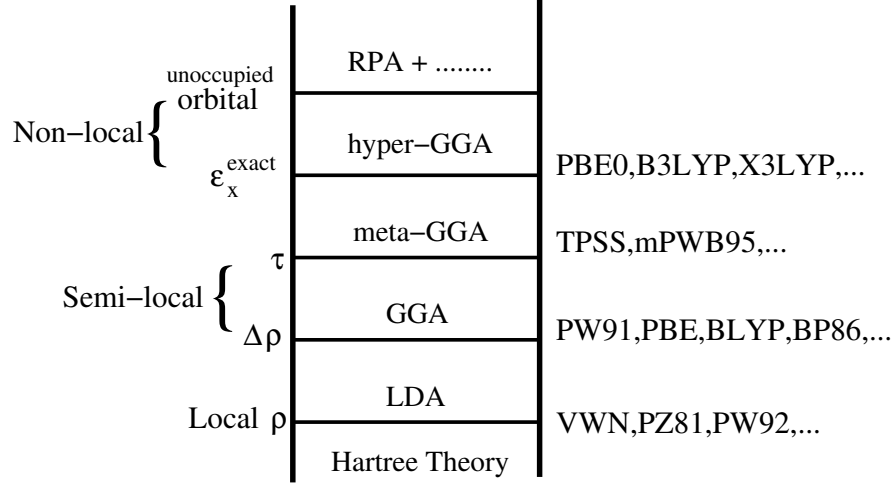
Figure 2.1: Schematic representation of the Jacob's ladder of the exchange-correlation functional approximations.

Local Density Approximation (LDA): In this approximation, a real inhomogeneous system is divided into infinitesimal volumes and within each infinitesimal volume, the density is taken to be uniform. The XC energy for each volume can be calculated using the XC energy for the uniform electron gas at that density and the total XC energy for the system can be written as

$$E_{\text{xc}}^{\text{LDA}} = \int \rho(\mathbf{r})\epsilon_{\text{xc}}^{\text{unif}}[(\rho(\mathbf{r}))]d\mathbf{r}, \tag{2.31}$$

where $\epsilon_{\text{xc}}^{\text{unif}}[(\rho(\mathbf{r}))]$ is the XC energy density for the interacting electron gas of density $\rho(\mathbf{r})$. The E_{rmxc}^{LDA} has two parts: $E_{\text{x}}^{\text{LDA}}$ and $E_{\text{c}}^{\text{LDA}}$. The analytical form of the exchange energy ($E_{\text{x}}^{\text{LDA}}$) is known in this case and given by[29,30]

$$E_{\text{x}}^{\text{LDA}} = -\frac{3}{4}\left(\frac{3}{\pi}\right)^{1/3}\int \rho(\mathbf{r})^{4/3}d\mathbf{r}. \tag{2.32}$$

However, there is no simple form available for the correlation energy and generally obtained by analysis and interpolation of highly accurate quantum Monte-Carlo simulations of the uniform electron gas.[31] Some of the popularly used LDA functionals are the Vosko-Wilk-Nusair (VWN),[32] Perdew-Zunger (PZ)[33] and Perdew-Wang

(PW).[34]

The LDA shows good performance for various properties of solid-state systems such as equilibrium structures, vibrational frequencies etc.. LDA works remarkably well for metallic systems. A possible explanation for this success can be related to the error cancellation between the exchange and correlation energies in LDA. Typically, LDA overestimates the exchange and underestimates the correlation energies for real systems and as a result of which it fortuitously gives good values of $E_{\mathrm{xc}}^{\mathrm{LDA}}$. This error cancellation likely because the LDA satisfies the exact sum rule[35,36] of XC potential which however does not necessarily guarantee accurate estimation of XC energy.

Generalized Gradient Approximation (GGA): The first step to improve the performance of LDA is to include the gradient of density ($\nabla\rho(\mathbf{r})$) into the XC functional in order to capture the varying electron densities of many materials. The earliest attempt was called the gradient-expansion approximation (GEA), where the gradient correction terms in powers of $\nabla\rho(\mathbf{r})$, $|\nabla\rho(\mathbf{r})|^2$, $\nabla^2\rho(\mathbf{r})$, etc. are added to LDA. A more appropriate way of incorporating the gradient of density beyond the LDA was found possible as:

$$E_{\mathrm{x}}^{\mathrm{GGA}} = \int \rho(\mathbf{r})\epsilon_{\mathrm{x}}^{\mathrm{unif}}(\rho(\mathbf{r}))F_{\mathrm{x}}^{\mathrm{GGA}}(s)d\mathbf{r}, \qquad (2.33)$$

where $F_x^{GGA}(s)$ is the exchange enhancement factor which determines the enhanced exchange energy over the LDA for a given density and s is the dimensionless reduced density gradient

$$s = \frac{|\nabla\rho(\mathbf{r})|}{2\left(3\pi^2\right)^{1/3}\rho(\mathbf{r})^{4/3}}. \qquad (2.34)$$

Some widely used GGA functionals are PBE,[37] PW91,[38] LYP[39] and AM05.[40]

In particular GGAs improve binding energies, atomic energies and dynamical properties of water, ice and water clusters[41] over the LDA results.

Hybrid Functional: The observation that trends rendered by semi-local approximations briefly discussed above are different to those rendered by the HF ap-

proximation mainly in semiconductors and insulators led to attempts to mix these two approaches. Formally the concept of hybrid functionals can be derived from the adiabatic connection"[42] for the XC energy as :

$$E_{\text{xc}} = \int_0^1 U_{\text{xc}}^\lambda d\lambda, \qquad (2.35)$$

$\lambda = 0$ correspond to non-interacting limit where E_{xc} is exactly represented by HF exchange in terms of the Kohn-Sham orbitals. The upper limit ($\lambda = 1$) corresponds to the fully interacting real system which can be approximately described by a local spin density approximations. The Eqn.(2.35) connects the non-interacting Kohn-Sham system for $\lambda = 0$ which does not incorporate any form of correlation to the fully interacting system for $\lambda = 1$ through a series of partially interacting systems in between $0 < \lambda < 1$ and all of the intermediate systems have the same density as the interacting one. As the non-interacting limit ($\lambda = 0$) is exactly described by the HF exchange, we expect an important role of the exact exchange for the improvement of the XC functionals as we switch on interaction (λ). Thus in the hybrid functionals semi-local XC approximation is mixed with the HF exchange in the following way

$$E_{\text{xc}}^{\text{hyb}} = \alpha E_{\text{x}}^{\text{HF}} + (1 - \alpha)E_{\text{x}}^{\text{DFT}} + E_c^{\text{DFT}}. \qquad (2.36)$$

The most popular and widely used hybrid functional is the B3LYP[43] which uses three parameters for controlling the mixing of the HF exchange and the DFT XC and the functional form can be written as :

$$E_{\text{xc}}^{\text{B3LYP}} = E_{\text{xc}}^{\text{LDA}} + \alpha_0(E_{\text{x}}^{\text{HF}} - E_{\text{x}}^{\text{LDA}}) + \alpha_{\text{x}}\Delta E_{\text{x}}^{\text{B88}} + \alpha_{\text{c}}\Delta E_{\text{c}}^{\text{LYP}}, \qquad (2.37)$$

where $\alpha_0 = 0.20$, $\alpha_{\text{x}} = 0.72$ and $\alpha_{\text{c}} = 0.81$ are determined empirically by fitting to experimental data, $\Delta E_{\text{x}}^{\text{B88}}$ and $\Delta E_{\text{c}}^{\text{LYP}}$ are the gradient corrections for the exchange and correlation respectively.[39,44] In the case of PBE0[45] functional, PBE GGA is used in Eqn.(2.36). In this case, the mixing coefficient α is taken to be 0.25 from the

perturbative calculation.[46] These functionals improve the performance over semi-local functionals for several molecular properties.[47,48] The hybrid functionals are called the global hybrids as the mixing coefficient is constant over the whole range. There are other class of hybrid functionals where the HF exchange and the semilocal XC functionals are mixed using the range separation of the Coulomb interaction operator. These are called range separated functionals and popular examples of this type of functionals are the CAM-B3LYP,[49] HSE06,[50] LC-ωPBE,[51] LC-ωPBEh[52] etc.. Although, it is expected to get improved results by climbing higher on Jacob's ladder but it is not always be the case.[53] Most of the proposed XC functionals have been implemented in the library of exchange-correlation functional (LIBXC)[54] which can be interfaced with several first-principle codes for the DFT calculations.

2.6 Pseudopotential Method

The idea of pseudopotential is to write an effective potential felt by valence electron in presence of core electrons. Technically pseudopotential replace the complicated structure of actual potential around the core region by smoother function. In a systems, the electronic structure have different contribution due to the core electrons and valence electrons because the core electrons are more bound to nuclei respect to the valence electrons which are relatively free due to the screening of the nuclei potential by the core electrons. In the low energy physical properties such as optical excitation, chemical bonding, conductivity etc. the core electrons have negligible contribution.

The pseudopotential or effective potential is constructed by replacing all atomic electron potential (full-potential) in such a way that core states are eliminated and the valence electrons are described by pseudo wavefunctions with significantly fewer nodes which can be effectively described by plane-wave basis sets.

First-principles pseudopotentials are derived from an atomic reference state, requiring that the pseudo- and all-electron valence eigenstates have the same energies and amplitude (and thus density) outside a chosen core cut-off radius R_c. Pseu-

dopotentials with larger R_c are said to be softer, that is more rapidly convergent, but at the same time less transferable, that is less accurate to reproduce realistic features in different environments.

Valence wave functions, with complex nature in the core region(r< R_c) due to presence of nodes, which demands a large set of plane wave basis for adequate representation set by kinetic energy cut-off(E_{cutoff})[Eqn.(2.38)].

$$\frac{1}{2}G^2 \leq E_{cutoff}. \tag{2.38}$$

where G is reciprocal lattice vector.

In standard DFT calculation like ours, we considered the valence electrons in an effective smooth pseudopotential. This way the valence wave functions becomes smooth enough within the core region to be described by a reasonably small set of plane waves. These pseudopotentials are generated from all electron calculations of atoms such that the pseudo wave functions satisfy the properties of valence electrons outside the cut-off radius R_c[Fig. 2.2]. Depending on the choice of certain constraints and division of core/semi-core and valence shell of electronic configurations there are different types of pseudopotentials.[55] The accuracy of the pseudopotentials depends on their 'transferability' such that the same pseudopotential for a given element can be used in various chemical environment and maximally reproduce scattering properties of the true potential. Therefore, the pseudopotentials should be accurate as well as smooth which requires less no of basis sets in order to reduce the computational cost. Norm-conserving ones[57] are the most commonly used pseudopotential which, as the name suggests conserve the normalization of the pseudo wave function inside R_c so that the total charge within the core region remain preserved. Ultrasoft[58] ones constitute the other set of commonly used variant of pseudopotentials, which maximally smoothen(delocalizes) the pseudo wave functions inside the core region at the cost of nonconservation of total charge, leading to requirement of additional correction term, namely, the augmented charges while substantially reducing the requirement of plane wave basis.
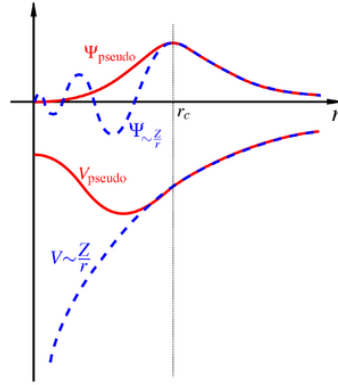
Figure 2.2: Wave function(blue) in real Coulomb potential(blue) and representation of pseudopotential(red) and pseudo wave function(red).[56]

2.6.1   Limitations

However, with increased correlation due to occupation of the d or higher orbitals which have sharper localization than the s and p electrons due to higher number of nodal plane and cones, the inadequacy of representation of correlation in XC functionals, which inherently borough from node-less charge distribution, show up as deviation of the calculated band gap and related properties from their experimental observed values.

In terms of matching the experimental band gap, which is estimated as the difference between the ionization potential(IP) and the electron affinity(EA), both LDA and GGA fails even for the $2p$ block diamond and zinc-blende structures of bulk C, Si, BN etc. Fundamentally, these failures of LDA and GGA can be attributed to the inherent lack of discontinuity of the derivative of the local and static mean-field approximation of the exchange-correlation functional, upon addition or removal of electron. As a state get filled or emptied once the electron number changes by one, the overall behaviour of the system is expected to change, depending on the effect of the charge density of that state on interaction among electrons in its vicinity. However, the static nature of the XC functional does not support any such change in the nature of many-electron interactions they represent. In principle, inclusion of dynamic correlation in the form of dynamic screening should largely address this

issue since it would in effect allow the inherent collective oscillatory (plasmonic) response of electrons to any evolution of charge density. Towards such correlation in the next section I will discuss the GW approximation of the many-body perturbation theory (MBPT), which naturally incorporates dynamical screening leading to a quasi-particle description of interacting electron.

2.7　GW approximation of Many-body perturbation theory

The Green's function based many-body perturbation theory (MBPT)[4,5,59,60] presents an exhaustive self-consistent approach to account for dynamic correlation starting from a reasonable set of occupied and unoccupied single particle states. The GW approximation[5,61] of the MBPT is the state of the art method which allows accurate estimation of energetic of interacting electrons through computation of self-energy correction to single particle levels.

In a simple case of non-interacting particles with Hamiltonian $H(\mathbf{r})$, we can define a non-interacting single-particle Green's function for the Schrödinger equation $H(\mathbf{r})\psi(\mathbf{r}) = E\psi(\mathbf{r})$ as :

$$[H(\mathbf{r}) - E]G_0(\mathbf{r}, \mathbf{r}', E) = \delta(\mathbf{r} - \mathbf{r}') \tag{2.39}$$

where $G_0(\mathbf{r}, \mathbf{r}', E)$ satisfies the same boundary conditions as $\psi(\mathbf{r})$. Returning back to the definition of Green's function Eqn.(2.39) we note that it is the representation of the operator equation:

$$(E - \hat{H})\hat{G}_0(E) = 1 \tag{2.40}$$

Using the completeness of the eigenstates of the unperturbed Hamiltonian, we can

write in the $\{|\mathbf{r}\rangle\}$ basis as:

$$\hat{G}_0(E, \mathbf{r}, \mathbf{r}') = \sum_n \frac{\psi_n^*(\mathbf{r})\psi_n(\mathbf{r}')}{E - E_n} \tag{2.41}$$

where, $\psi_n(\mathbf{r})$'s and E_n's are the eigenfunctions and eigenvalues of H respectively.

Generalizing the propagator interpretation of Green's function in the realm of N electrons systems, the generic one particle Green's function (describing propagation of one particle) is defined as :

$$G_{\alpha\beta}(\mathbf{r}, t, \mathbf{r}', t') = -i\langle N, 0 \mid \hat{T}[\hat{\psi}_\alpha(\mathbf{r}, t)\hat{\psi}_\beta^\dagger(\mathbf{r}', t')] \mid N, 0\rangle \tag{2.42}$$

where $\mid N, 0\rangle$ is an N electron ground state, $\psi_\alpha^\dagger(\mathbf{r}, t)$ and $\psi_\alpha(\mathbf{r}, t)$ are respectively the creation and annihilation field operator and T is time ordering operator to ensure that the sequence of operation of the operators from right to left are causal in time:

$$\begin{aligned} T\left[\hat{\psi}_\alpha(\mathbf{r}, t)\hat{\psi}_\beta^\dagger(\mathbf{r}', t')\right] &= \hat{\psi}_\alpha(\mathbf{r}, t)\hat{\psi}_\beta^\dagger(\mathbf{r}', t'), \quad t > t' \\ &= \pm\hat{\psi}_\alpha^\dagger(\mathbf{r}', t')\hat{\psi}_\beta(\mathbf{r}, t), \quad t < t' \end{aligned} \tag{2.43}$$

Implying:

$$\begin{aligned} iG(x, t, x', t') &= \langle N, 0 \mid \hat{\psi}(x, t)\hat{\psi}^\dagger(x', t')) \mid N, 0\rangle\theta(t - t') \\ &\pm\langle N, 0 \mid \hat{\psi}^\dagger(x', t')\hat{\psi}(x, t)) \mid N, 0\rangle\theta(t' - t) \end{aligned} \tag{2.44}$$

where, $\theta(t - t')$ is a step function.

We now move on to derive description of interaction approximately in terms of one particle Green's function by considering the two body interaction as perturbation.

Let us consider a generic two body interaction described by the Hamiltonian :

$$\hat{H}(x_1, t_1) = \hat{H}_0(x_1) + \frac{1}{2}v(x_1, x_2)\delta(t_1 - t_2) \tag{2.45}$$

where $\hat{H}_0(x_1)$ is the one-particle part and $v(x_1, x_2)$ can be the coulomb interaction i.e., $\frac{e^2}{|\vec{r_1}-\vec{r_2}|}$.

Representing Eqn.(2.45) in term of field operator in the Heisenberg equation of motion, we can write

$$i\hbar\frac{\partial}{\partial t_1}\hat{\psi}(x_1, t_1) = \hat{H}_0(x_1)\hat{\psi}(x_1, t_1) + \int v(x_1, x_3)\hat{\psi}^{\dagger}(x_3, x_1)\hat{\psi}(x_3, t_1)dx_3\hat{\psi}(x_1, t_1)$$
(2.46)

We can multiplying Eqn.(2.46) by field operator $\hat{\psi}^*(x_2, t_2)$ with appropriate time ordering and take expectation value with respect to ground state on both side to write the duel Eqn(2.46) in term of Green's function as :

$$G(x_1, t_1, x_2, t_2) + i\int v(x_1, x_3)\langle N|T[\hat{\psi}^{\dagger}(x_3, t_1)\hat{\psi}(x_3, t_1)\hat{\psi}(x_1, t_1)\hat{\psi}^{\dagger}(x_2, t_2)]|N\rangle dx_3$$

$$= \hbar\delta(x_1 - x_2)\delta(t_1 - t_2)$$
(2.47)

Above equation can be interpreted as:

Non-interacting one-particle term $+$ interaction term $= \hbar\delta(x_1 - x_2)\delta(t_1 - t_2)$

In our case, we use DFT to represent the non-interacting regime.

The interaction term, on account of the two particle interaction, naturally involves a two particle Green's function:

$$\langle N|T[\hat{\psi}^{\dagger}(x_3, t_1)\hat{\psi}(x_3, t_1)\hat{\psi}(x_1, t_1)\hat{\psi}^{\dagger}(x_2, t_2)]|N\rangle$$
(2.48)

In the non-interacting limit, where we assume the two particles to propagate independently to each other we can approximate the two particle Green's function similar as combination of products of one particle Green's functions leading to the Hartree-Fock description.

To go beyond independent propagation approximation, we introduce a external

field ϕ in the equation of motion eqn.(2.47) as:

$$\{i\hbar\frac{\partial}{\partial t} - \hat{H}_0(x_1) - \phi(x_1, t_1)\}G(x_1, t_1, x_2, t_2) + i\int v(x_1, x_3)\langle N|T[\hat{\psi}^\dagger(x_3, t_1)$$
$$\hat{\psi}(x_3, t_1)\hat{\psi}(x_1, t_1)\hat{\psi}^\dagger(x_2, t_2)]|N\rangle dx_3 = \hbar\delta(x_1 - x_2)\delta(t_1 - t_2) \quad (2.49)$$

which enables us to define the two particle Green's function as:

$$G_2(1, 2, 3, 3^+) = \hbar\frac{\delta G(1, 2)}{\delta\phi(3)} + G(1, 2)G(3, 3^+) \quad (2.50)$$

using Gellmann-Low theorem in the interaction representation. As obvious, we denote the labels "1,2,...,N" as "$(x_1, t_1), (x_2, t_2), ..., (x_N, t_N)$".

Using the expression of two particle Green's function above in Eqn.(2.47), we obtain:

$$[i\frac{\partial}{\partial t} - H_0(x_1) - V_H]G(1, 2) + i\int v(1, 3)\frac{\delta G(1, 2)}{\delta\phi(3)}d(3) = \delta(1 - 2). \quad (2.51)$$

where

$$V_H = \int v(1, 3)G(3, 3^+)dx(3) \quad (2.52)$$

At this point we can introduce the "self-energy operator" which contain all the interaction terms in it as:

$$[i\frac{\partial}{\partial t} - H_0(x_1) - V(1)]G(1, 2) - \int \Sigma(1, 3)G(3, 2)d(3) = \delta(1 - 2). \quad (2.53)$$

where $V(1) = \phi(1) + V_H(1)$.

Comparing Eqn.(2.51) and Eqn.(2.53)

$$\Sigma(1, 2) = -i\int v(1, 3)G(1, 4)\frac{\delta G^{-1}(4, 2)}{\delta\phi(3)}d(3)d(4) \quad (2.54)$$

Noting $G^{-1}G = 1$ which lead to

$$\frac{\partial G}{\partial \phi} = -G\frac{\partial G^{-1}}{\partial \phi}G \tag{2.55}$$

We find:

$$\Sigma(1,2) = -i\int v(1,3)G(1,4)\frac{\delta G^{-1}(4,2)}{\delta\phi(3)}d(3)d(4) \tag{2.56}$$

consistent with Eqn.(2.53).

To interpret the Σ in terms of physically observable and measurable quantities we note that the dielectric response function defined as :

$$\epsilon^{-1}(x_1, t_1, x_2, t_2) = \frac{\delta V(x_1, t_1)}{\delta\phi(x_2, t_2)} \tag{2.57}$$

Recalling $v(1) = \phi(1) + V_H$, we can write:

$$\epsilon^{-1}(1,2) = \delta(1-2) + \int v(1,3)\frac{\delta\rho(3)}{\delta\phi(2)}d(3) \tag{2.58}$$

Polarization function is defined as :

$$\begin{aligned} P(1,2) &= \frac{\delta\rho(1)}{\delta V(2)} \\ &= -i\int G(1,3)\Gamma(3,4,2)G(4,1^+)d(3) \end{aligned} \tag{2.59}$$

where

$$\Gamma(1,2,3) = -\frac{\delta G^{-1}(1,2)}{\delta V(3)} \tag{2.60}$$

which is known as vertex function.

In most of the system, it is found reasonable to approximate the vertex function Γ as

$$\Gamma(1,2,3) = -\frac{\delta G^{-1}(1,2)}{\delta V(3)} \simeq \frac{\delta G_0^{-1}(1,2)}{\delta V(3)} = \delta(1-2)\delta(1-3) \tag{2.61}$$

Leading to:

$$P_0(1,2) = -iG_0(1,2)G_0(2,1^+) \tag{2.62}$$

and the self-energy operator takes a simple form as

$$\Sigma(1,2) = iG_0(1,2)W(1,2) \tag{2.63}$$

where

$$W(1,2) = \int \epsilon^{-1}(1,3)v(3,2)d(3) \tag{2.64}$$

Finally transforming expression for P_0, ϵ, Σ, W in terms of ω, we have

$$P_0(\vec{r}_1, \vec{r}_2, \omega) = -\frac{i}{2\pi} \int G_0(\vec{r}_1, \vec{r}_2, \omega - \omega')G_0(\vec{r}_1, \vec{r}_2, \omega')d\omega' \tag{2.65}$$

$$\epsilon(\vec{r}_1, \vec{r}_2, \omega) = \delta(\vec{r}_1 - \vec{r}_2) - \int v(\vec{r}_1, \vec{r}_3)P_0(\vec{r}_3, \vec{r}_2, \omega)d\vec{r}_3 \tag{2.66}$$

$$W(\vec{r}_1, \vec{r}_2, \omega) = \int \epsilon^{-1}(\vec{r}_1, \vec{r}_3, \omega)v(\vec{r}_3, \vec{r}_2)d\vec{r}_3 \tag{2.67}$$

$$\Sigma(\vec{r}_1, \vec{r}_2, \omega) = \frac{i}{2\pi} \int G_0(\vec{r}_1, \vec{r}_2, \omega - \omega')W(\vec{r}_1, \vec{r}_2, \omega')d\omega' \tag{2.68}$$

We now recall Eqn.(2.51) and write the corresponding homogeneous equation as:

$$\left(-\frac{1}{2}\nabla^2 + V_{ext} + V_H\right)\psi_{nk}(\mathbf{r}) + \int \Sigma(\mathbf{r}, \mathbf{r}', E_{nk})\psi_{nk}(\mathbf{r}')d\mathbf{r}' = E_{nk}\psi_{nk}(\mathbf{r}) \tag{2.69}$$

With the approximation that the single particle states remain unaltered upon self-energy correction we calculate the quasi-particle energy at zeroth level as

$$E_{n\mathbf{k}}^{QP} = E_{n\mathbf{k}}^{KS} + \left\langle \phi_{n\mathbf{k}}^{KS} \left| \Sigma^{GW}\left(E_{n\mathbf{k}}^{QP}\right) - V_{xc} \right| \phi_{n\mathbf{k}}^{KS} \right\rangle \tag{2.70}$$

This is only one iteration known as one-shot G_0W_0 which gives reasonably accurate results for the systems we are interested. In a typial GW implementation, however, the computational cost scales as $O(N^4)$ which is prohibitively expensive and restrict its application to systems of having hundreds of electrons in it.

The key convergenced parameters are ϵ and G and thereby Σ in terms of the unoccupied state used in their calculation. The dynamic estimation of ϵ is performed within the plasmon pole approximation starting with the static limit ($\omega = 0$) calculated using the linear response based formulation as :

$$P_0(\vec{r}, \vec{r}'; \omega = 0) = \sum_{j,k=1}^{\infty} (f_k - f_j) \frac{\varphi_j^0(\vec{r})\varphi_k^{0*}(\vec{r})\varphi_j^{0*}(\vec{r}')\varphi_k^0(\vec{r}')}{-\omega_{jk} + i\eta} \tag{2.71}$$

where f_j and f_k are occupation number of the Kohn-Sham ground state(1 for occupied and 0 for unoccupied orbitals).

2.8 Electron in periodic potential: Tight-binding framework

In this section I will briefly introduce the Bloch formalism and the conceptual basis of Wannier function and the tight-binding framework based on it.

A periodic system is characterized by an effective periodic potential that an electron in it is subjected to, satisfying :

$$V(\mathbf{r}) = V(\mathbf{r} + \mathbf{R}), \tag{2.72}$$

where

$$\mathbf{R} = n_1\mathbf{a}_1 + n_2\mathbf{a}_2 + n_3\mathbf{a}_3 \tag{2.73}$$

is any real space lattice vector with $\{n_i\} \to \mathbb{Z}$, $\mathbf{a}_i$(i=1,2,3) being three lattice vectors enclosing a finite volume which is defined as an unit-cell which defines the periodicity of the system. A unit cell can be a primitive with smallest volume or multiple of that. For a given system, although the volume of the primitive unit-cell is uniquely defined, the primitive unit-cell itself is not.

The potential defines a single particle Hamiltonian which satisfies:

$$H(\mathbf{r}) = H(\mathbf{r} + \mathbf{R}), \tag{2.74}$$

Within the Born-von Karman(BVK) periodic boundary condition(PBC), central to the Bloch formalism, the infinitely extended perfect crystal is divided into chunks of crystals containing, say, $N_1 \times N_2 \times N_3$ number of unit-cells. Analytic description, namely, the Bloch formalism, is derived for finite $\{N_i\}$, which are then notionally set to ∞ to represent a perfect crystal.

For such a chunk of crystal, wave functions describing an electron within the BVK PBC satisfy:

$$\psi(\mathbf{r}) = \psi(\mathbf{r} + N_1\mathbf{a}_1 + N_2\mathbf{a}_2 + N_3\mathbf{a}_3). \tag{2.75}$$

which allows expansion in the Fourier basis $\{e^{i\mathbf{f}.\mathbf{r}}\}$ defined by wave-vectors:

$$\mathbf{f} = \sum_{i=1}^{3} \frac{m_i}{N_i}\mathbf{b}_i, \tag{2.76}$$

with $m_i \to \mathbb{Z}$ and $\mathbf{b}_i$(i=1,2,3) being primitive reciprocal lattice vectors which satisfy $\mathbf{b}_i.\mathbf{a}_j = 2\pi\delta_{ij}$.

However, such a solution to the periodic Hamiltonian defined in Eqn.(2.74) becomes possible only if the Fourier coefficients $\{C_\mathbf{f}\}$ separates out into $N_1 \times N_2 \times N_3$ linearly independent sets each identified by a unique $\mathbf{f}$ defined by $\{m_i = 0, 1, 2, ..., N_i - 1\}_{i=1,2,3}$.

Denoting the unique set of wave-vectors $\{\mathbf{f}\}$ as $\{\mathbf{k}\}$, referred as the allowed values of crystal momentum, we therefore have for each unique $\mathbf{k}$:

$$\psi_\mathbf{k}(\mathbf{r}) = \frac{1}{\sqrt{\Omega}} \sum_\mathbf{G} C_{\mathbf{k}-\mathbf{G}} e^{i(\mathbf{k}-\mathbf{G}).\mathbf{r}} \tag{2.77}$$

where $\Omega = N_k\Omega_{cell}$, with $N_k = N_1N_2N_3$, and $\mathbf{k} = \sum_{i=1}^{3} \frac{m_i}{N_i}\mathbf{b}_i$ with $m_i = 0, 1, 2, ..., N_i - 1$ and $\mathbf{G} = l_1\mathbf{b}_1 + l_2\mathbf{b}_2 + l_3\mathbf{b}_3$ is a reciprocal lattice vector with $l_i \to \mathbb{Z}$

Eqn.(2.77) implies

$$\psi_{\mathbf{k}}(\mathbf{r}) = \frac{1}{\sqrt{N_k}} u_{\mathbf{k}}(\mathbf{r}) e^{i\mathbf{k}.\mathbf{r}} \tag{2.78}$$

where $u_{\mathbf{k}}(\mathbf{r})$ has the same periodicity as the Hamiltonian, and obtained as:

$$u_{\mathbf{k}}(\mathbf{r}) = \frac{1}{\sqrt{\Omega_{cell}}} \sum_{\mathbf{G}} C_{\mathbf{k}-\mathbf{G}} e^{i\mathbf{G}.\mathbf{r}}. \tag{2.79}$$

The cell periodic functions $u_{\mathbf{k}}(\mathbf{r})$ can be obtained as eigen function of the Bloch Hamiltonian:

$$H(\mathbf{k}) = -\frac{(\hat{\mathbf{p}} + \hbar\mathbf{k})^2}{2m_e} + V(\mathbf{r}). \tag{2.80}$$

The eigenvalues and eigenstates of $H(\mathbf{k})$ provides the description of energy levels and charge density of an electron in a periodic potential. In the Kohn-Sham analogue to Bloch Hamiltonian $V = V_H + V_{XC} + V_{ext}$.

Introducing the band index (m) which are essentially the symmetry matched order of the eigenstates obtained through diagonalization of H_k for every allowed k values, the cell periodic function and the Bloch functions satisfy the following orthoronmality conditions:

$$\int_{\Omega_{cell}} u_{m\mathbf{k}}^*(\mathbf{r}) u_{m'\mathbf{k}}(\mathbf{r}) d\mathbf{r} = \delta_{mm'} \tag{2.81}$$

$$\int_{\Omega} \psi_{m\mathbf{k}}^*(\mathbf{r}) \psi_{m'\mathbf{k}'}(\mathbf{r}) d\mathbf{r} = \delta_{mm'} \delta_{\mathbf{k}\mathbf{k}'} \tag{2.82}$$

Following Eqn.(2.77) we note that

$$\psi_{\mathbf{k}+\mathbf{G}'}(\mathbf{r}) = \psi_{\mathbf{k}}(\mathbf{r}) \tag{2.83}$$

Noting the periodicity of ψ in k-space, we recall that for a periodic function $f(q) = f(q + Q)$, we have:

$$f(q) = \sum_n C_n e^{in\frac{2\pi}{Q}q}. \tag{2.84}$$

For simplicity, we now resort to one dimension which can be easily generalized to

higher dimensions. Therefore in one dimension the periodicity of Bloch function :

$$\psi_{k+G_0}(x) = \psi_k(x) \tag{2.85}$$

would imply :

$$
\begin{aligned}
\psi_k(x) &= \sum_n C_n(x)e^{in\frac{2\pi}{G_0}k} \\
&= \sum_n C_n(x)e^{inak} \\
&= \sum_{R_n} C_{R_n}(x)e^{iR_n k}
\end{aligned} \tag{2.86}
$$

where we replace $G_0 = \frac{2\pi}{a}$ and $R_n = na$. The function $C_{R_n}(x)$ in real space is essentially the Wannier function[8,62,63] which we represent here onwards as $W_{R_n}(x)$.

Eqn.(2.86) implies an inverse relation as :

$$W_{R_n}(x) = A \int_{BZ} \psi_k(x)e^{-iR_n x}. \tag{2.87}$$

After normalization :

$$
\begin{aligned}
W_{R_n}(x) &= \frac{\sqrt{N_k}a}{2\pi} \int \psi_k(x)e^{-iR_n k}dk \\
&= \frac{1}{\sqrt{N}} \sum_k \psi_k(x)e^{-iR_n k}
\end{aligned} \tag{2.88}
$$

implying :

$$\psi_k(x) = \frac{1}{\sqrt{N_k}} \sum_{R_n} e^{ikR_n} W_{R_n}(x). \tag{2.89}$$

Generalizing to three dimensions

$$
\begin{aligned}
W_{\mathbf{R}}(\mathbf{r}) &= \frac{\sqrt{N}\Omega}{(2\pi)^3} \int \psi_{\mathbf{k}}(\mathbf{r})e^{-i\mathbf{R}.\mathbf{k}}d^3k \\
&= \frac{1}{\sqrt{N}} \sum_{\mathbf{k}} \psi_{\mathbf{k}}(\mathbf{r})e^{-i\mathbf{R}.\mathbf{k}}
\end{aligned} \tag{2.90}
$$

and

$$\psi_{m\mathbf{k}}(\mathbf{r}) = \frac{1}{\sqrt{N_k}} \sum_{\mathbf{R}} e^{i\mathbf{k}.\mathbf{R}} W_{m\mathbf{R}}(\mathbf{r}). \tag{2.91}$$

where we have reintroduced the band index (m) implying that Wannier function are to constructed band by band. More generally:

$$W_{m\mathbf{R}}(\mathbf{r}) = \frac{1}{\sqrt{N_k}} \sum_{\mathbf{k}} e^{-i\mathbf{k}.\mathbf{R}} \sum_{l} U_{ml} \psi_{l\mathbf{k}}(\mathbf{r}). \tag{2.92}$$

With proper choice of gauge $\underline{U}$, Wannier functions can be constructed to be localized within a desired unit-cell. Orthonormality condition satisfied by Wannier functions:

$$\langle W_{m\mathbf{R}}(\mathbf{r}) \mid W_{m'\mathbf{R}'}(\mathbf{r}) \rangle = \delta_{mm'} \delta_{\mathbf{R}\mathbf{R}'} \tag{2.93}$$

Localized set of orthonormal Wannier functions thus constitute an ideal set of localized orthogonal basis.

2.8.1   Tight-Binding model

Tight-binding (TB)[62] model is the simplest single particle approach for calculation of electronic structure of a system of atoms. To construct a representation of a given Hamiltonian is in the basis of a chosen set of N number of orthonormal localized functions $\{\phi_i(\mathbf{r})\}$. Wannier functions are considered as a linear combinations of the chosen basis functions as :

$$W_n(\mathbf{r}, \mathbf{R}) = \sum_{m}^{N} C_{nm} \phi_m(\mathbf{r}, \mathbf{R}). \tag{2.94}$$

where $\mathbf{R}$ is a lattice vector spanning the entire crystal and $\{\phi_n(\mathbf{r}, \mathbf{R})\}$ are considered translated to the unit-cell defined by $\mathbf{R}$. For isolated systems only $\mathbf{R} = 0$ is considered.

Depending on the range of the basis functions used, a TB model can be chosen to represent either only few bands about the Fermi energy, or a wide subspace of

bands covering not only the entire occupied subspace but also an equal number of bands from the unoccupied subspace, as is the case in this thesis.

Traditionally, $\{\phi_i(\mathbf{r})\}$ are chosen to be atomic orbitals obtained as:

$$H_{at}\phi_j(\mathbf{r}) = E_j\phi_j(\mathbf{r}). \tag{2.95}$$

H_{at} being the atomic Hamiltonian and E_j being the energy levels of a single atom.

Referring to the Bloch functions introduced in the previous section, Schrödinger equation for the crystal can be written as,

$$H\psi_{m\mathbf{k}}(\mathbf{r}) = (\sum_{atom} H_{at} + \Delta V)\psi_{m\mathbf{k}}(\mathbf{r}) = \varepsilon_m(\mathbf{k})\psi_{m\mathbf{k}}(\mathbf{r}), \tag{2.96}$$

where, H is the crystal Hamiltonian and ΔV contains the corrections to reproduce the full periodic potential of the crystal in terms of the ionic potentials.

Taking inner product of both sides of Eqn.(2.96) with $\phi_n^*(\mathbf{r})$ at $\mathbf{R} = 0$:

$$\int \phi_n^*(\mathbf{r})(\sum_{atom} H_{at} + \Delta V)\psi_{m\mathbf{k}}(\mathbf{r})d^3r = \varepsilon_m(\mathbf{k})\int \phi_n^*(\mathbf{r})\psi_{m\mathbf{k}}(\mathbf{r})d^3r. \tag{2.97}$$

using Eqn.(2.89) and Eqn.(2.94):

$$\varepsilon_m(\mathbf{k})\sum_l C_{ml}(\mathbf{k})\sum_{\mathbf{R}} \int d^3r\,\phi_n^*(\mathbf{r})\phi_l(\mathbf{r}-\mathbf{R})e^{i\mathbf{k}.\mathbf{R}} =$$

$$\sum_j C_{mj}(\mathbf{k})\sum_{\mathbf{R}'} \int d^3r\,\phi_n^*(\mathbf{r})(H_{at}+\Delta V)\phi_j(\mathbf{r}-\mathbf{R}')e^{i\mathbf{k}.\mathbf{R}'}$$

which simplifies to:

$$(\varepsilon_m(\mathbf{k}) - E_n)\sum_l C_{ml}(\mathbf{k})\sum_{\mathbf{R}} \alpha_{nl}(\mathbf{R})e^{i\mathbf{k}.\mathbf{R}} = \sum_j C_{mj}(\mathbf{k})\sum_{\mathbf{R}'} \gamma_{nj}(\mathbf{R}')e^{i\mathbf{k}.\mathbf{R}'} \tag{2.98}$$

with

$$\alpha_{mn}(\mathbf{R}) = \int d^3r \ \phi_m^*(\mathbf{r})\phi_n(\mathbf{r} - \mathbf{R}) \tag{2.99}$$

$$\gamma_{mn}(\mathbf{R}) = -\int d^3r \ \phi_m^*(\mathbf{r})\Delta V \phi_n(\mathbf{r} - \mathbf{R}). \tag{2.100}$$

Overlap of m-th and n-th atomic orbitals located at different unit-cells is often considered negligible. The parameter is $\gamma_{m,n}(\mathbf{R})$, is known as 'hopping' parameter, which is also often considered negligible beyond neighboring unit-cells due to localized nature of the basis.

For an orthonormal basis, as we have constructed in this work, $\alpha_{mn}(\mathbf{R}) = \delta_{mn}\delta_{\mathbf{R},0}$ which reduces Eqn.(2.98) to

$$\varepsilon_m(\mathbf{k})C_{mn}(\mathbf{k}) = E_n C_{mn}(\mathbf{k}) + \sum_j C_{mj}(\mathbf{k}) \sum_{\mathbf{R}'} \gamma_{nj}(\mathbf{R}')e^{i\mathbf{k}.\mathbf{R}'} \tag{2.101}$$

In this thesis, we calculate the tight binding parameters in the basis of directed hybrid atomic Wannier orbitals (HAWO) described in chapter3 and consider beyond nearest neighborhood. Due to directed nature of the HAWO basis, each inter-atomic hopping is predominantly represented by a single off-diagonal element.

2.9 The formal framework of linear-response within TDDFT

2.9.1 General linear response theory

We consider the application of perturbation to the total Hamiltonian H_0 as :

$$\hat{H}(t) = \hat{H}_0 + \hat{H}'(t)\theta(t - t_0) \tag{2.102}$$

At times before t_0 the system is in equilibrium, after which the perturbation is turned on. The system is now evolving according to new Hamiltonian and is in a non-equilibrium state. The time dependence of the state $|n(t)\rangle$ is of course governed by the Schrödinger equation

$$i\delta_t|n(t)\rangle = \hat{H}(t)|n(t)\rangle \tag{2.103}$$

Since $\hat{H}'$ is to be regarded as a small perturbation, it is convenient to utilize the interaction picture representation $|\hat{n}_I(t)\rangle$. The time dependence in this representation is given by -

$$|n_I(t)\rangle = e^{i\hat{H}_0 t}|n_S(t)\rangle \tag{2.104}$$

$$A_I(t) = e^{i\hat{H}_0 t} A_S e^{-i\hat{H}_0 t} \tag{2.105}$$

where by definition

$$|n_S(t)\rangle = e^{i\hat{H}_0 t}\hat{U}_I(t,t_0)|n_H\rangle = e^{-i\hat{H}_0 t}(1 - i\int_{t_0}^{t} dt' \hat{H}'(t))|n_H\rangle \tag{2.106}$$

The expectation value of A upto linear order in the perturbation using eqn. 2.106:

$$
\begin{aligned}
\langle \hat{A}(t) \rangle &= \sum_n^{occu} \langle n_S(t) | \hat{A} | n_S(t) \rangle \\
&= \sum_n^{occu} \left\{ \langle n_H | \hat{U}_I^\dagger e^{i\hat{H}_0 t} \right\} \hat{A} \left\{ e^{-i\hat{H}_0 t} \hat{U}_I | n_H \rangle \right\} \\
&= \sum_n^{occu} \langle n_H | \left(1 + i \int_{t_0}^t dt' \hat{H}'(t') \right) e^{i\hat{H}_0 t} \hat{A} e^{-i\hat{H}_0 t} \left(1 - i \int_{t_0}^t dt' H'(t') \right) | n_H \rangle \\
&= \sum_n^{occu} \left[\left(\langle n_H | e^{i\hat{H}_0 t} \right) \hat{A} \left(e^{-i\hat{H}_0 t} | n_H \rangle \right) + i \int_{t_0}^t \langle n_H | \hat{H}'(t') e^{i H_0 t} \hat{A} e^{-i\hat{H}_0 t} | n_H \rangle dt' \right] \\
&\quad - i \sum_n^{occu} \left[\int_{t_0}^t \langle n_H | e^{i\hat{H}_0 t} \hat{A} e^{-i\hat{H}_0 t} \hat{H}'(t') | n_H \rangle \right] \\
&= \sum_n^{occu} \left[\langle n_H | \hat{A} | n_H \rangle + i \int_{t_0}^t \langle n_H | \left\{ \hat{H}'(t') \hat{A}_I(t) - \hat{A}_I(t) \hat{H}'(t') \right\} | n_H \rangle \right] \\
&= \langle A \rangle_0 + i \int_{t_0}^t \langle [\hat{H}'(t'), \hat{A}_I(t)] \rangle_0 dt'
\end{aligned}
\tag{2.107}
$$

where "0" implies in term of all unperturbed occupied state.

Now assume that the system is acted upon a time dependent perturbation

$$
\hat{H}'(t) = F(t)\hat{\beta}, t \geq_0
\tag{2.108}
$$

where $F(t)$ is an external field that couples to an observable $\hat{\beta}$ and which is switched on at time t_0. Then

$$
\langle \hat{A}(t) \rangle - \langle \hat{A} \rangle_0 = i \int_{t_0}^t dt' \langle [\hat{\beta}, \hat{A}_I(t)] \rangle_0 F(t')
\tag{2.109}
$$

We rewrite the linear response result as

$$
\delta \langle \hat{A}(t) \rangle = \langle \hat{A}(t) \rangle - \langle \hat{A} \rangle_0 = \int_{t_0}^\infty dt' \chi_{A\beta}^R(t, t') F(t')
\tag{2.110}
$$

where

$$
\chi_{A\beta}^R(t, t') = -i\theta(t - t') \langle [\hat{A}_I(t), \hat{\beta}] \rangle_0
\tag{2.111}
$$

Then, $A(t) - A_0$ is called the response of $\hat{A}$ due to the perturbation. Here A_0 is the expectation value of $\hat{A}$ corresponding to the ground state wavefunction.

The response of $\hat{A}$, can be expanded in power of the field F(t):

$$A(t) - A_0 = A_1(t) + A_2(t) + A_3(t) + \cdots \tag{2.112}$$

where $A_1(t)$ is the linear response, $A_2(t)$ is the quadratic response, $A_3(t)$ is the third order response and so on.

Using eqn.2.109, we can write the linear response as:

$$A_1(t) = -i \sum_n \int_{t_0}^t dt' \langle n_0 | [\hat{A}(t), \hat{\beta}(t')] | n_0 \rangle F(t') \tag{2.113}$$

Since the initial state Hamiltonian $\hat{H}_0$ is time-independent, we can replace the commutator $[\hat{A}(t), \hat{\beta}(t)]$ with $[\hat{A}(t - t'), \hat{\beta}]$. Similar to Eqn.(5.10), we now define the retarded response function as-

$$\chi_{A\beta}(t - t') = -i\theta(t - t') \sum_n \langle n_0 | [\hat{A}(t - t'), \beta] | n_0 \rangle \tag{2.114}$$

Where the word 'retarded' indicates that the response at time t is due to a potential at an earlier time $t' \le t$. The linear response $A_1(t)$ is therefore given by-

$$A_1(t) = \int_{-\infty}^{\infty} dt' \chi_{A\beta}(t - t') F(t') \tag{2.115}$$

where we are allowed to replace the lower integration limit t_0 by $-\infty$, since the external field $F(t)$ is zero for all times before t_0.

Next we define the density density response. Here the external perturbation is a scaler potential $v_1(\mathbf{r}, t)$ which is switched on at t_0 and couples to the density operator as :

$$\hat{H}_1'(t) = \int d^3r' v_1(\mathbf{r}, t) \hat{n}(\mathbf{r}') \tag{2.116}$$

Using the Eqn.(2.109) and Eqn.(5.10), we can write linear response of the density as:

$$n_1(\mathbf{r}, t) = \int_{-\infty}^{\infty} dt' \int d^3r' \chi_{nn}(\mathbf{r}, \mathbf{r}', t - t') v_1(\mathbf{r}', t') \tag{2.117}$$

comparing the Eqn.(2.117) with Eqn.(2.114), we get $\hat{A}_I(t - t') = \hat{n}_I(\mathbf{r}, t - t')$ and $\hat{\beta} = \hat{n}(\mathbf{r}')$, implying a density-density response function as:

$$\chi_{nn}(\mathbf{r}, \mathbf{r}'; t - t') = -i\theta(t - t') \sum_n \langle n_0 | [\hat{n}_I(\mathbf{r}, t - t'), \hat{n}(\mathbf{r}')] | n_0 \rangle \tag{2.118}$$

2.9.2 Frequency-dependent response

We define the Fourier transform of the perturbing field as-

$$F(t) = \int_{-\infty}^{\infty} \frac{d\omega}{2\pi} F(\omega) e^{-i\omega t} \tag{2.119}$$

and

$$F(\omega) = \int_{-\infty}^{\infty} dt F(t) e^{i\omega t} \tag{2.120}$$

Inserting the Eqn.(2.120) into Eqn.(2.115)

$$
\begin{aligned}
\int_{-\infty}^{\infty} \frac{d\omega}{2\pi} A_1(\omega) e^{-i\omega t} &= \int_{-\infty}^{\infty} dt' \int_{-\infty}^{\infty} \frac{d\omega}{2\pi} \chi_{A\beta}(\omega) e^{-i\omega(t-t')} \int_{-\infty}^{\infty} \frac{d\omega'}{2\pi} F(\omega') e^{-i\omega' t'} \\
&= \int_{-\infty}^{\infty} dt' \int_{-\infty}^{\infty} \frac{d\omega}{2\pi} \int_{-\infty}^{\infty} \frac{d\omega'}{2\pi} \chi_{A\beta}(\omega) e^{-it'(\omega-\omega')} F(\omega') e^{-i\omega t} \\
&= \int_{-\infty}^{\infty} \frac{d\omega}{2\pi} \chi_{A\beta}(\omega) e^{-i\omega t} \int_{-\infty}^{\infty} F(\omega') \frac{d\omega'}{2\pi} \int_{-\infty}^{\infty} dt' e^{-it'(\omega-\omega')} \\
&= \int_{-\infty}^{\infty} \frac{d\omega}{2\pi} \chi_{A\beta}(\omega) e^{-i\omega t} \int_{-\infty}^{\infty} F(\omega') d\omega' \delta(\omega - \omega') \\
&= \int_{-\infty}^{\infty} \frac{d\omega}{2\pi} \chi_{A\beta}(\omega) e^{-i\omega t} F(\omega) \tag{2.121}
\end{aligned}
$$

Finally,

$$\int_{-\infty}^{\infty} \frac{d\omega}{2\pi} A_1(\omega) e^{-i\omega t} = \int_{-\infty}^{\infty} \frac{d\omega}{2\pi} \chi_{A\beta} e^{-i\omega t} F(\omega) \tag{2.122}$$

Since all exponential term are linearly independent, the Eqn.(2.122) becomes:

$$A_1(\omega) = \chi_{A\beta}(\omega)F(\omega) \tag{2.123}$$

Next, we define the response function in omega space. We take the Fourier transform of Eqn.(2.114)

$$\int_{-\infty}^{\infty} d\tau \chi_{A\beta}(\tau)e^{i\omega\tau} = -i\sum_{n}\int_{-\infty}^{\infty} d\tau \theta(\tau)\langle n_0|[\hat{A}(\tau),\hat{\beta}]|n_0\rangle e^{i\omega\tau} \tag{2.124}$$

where $\tau = t - t'$. Then,

$$
\begin{aligned}
\chi_{A\beta}(\omega) &= -i\sum_{n}\int_{-\infty}^{\infty} d\tau \theta(\tau)\langle n_0|[\hat{A}_I(\tau),\beta]|n_0\rangle e^{i\omega\tau} \\
&= -i\sum_{n}\int_{-\infty}^{\infty} d\tau \theta(\tau)\langle n_0|\left[\hat{A}_I(\tau)\beta - \beta\hat{A}(\tau)\right]|n_0\rangle e^{i\omega\tau} \tag{2.125}
\end{aligned}
$$

Using the completeness relation $\sum_{n=0}^{\infty}|n_0\rangle\langle n_0| = 1$ in Eqn.(2.125)

$$\chi_{A\beta}(\omega) = -i\sum_{n=1}^{\infty}\sum_{l=1}^{\infty}\int_{-\infty}^{\infty} d\tau \theta(\tau)e^{i\omega\tau}\left\{\langle n_0|\hat{A}_I(\tau)|l_0\rangle\langle l_0|\hat{\beta}|n_0\rangle - \langle n_0|\hat{\beta}|l_0\rangle\langle l_0|\hat{A}_I(\tau)|n_0\rangle\right\} \tag{2.126}$$

Now putting the value of $\hat{A}(\tau)$ from the interaction picture $[\hat{A}_I(\tau) = e^{iH_0\tau}\hat{A}_S e^{-iH_0\tau}]$ into Eqn.(2.126)

$$
\begin{aligned}
\chi_{A\beta}(\omega) &= -i\sum_{n=0}^{\infty}\sum_{l=1}^{\infty}\int_{-\infty}^{\infty} d\tau \theta(\tau)e^{i\omega\tau} \times \\
&\quad \left\{\langle n_0|e^{iH_0\tau}\hat{A}e^{-iH_0\tau}|l_0\rangle\langle l_0|\hat{\beta}|n_0\rangle - \langle n_0|\hat{\beta}|l_0\rangle\langle l_0|e^{iH_0\tau}\hat{A}e^{-iH_0}|n_0\rangle\right\} \\
&= -i\sum_{n=0}^{\infty}\sum_{l=1}^{\infty}\int_{-\infty}^{\infty} d\tau \theta(\tau)e^{i\omega\tau}\left\{\langle n_0|\hat{A}|l_0\rangle\langle l_0|\hat{\beta}|n_0\rangle e^{-i\Omega_{nl}\tau} - \langle n_0|\hat{\beta}|l_0\rangle\langle l_0|\hat{A}(\tau)|n_0\rangle e^{i\Omega_{nl}\tau}\right\} \tag{2.127}
\end{aligned}
$$

where $\Omega_{nl} = E_n - E_l$ is the excitation energy.

Next we use the integral representation of the step function :

$$\theta(\tau) = \lim_{n \to 0^+} \frac{i}{2\pi} \int_{-\infty}^{\infty} d\omega' \frac{e^{-i\omega'\tau}}{\omega' + i\eta} \tag{2.128}$$

Using Eqn.(2.128) into Eqn.(2.9.2) :

$$
\begin{aligned}
\chi_{A\beta}(\omega) &= -i \lim_{n \to 0^+} \frac{i}{2\pi} \sum_{n=1}^{\infty} \sum_{l=1}^{\infty} \int_{-\infty}^{\infty} d\tau \int_{-\infty}^{\infty} d\omega' \frac{e^{-i\omega'\tau}}{\omega' + i\eta} \\
&\quad \left\{ e^{i\omega\tau} \langle n_0|\hat{A}|l_0\rangle \langle l_0|\hat{\beta}|n_0\rangle e^{-i\Omega_{nl}\tau} - \langle n_0|\hat{\beta}|l_0\rangle \langle l_0|\hat{A}|n_0\rangle e^{i\Omega_{nl}\tau} \right\} \\
&= \lim_{n \to 0^+} \sum_{n=1}^{\infty} \sum_{l=1}^{\infty} \frac{1}{2\pi} \int_{-\infty}^{\infty} \frac{d\omega}{\omega' + i\eta} \int_{-\infty}^{\infty} e^{i(\omega - \omega' - \Omega_n)\tau} d\tau \langle n_0|\hat{A}|l_0\rangle \langle l_0|\hat{\beta}|n_0\rangle \\
&\quad - \lim_{n \to 0^+} \sum_{n=1}^{\infty} \sum_{l=1}^{\infty} \frac{1}{2\pi} \int_{-\infty}^{\infty} \frac{d\omega}{\omega' + i\eta} \int_{-\infty}^{\infty} e^{i(\omega - \omega' + \Omega_n)\tau} d\tau \langle n_0|\hat{\beta}|l_0\rangle \langle l_0|\hat{A}|n_0\rangle \\
&= \lim_{n \to 0^+} \sum_{n=1}^{\infty} \sum_{l=1}^{\infty} \left\{ \int_{\infty}^{\infty} \frac{1}{2\pi} \frac{d\omega}{\omega' + i\eta} 2\pi\delta(\omega - \omega' - \Omega_n) - \int_{\infty}^{\infty} \frac{1}{2\pi} \frac{d\omega}{\omega' + i\eta} 2\pi\delta(\omega - \omega' + \Omega_n) \right\}
\end{aligned}
\tag{2.129}
$$

Finally:

$$\chi_{A\beta}(\omega) = \lim_{n \to 0^+} \sum_{n=1}^{occu} \sum_{l=1}^{\infty} \left\{ \frac{\langle n_0|\hat{A}|l_0\rangle \langle l_0|\hat{\beta}|n_0\rangle}{\omega - \Omega_{nl} + i\eta} - \frac{\langle n_0|\hat{\beta}|l_0\rangle \langle l_0|\hat{A}|n_0\rangle}{\omega + \Omega_{nl} + i\eta} \right\} \tag{2.130}$$

Eqn.(2.130) is called the Lehmann representation of the linear response function which show how a frequency dependent perturbation couples to the excitation spectrum of a system.

Similarly the frequency-dependent density response [Eqn.(2.117)] is given by

$$n_1(\mathbf{r}, \omega) = \int d^3 r' \chi_{nn}(\mathbf{r}, \mathbf{r}', \omega) v_1(\mathbf{r}', \omega) \tag{2.131}$$

Corresponding Lehmann representation of the density density response function

[Eqn.(2.118)] is

$$\chi_{nn}(\mathbf{r}, \mathbf{r}'\omega) = \sum_{n=1}^{occu} \sum_{l=1}^{\infty} \left\{ \frac{\langle n_0|\hat{n}(\mathbf{r})|l_0\rangle\langle l_0|\hat{n}(\mathbf{r}')|n_0\rangle}{\omega - \Omega_{nl} + i\eta} - \frac{\langle n_0|\hat{n}(\mathbf{r}')|l_0\rangle\langle l_0|\hat{n}(\mathbf{r})|n_0\rangle}{\omega + \Omega_{nl} + i\eta} \right\}$$

$$(2.132)$$

Noting that $\hat{n}(\mathbf{r}) = |\mathbf{r}\rangle\langle\mathbf{r}|$ we therefore have

$$
\begin{aligned}
\chi_{nn}(\mathbf{r}, \mathbf{r}'\omega) &= \sum_{n=1}^{occu} \sum_{l=1}^{\infty} \left\{ \frac{n_0^*(\mathbf{r})l_0(\mathbf{r})l_0^*(\mathbf{r}')n_0(\mathbf{r}')}{\omega - \Omega_{nl} + i\eta} - \frac{n_0^*(\mathbf{r}')l_0(\mathbf{r}')l_0^*(\mathbf{r})n_0(\mathbf{r})}{\omega + \Omega_{nl} + i\eta} \right\} \\
&= \sum_{n=1}^{\infty} \sum_{l=1}^{\infty} (f_{n_0} - f_{l_0}) \frac{n_0^*(\mathbf{r})l_0(\mathbf{r})l_0^*(\mathbf{r}')n_0(\mathbf{r}')}{\omega - \Omega_{nl} + i\eta}
\end{aligned}
$$

$$(2.133)$$

obtained by swapping the index of the second term.

2.9.3   The Runge-Gross theorem in linear response

So far our discussion has been exclusively within the independent particle approximation, wherein the effect of electric field on the charge density and thereby the electronic structure has not been considered self consistently. To address this shortcoming, it turns out that the correspondence of the ground state charge density and the external potential which is central to density functional theory is also valid if the external potential is time dependent.

We consider time dependent external potential of the form-

$$v(\mathbf{r}, t) = v_0(\mathbf{r}) + v_1(\mathbf{r}, t)\theta(t - t_0) \tag{2.134}$$

That is the system is in its ground state before t_0 and $v_1(\mathbf{r}, t)$ is the small time dependent perturbation which is switched on at t_0

The initial many-body ground state is uniquely determined by the Hohenberg-Kohn theorem of static DFT. But for time dependent potential we use the Runge-Gross theorem.

According to Runge-Gross theorem, there exists a unique one-to-one correspondence between $v(\mathbf{r}, t)$ and the time-dependent density $n(\mathbf{r}, t)$.

This means that we can formally write the time-dependent density as a function of external potential with out any dependence on the initial many-body state.

$$n(\mathbf{r}, t) = n[v](\mathbf{r}, t) \tag{2.135}$$

We expand the density response in powers of the perturbation v_1:

$$n(\mathbf{r}, t) - n_0(\mathbf{r}) = n_1(\mathbf{r}, t) + n_2((\mathbf{r}, t) + n_3(\mathbf{r}, t) + \text{...............} \tag{2.136}$$

The first order density response is given by

$$n_1(\mathbf{r}, t) = \int dt^{'} \int d^3 r^{'} \chi(\mathbf{r}, t, \mathbf{r}^{'}, t^{'}) v_1(\mathbf{r}^{'}, t^{'}) \tag{2.137}$$

We define the density-density response function of the many body system :

$$\chi(\mathbf{r}, t, \mathbf{r}^{'}, t^{'}) = \frac{\delta n[v](\mathbf{r}, t)}{\delta v(\mathbf{r}^{'}, t^{'})} \tag{2.138}$$

This equation shows that the linear response function is a function of the ground state density only.

The one to one correspondence between time dependent densities and potentials implies that one should also be able to calculate the perturbing potential from the linear density response as :

$$v_1(\mathbf{r}, t) = \int dt^{'} \int d^3 r^{'} \chi^{-1}(\mathbf{r}, t, \mathbf{r}^{'}, t^{'}) n_1(\mathbf{r}^{'}, t^{'}) \tag{2.139}$$

where χ^{-1} is the inverse response function, whose existence is indeed guaranteed by the Runge-Gross theorem.

2.9.4 Linear response of the Kohn-Sham system

The time dependent $n(\mathbf{r}, t)$ corresponding to the external potential

$$v(\mathbf{r}, t) = v_0(\mathbf{r}) + v_1(\mathbf{r}, t)\theta(t - t_0) \tag{2.140}$$

can also be reproduced in a noninteracting, time dependent Kohn-Sham system with the effective potential

$$v_s[n](\mathbf{r}, t) = v(\mathbf{r}, t) + \int d^3 r' \frac{n(\mathbf{r}', t)}{\mathbf{r} - \mathbf{r}'} + v_{xc}[n](\mathbf{r}, t) \tag{2.141}$$

Then we can express the time dependent density as a function of the Kohn-Sham potential as :

$$n(\mathbf{r}, t) = n[v_s(\mathbf{r}, t)] \tag{2.142}$$

Within the linear response the first order correction to density [Eqn.(2.142)] can be obtained from the first order correction to the v_s as:

$$n_1(\mathbf{r}, t) = \int dt' \int d^3 r' \chi_s(\mathbf{r}, t, \mathbf{r}', t') v_{s1}(\mathbf{r}', t') \tag{2.143}$$

where

$$\chi_s(\mathbf{r}, t, \mathbf{r}', t) = \left. \frac{\delta n[v_s](\mathbf{r}, t)}{\delta v_s(\mathbf{r}', t')} \right|_{v_s[n_0](\mathbf{r})} \tag{2.144}$$

is the non-interaction Kohn-Sham particle density-density response and the first order correction to the effective potential is

$$v_{s1}[n](\mathbf{r}, t) = v_1(\mathbf{r}, t) + \int d^3 r' \frac{n_1(\mathbf{r}', t)}{|\mathbf{r} - \mathbf{r}'|} + v_{xc1}(\mathbf{r}, t) \tag{2.145}$$

The first two term represent the external perturbation and the linearized [first order correction] time dependent Hartree potential. The last term is the linearized XC

potential, which is obtained by functional Taylor expression.

$$v_{xc1}(\mathbf{r}, t) = \int dt' \int d^3r' \frac{\delta v_{xc}[n](\mathbf{r}, t)}{\delta n(\mathbf{r}', t')}\bigg)\bigg|_{n_0(\mathbf{r})} n_1(\mathbf{r}'t') \tag{2.146}$$

where $\frac{\delta v_{xc}[n](\mathbf{r},t)}{\delta n(\mathbf{r}',t')}\big|_{n_0(\mathbf{r})}$ is the XC kernel, which is a functional of the ground state density.

The XC kernel is the key quantity of TDDFT in the linear response regime. We substitute v_{s1} in Eqn.(2.143) by Eqn.(2.145):

$$
\begin{aligned}
n_1(\mathbf{r}, t) &= \int dt' \int d^3r' \chi_s(\mathbf{r}, t, \mathbf{r}', t') \left[v_1(\mathbf{r}', t') + \int d^3r' \frac{n_1(\mathbf{r}', t')}{|\mathbf{r} - \mathbf{r}'|} + v_{xc1}(\mathbf{r}', t') \right] \\
&= \int dt' \int d^3r' \chi_s(\mathbf{r}, t, \mathbf{r}', t') \left[v_1(\mathbf{r}', t') + \int d\tau \int d^3x \left\{ \frac{\delta(t - \tau')}{|\mathbf{r}' - \mathbf{x}|} \right.\right. \\
&\quad \left.\left. + f_{xc}(\mathbf{r}', t', \mathbf{x}, \tau) \right\} n_1(\mathbf{x}, \tau) \right]
\end{aligned}
\tag{2.147}
$$

For interacting system we define a net interacting response function χ as :

$$n_1(\mathbf{r}, t) = \int dt' \int d^3r' \chi(\mathbf{r}, t, \mathbf{r}', t') v_1(\mathbf{r}', t') \tag{2.148}$$

Next we can establish a relation between the interacting and noninteracting response function by inserting the Eqn.(2.148) into Eqn.(2.147):

$$
\begin{aligned}
\int dt' \int d^3r' \chi(\mathbf{r}, t, \mathbf{r}', t') v_1(\mathbf{r}', t') &= \int dt' \int d^3r' \chi_s(\mathbf{r}, t, \mathbf{r}', t') \\
&\quad \left[v_1(\mathbf{r}', t') + \int d\tau \int d^3x \left\{ \frac{\delta(t - \tau')}{|\mathbf{r}' - \mathbf{x}|} + f_{xc}(\mathbf{r}', t', \mathbf{x}, \tau) \right\} \times \right. \\
&\quad \left. \int d\tau' \int dx' \chi(\mathbf{x}, \tau, \mathbf{x}', \tau') v_1(\mathbf{x}', \tau') \right]
\end{aligned}
\tag{2.149}
$$

Since Hartree and XC integral kernels are the ground state properties of the system and independent on the perturbation, the Eqn.(2.149) becomes :

$$
\begin{aligned}
\chi(\mathbf{r}, t, \mathbf{r}', t') &= \chi_s(\mathbf{r}, t, \mathbf{r}', t') + \\
&\int d\tau \int d^3r \int d\tau' \int d^3x' \chi_s(\mathbf{r}, t, \mathbf{x}, \tau) \Big\{ \frac{\delta(\tau - \tau')}{|\mathbf{x} - \mathbf{x}'|} \\
&+ f_{xc}(\mathbf{x}, \tau, \mathbf{x}', \tau') \Big\} \chi(\mathbf{x}, \tau, \mathbf{x}', \tau') v_1(\mathbf{r}', t')
\end{aligned}
\tag{2.150}
$$

Eqn.(2.150) known as Dyson equations to be solved self-consistently.

In standard TDDFT implementation the Dyson equation is converged in the frequency domain where the noninteracting frequency dependent density-density response function derived above in Eqn(2.133) can be used as the initial noninteracting χ_s

2.9.5 Spectroscopic observables

Using the density-density response function we can calculate the spectroscopic observables of a system. We start by defining the dipole polarizability within linear response in the presence of an external electric field $E_j(t) = E_0 \sin(\omega t)$, applied along j-direction as :

$$
p_i(t) = \int_0^t dt' \sum_j \alpha_{ij}(t - t') E_j(t')
\tag{2.151}
$$

Fourier transform of which is

$$
p_i(\omega) = \sum_j \alpha_{ij}(\omega) E_j(\omega).
\tag{2.152}
$$

where $\underline{\underline{\alpha}}(\omega)$ is the dynamic polarizability tensor.

The z-component of the dipole polarizability is

$$
p_{1z}(t) = - \int d^3r\, z n_1(\mathbf{r}, t).
\tag{2.153}
$$

In Eqn.(2.153), the negative sign accounts for the negative sign of the change density. The dynamic dipole polarizability tensor :

$$\alpha_{zz}(\omega) = -\frac{2}{E_0} \int d^3r z n_1(\mathbf{r}, \omega) \qquad (2.154)$$

where $E_j(\omega) = \frac{1}{2}E_0$

Putting Eqn.(2.131) into Eqn.(5.2), we get

$$\alpha_{zz}(\omega) = -\int d^3r \int d^3r' z z' \chi_{nn}(\mathbf{r}, \mathbf{r}', \omega) \qquad (2.155)$$

where χ_{nn} is the dynamic dielectric susceptibility obtained as the density-density (nn) response function in Eqn.(2.132). According to the fermi's Golden Rule formula, the photo absorption cross-section-

$$\sigma_{zz}(\omega) = \frac{4\pi\omega}{c}\Im\alpha_{zz}(\omega) \qquad (2.156)$$

So the primary computation involve calculation of dielectric response function χ_{nn} in-terms of the available description of the electronic structure.

2.10 Description of optical properties using Bethe-Salpeter Equation (BSE)

In section 2.7, we have introduced the single-particle Green's function, which describe the motion of a single particle or hole in an N particle system in the ground state. Optical excitation involve creation of an electron in the conduction band and hole in the valence band which interact through coulomb attraction screened by other charge particles. An electron-hole pair thus essentially constitute the two particle bound system. Motion of such a system is thus described by the two particle Green's function. Starting with the simplest approximation for a two particle

correlation function for an non-interacting electron-hole pair as:

$$L_0(12;1^{'}2^{'}) = G_1(1,2^{'})G_1(2,1^{'}) \tag{2.157}$$

where the electron and the hole are represented by one particle Green function, the correlation function L in the presence of electron-hole interaction kernel K can be written as:

$$L(12;1^{'}2^{'}) = L_0(12;1^{'}2^{'}) + \int d(3456)L_0(14;1^{'}3)K(35;46)L(62;52^{'}) \tag{2.158}$$

which is a form of the Bathe-salpeter equation[64] used to describe bound two particle system. The electron-hole interaction kernel K is given by the functional derivative

$$K(35;46) = \frac{\delta[V_{Coul}(3)\delta(3,4) + \Sigma(3,4)]}{\delta G_1(6,5)} \tag{2.159}$$

where Σ is self-energy operator discuss in section 2.7 in GW approximation. L can be constructed using electron-hole amplitude of form

$$\Phi(\mathbf{x},\mathbf{x}^{'}) = \sum_{v}^{occu} \sum_{c}^{empty} A_{vc}\psi_c(\mathbf{x})\psi_v^{\star}(\mathbf{x}^{'}) + B_{vc}\psi_v(\mathbf{x})\psi_c^{\star}(\mathbf{x}^{'}), \tag{2.160}$$

which results into two set of identical eigenvalue problems for the co-efficient A_{vc} and B_{vc}. For isolated system like molecules and cluster, considering only the dominant diagonal contributions, Eqn.(2.158) further results into an eigenvalue problem of form:

$$(E_c - E_v)A_{cv} + \sum_{c^{'}v^{'}}(K_{cv,c^{'}v^{'}}^x + K_{cv,c^{'}v^{'}}^d)A_{c^{'}v^{'}} = \Omega A_{cv} \tag{2.161}$$

where the e-h bare exchange :

$$K_{cv,c^{'}v^{'}}^x = \int dr \int dr^{'} \psi_{v^{'}}^{\star}(\mathbf{r})\psi_c^{\star}(\mathbf{r}^{'})v(\mathbf{r},\mathbf{r}^{'})\psi_v(\mathbf{r}^{'})\psi_{c^{'}}(\mathbf{r}) \tag{2.162}$$

screened direct :

$$K^d_{cv,c'v'} = - \int dr \int dr' \, \psi_v(\mathbf{r}')\psi_c^\star(\mathbf{r})W(\mathbf{r},\mathbf{r}')\psi_{v'}^\star(\mathbf{r}')\psi_{c'}(\mathbf{r}) \tag{2.163}$$

The eigenvalues of Eqn.(2.161) thus render the excitation energies Ω. The co-efficient A_{vc} can also be used to construct the dielectric function whose imaginary part renders the optical absorption cross-section. However computationally the BSE based approach is expensive on two counts: (1) convergence of the interaction kernel with respect to screening in Eqn.(2.163), and (2) convergence of the Ω with respect to the states in conduction band (ψ_c) consider in electron-hole amplitude.

2.11   Real-time dynamics approach

In this approach the interaction of matter is studied in real time using the time dependent Schrödinger equation.

$$i\hbar\frac{\partial\Psi}{\partial t} = H\Psi \tag{2.164}$$

whose solution is

$$\Psi(t) = U(t,0)\Psi(0) = T\exp\left(-i\int_0^t H(t')dt'\right)\Psi(0) \tag{2.165}$$

where T is the time ordering operator. The most elementary solution is obtained by breaking the total evolution operator into evolution operators of small time durations

$$U(t,0) \simeq \prod_{n=0}^{N-1} U((n+1)\triangle t, n\triangle t) \tag{2.166}$$

where $\triangle t = T_{tot}/N$ and

$$U(t+\triangle t, t) = \exp[-iH(t)\triangle t] \tag{2.167}$$

T_{tot} is the total time for which we allow the system to evolve. But in this method the operator itself is not unitary. Therefore wave functions do not remain orthonormal after evolution over a long time. This problem is solved by introducing a unitary approximate form of time evolution operator discussed in the next section .

2.11.1 Cranck-Nicolson scheme

Time dependent Schrödinger equation can be discretized using finite difference approach in two ways. Using the forward time centered space (FTCS) scheme where the wave function at any point in space at time $t + \Delta t$ is computed based on hamiltonian operating on wave function at time t :

$$i\hbar \frac{\Psi_j^{n+1} - \Psi_j^n}{\delta t} = -\frac{\hbar^2}{2m} \frac{\Psi_{j+1}^n + \Psi_{j-1}^n - 2\Psi_j^n}{\delta_{x^2}} + V_j \Psi_j^n \qquad (2.168)$$

where the superscript {n} represent the time index and the subscript {j} represent the space index, implying

$$\Psi_j^{n+1} = \Psi_j^n - \frac{i\delta t}{\hbar} \Big[-\frac{\hbar^2}{2m} \frac{\Psi_{j+1}^n + \Psi_{j-1}^n - 2\Psi_j^n}{\delta_{x^2}} + V_j \Psi_j^n \Big]. \qquad (2.169)$$

which in a compact form implies

$$\Psi^{n+1} - \Big(I - \frac{i\delta_t}{\hbar} H\Big)\Psi^n = 0 \qquad (2.170)$$

where the H is written as a matrix in the finite difference scheme as per Eqn.(2.169). In the Backward Time Space centered scheme (BTCS) where the wave function at any point in space at time t is computed based on hamiltonian operating on the wave function at time $t + \Delta t$ as :

$$i\hbar \frac{\Psi_j^{n+1} - \Psi_j^n}{\delta t} = -\frac{\hbar^2}{2m} \frac{\Psi_{j+1}^{n+1} + \Psi_{j-1}^{n+1} - 2\Psi_j^{n+1}}{\delta_{x^2}} + V_j \Psi_j^{n+1} \qquad (2.171)$$

implying

$$\Psi_j^{n+1} + \frac{i\delta t}{\hbar}\Big[-\frac{\hbar^2}{2m}\frac{\Psi_{j+1}^{n+1} + \Psi_{j-1}^{n+1} - 2\Psi_j^{n+1}}{\delta_{x^2}} + V_j\Psi_j^{n+1}\Big] = \Psi_j^n \tag{2.172}$$

which further implies

$$\Big(I + \frac{i\delta_t}{\hbar}H\Big)\Psi^{n+1} - \Psi^n = 0 \tag{2.173}$$

In the Symmetric Time Space centered Cranck-Nicolson scheme the averages of the FTCS and BTCS schemes is made by adding Eqn.(2.170) and Eqn.(2.173) as :

$$\Big[\Psi^{n+1} - \Big(I - \frac{i\delta_t}{\hbar}H\Big)\Psi^n - \Psi^n + \Big(I + \frac{i\delta_t}{\hbar}H\Big)\Psi^{n+1}\Big] = 0 \tag{2.174}$$

which implies

$$\Psi^{n+1} = \frac{\Big(I - \frac{i\delta_t}{2\hbar}H\Big)}{\Big(I + \frac{i\delta_t}{2\hbar}H\Big)}\Psi^n \tag{2.175}$$

We can increase the stability of the solution if we include more terms in the expansion of the derivatives both in numerator and denominator :

$$\Psi^{n+1} = \frac{\Big(I - \frac{i\delta_t}{2\hbar}H - 1/2(H\delta t/2)^2 + i1/6(H\delta t/2)^3\Big)}{\Big(I + \frac{i\delta_t}{2\hbar}H - 1/2(H\delta t/2)^2 - i1/2(H\delta t/2)^3\Big)}\Psi^n \tag{2.176}$$

This method is unitary, strictly preserving the orthonormality of the states for the an arbitrary time evolution. For time-independent Hamiltonians it is also explicitly time reversal invariant and exactly conserves energy. In practice , with a suitable choice of Δt, the energy is satisfactorily conserved even when the Hamiltonian changes with time. The method is stable when $\Delta E\Delta T \ll 1$.

2.11.2   Calculation of the polarizabilities

In a part of this thesis work we have adopted the Cranck-Nicolson scheme to study the response of finite systems to a pulsed electric field of form

$$v_1(\vec{r}, t) = A\delta(t - t_0)z \tag{2.177}$$

The dipole-moment is calculated as :

$$d_z(t) = \sum_{n_{occ}} \int |\Psi_n(\vec{r}, t)|^2 z d^3 r \tag{2.178}$$

For finite system, the dipole polarizability α_{zz} for a particular ω can be defined as the ratio between the induced dipole-moment $d_z(t)$ and the applied external electric field $E_z(t)$ of form $E_z(t) = E_0 e^{-i\omega t}$. Therefore for an arbitrary time dependence of $E_z(t)$ and the consequent $d_z(t)$, their ω component should be related by the dipole polarizability $\alpha_{zz}(\omega)$ as :

$$\int_0^\infty dt e^{i\omega t} d_z(t) = \alpha_{zz}(\omega) \int_0^\infty dt e^{i\omega t} E_z(t) \tag{2.179}$$

implying

$$\alpha_{zz}(\omega) = \frac{1}{\tilde{E}_z(\omega)} \int_0^\infty dt e^{i\omega t} d_z(t) \tag{2.180}$$

where $\tilde{E}_z(\omega) = \int dt e^{i\omega t} E_z(t)$ is the Fourier transform of $E_z(t)$ for frequency ω.

Since we chose an impulsive external potential [Eqn.(2.177)], which includes all the frequency component uniformly, implying a frequency independent Fourier transform, we can obtain the polarizability for the whole spectral region from a single time evolution as:

$$\alpha_{zz}(\omega) = -\frac{e^2}{A} \int_0^\infty dt e^{i\omega t} d_z(t). \tag{2.181}$$

In my work the time evaluation has been performed in the tight-binding basis described in the first part of this thesis.

Chapter 3

Hybrid atomic orbital basis from first principles: Bottom-up mapping of self-energy correction to large covalent systems

In this chapter the key outcome is a numerical scheme to construct degenerate hybrid atomic Wannier orbital basis from first principles which are naturally oriented towards direction of coordination in systems with ideal bond angle. In chapter 4 we have generalized the construction for non-ideal bond angles. I have contributed jointly with another colleague in developing and testing the methodology described in this chapter. I will first reproduce the methodological part and then focus on system which I worked on primarily. The proposed Wannier orbitals constitute a directed multi-orbital orthonormal basis. Beyond the construction of the directed basis, in this chapter I describe strategies to transfer of tight-binding parameters calculated in basis of the constructed orbitals in reference systems to larger isomorphic target systems through mapping of neighborhoods and projected Wannier charge centres. The proposed directed basis is demonstrated here to be promis-

ing of facilitating transfer of self-energy correction from smaller covalent systems to their larger variants with thousands of atoms. I will be using transferred self-energy corrected tight binding parameters in large nano-diamonds in chapter 5 where I propose a modified real time dynamic scheme in the directed basis towards inexpensive estimation of optical absorption threshold.

3.1   Introduction

Setting a minimal TB basis for a given systems of atoms calls for appropriate orientation of orbitals at each atomic site in accordance with their immediate atomic neighborhood, so that the nearest neighbor interactions can be represented by the least number of orbitals. In this direction, hybrid atomic orbitals have been used by quantum chemists since their introduction[65,66] almost a century ago. Rational approaches for their construction[67,68,69,70,71] over the last several decades have been primarily focussed on partitioning systems into substructures which are spanned by groups of hybrid orbitals, leading to unambiguous partitioning of electrons into bonding orbitals and lone-pairs, and further into atomic orbitals. For such partitioning, notionally similar several approaches[68,70,72,73,74,75] have been proposed grossly based on the maximum overlap condition which in effect leads to localization of orbitals within the chosen subspace of molecular orbitals. In these approaches, either the overlap matrix[68,70] or the first-order density matrices,[74,76] both of which are calculated typically in the basis of either the Slater type orbitals(STO)[77] or the Gaussian type orbitals(GTO),[78,79] are generally transformed into block diagonal forms each spanned by orbitals centered on nearest neighbor atoms. The resultant hybrid orbitals involving atomic orbitals centred on more than one atoms[71,80] render unambiguous bonding orbitals and bond-orders, while the ones like the *natural hybrid orbitals*(NHO),[76] the *effective atomic orbital*(EAO),[75] the *oriented quasi-atomic orbitals*,[81] or the ones constructed using the *maximal orbital analysis*[82] approach, attempts to describe the state of the orbitals of the atoms as they participate in bonds. Hybrid orbitals in the line of NHOs have been popularly constructed ab-initio at

the HF level.[83,84]

A more explicit approach[85,86] has been to construct the *generalized hybrid orbitals*(GHO) as combinations of STO with common Slater exponent and fixed position of nodes along bonds to assign their orientation. Expedient to clarify that in this paper we refer to bonds simply as the linear connectivity between atoms which are primarily nearest neighbors if not mentioned specifically. Much of these efforts were undertaken in aid to molecular mechanics calculation[87,88] where the description of interactions between sub-structures eases with use of orbitals which are directed along bonds. Effective analytical models for such interactions have also been developed[89] recently for inexpensive deductive computation of properties of bulk as well as clusters of sp^x hybridized covalent systems. Notably unlike the GHOs, the NHOs or the EAOs by construction may not be oriented exactly along the bonds. In general for all such hybrid orbitals, their directed nature, maximal localization and ortho-normality are not guaranteed simultaneously by construction. In a part of this work we explore simultaneity of these conditions in construction of hybrid atomic orbitals from first-principles proposed in this work.

Instead of overlap or density matrices, in this work we take recourse to the first moment matrices (FMM) due to their direct correspondence to localization. FMMs are known not to commute among each other in more than one dimension if projected on to a finite subspace of orthonormal states. We propose construction of hybrid atomic orbitals(HAO) as approximate eigenstates of the FMMs within a finite subspace of Kohn-Sham (KS) states of isolated atoms. Orientation and hybridization of the proposed orbitals can be a-priori naturalized as per their anticipated neighborhood. This substantially eases the effort of orientating them appropriately while transferring them from isolated atoms to the real systems, which eventually eases the interpretation of elements of the Hamiltonian. An orthonormal set of localized Wannier orbitals resembling the HAOs is further constructed in the basis of KS single particle states of the given system. These Wannier orbitals, which we refer in this paper as the *hybrid atomic Wannier orbitals* (HAWO), constitute a multi-orbital tight-binding (TB) basis locked to their immediate atomic neighborhood by

construction, and render hopping parameters involving effectively only two orbitals per bond. HAWOs thus offer easy transfer of the corresponding TB parameters to other iso-structural systems exclusively through mapping of neighborhoods and projection of charge centres learned from HAOs. Effective transfer of TB parameters is demonstrated in nano-ribbons of graphene and hexagonal boron-nitride, C_{60}, and nano-diamonds and their silicon based counterparts. In particular, we show in the HAWO basis that it is possible to effectively transfer self-energy(SE) correction(SEC) of single particle levels from smaller reference systems to much larger iso-structural systems through TB parameters with minimal additional computational expense through the proposed mapping of multi-orbital TB parameters beyond the nearest neighborhood.

3.2 Methodological details

3.2.1 Construction of hybrid orbitals

In a given direction, for example along $\hat{x}$, the most localized orbitals $\{\phi\}$ would diagonalize the corresponding FMM:

$$X_{ij} = \langle \phi_i \mid x \mid \phi_j \rangle. \tag{3.1}$$

This becomes clear by noting that the total spread of a finite set of N number of orbitals along $\hat{x}$ is given by:

$$\Omega_x = \sum_{i=1,N} \left[\langle \phi_i | x^2 | \phi_i \rangle - |\langle \phi_i | x | \phi_i \rangle|^2 \right], \tag{3.2}$$

which can be expressed as:

$$
\begin{aligned}
\Omega_x &= \sum_{i=1,N} \left(\sum_{j=1}^{\infty} X_{ij} X_{ji} - X_{ii} X_{ii} \right) \\
&= \sum_{i=1,N} \sum_{j \neq i}^{\infty} |X_{ij}|^2 \\
&= \sum_{i=1,N} \left(\sum_{j \neq i}^{N} |X_{ij}|^2 + \sum_{j=N+1}^{\infty} |X_{ij}|^2 \right).
\end{aligned}
\tag{3.3}
$$

Diagonalization of X in the $N \times N$ subspace would therefore sets the first term in Eqn.(4.2) to zero, leading to minimization of total spread. Notably, X can be calculated directly as in Eqn.(3.1) only for isolated systems well separated from their periodic images. For periodic system with non-zero crystal momentum, computation of X would essentially involve evaluation of geometric phases[90] of Bloch electrons evolved across the Brillouin Zone.[91,92] Nevertheless, there exists therefore a unique set of orbitals which completely diagonalize X, and would also thereby have maximum localization along $\hat{x}$. Similar unique sets exist for $\hat{y}$ and $\hat{z}$ directions as well. However, the matrices X, Y and Z, when projected into a finite subspace of orthonormal states, do not commute with each other in general unless mandated by symmetries. This implies that a unique set of orbitals with maximum localization simultaneously in all three orthogonal directions would not exist in general. The same is true for Wannier functions (WF) in case of periodic systems with non-zero wave-vectors. Numerically localized Wannier functions[93,94]therefore are not be unique and the choice of gauge used for their construction depends on the chosen criteria of localization.

We chose to look for the possibility to construct a set of localized orbitals which will be a reasonable compromise between the three unique sets of orbitals having maximum localization along the three orthogonal directions. We thus resorted to the condition of simultaneous approximate joint diagonalization[95] of the three FMMs: X, Y and Z. To compute such an approximate eigen sub-space of the three FMMs, we adopted an iterative scheme based on generalization of the Jacobi method of

56

Hybrid atomic orbital basis from first principles: Bottom-up mapping of self-energy correction to large covalent systems

matrix diagonalization,[96] wherein, off-diagonal elements are iteratively minimized by applying rotation of coordinates by an optimally chosen angle. The extension of the method to more than one square matrices irrespective of whether they are commuting or not, is based on a proposed[95] choice of angle of rotation leading to complex rotation matrix U which has been proven[95] to minimize the composite objective function defined as :

$$\text{off}(UXU^\dagger) + \text{off}(UYU^\dagger) + \text{off}(UZU^\dagger) \tag{3.4}$$

where $\text{off}(A) = \sum_{1 \leq i \neq j \geq N} |A_{ij}|^2$ for an $N \times N$ matrix A. N being the number of orthonormal states used to compute X, Y and Z. U is a product of all the $N(N-1)/2$ complex plane rotations, one each for each pairs of (ij) for $i \neq j$. For a given (ij) the plane rotation $R(i,j)$ is an $N \times N$ identity matrix except for:

$$\begin{pmatrix} r_{ii} & r_{ij} \\ r_{ji} & r_{jj} \end{pmatrix} = \begin{pmatrix} c & \overline{s} \\ -s & \overline{c} \end{pmatrix} \tag{3.5}$$

where $c, s \in C, |c|^2 + |s|^2 = 1$.

It has been shown[95] that the objective function defined in Eqn.(3.4) is minimized if U is a product of $R(i,j)$ matrices as shown in Eqn.(3.5) whose elements are given as:

$$c = \sqrt{\frac{x+r}{2r}}; s = \frac{y - iz}{\sqrt{2r(x+r)}} \tag{3.6}$$

where

$$r = \sqrt{x^2 + y^2 + z^2}$$

and $[x, y, z]^\dagger$ being the eigen-vector corresponding to the highest eigen-value of a

3×3 matrix:

$$G(i,j) = \quad \text{Real}\left(h^\dagger(X,i,j)h(X,i,j)\right)$$
$$+ \quad \text{Real}\left(h^\dagger(Y,i,j)h(Y,i,j)\right)$$
$$+ \quad \text{Real}\left(h^\dagger(Z,i,j)h(Z,i,j)\right)$$

with:

$$h(A,i,j) = [a_{ii} - a_{jj}, a_{ij} + a_{ji}, i(a_{ji} - a_{ij})]. \tag{3.7}$$

Notably, given the form of $R(i,j)$, for a rotated matrix $A' = R(i,j)AR^\dagger(i,j)$ corresponding to plane rotation for the (ij)-th pair of elements of A, it is easily seen that $a'_{kk} = a_{kk}$ for $k \neq i$ and $k \neq j$, leading to the invariance:

$$\text{off}(A') + |a'_{ii}|^2 + |a'_{jj}|^2 = \text{off}(A) + |a_{ii}|^2 + |a_{jj}|^2.$$

owing to preservation of norm in similarity transformation. Therefore, minimizing off(A') would naturally imply maximizing $|a'_{ii}|^2 + |a'_{jj}|^2$, which further implies maximizing $|a'_{ii} - a'_{jj}|^2$ since:

$$2\left(|a'_{ii}|^2 + |a'_{jj}|^2\right) = |a'_{ii} + a'_{jj}|^2 + |a'_{ii} - a'_{jj}|^2$$

and

$$a'_{ii} + a'_{jj} = a_{ii} + a_{jj}$$

owing to invariance of trace under similarity transformation. Therefore in our case the minimization of the objective function[Eqn.(3.4)] implies maximizing the separation between the charge centres of the i-th and the j-th orbitals, which is thus similar to the principle of the Foster and Boys[97] scheme of orbital localization. This becomes clear by rewriting the total spread [Eqn.(4.2)] for N orbital $\{\phi_i, i = 1, N\}$ as:

$$\Omega = \sum_{k=1,3} \sum_{i=1,N} \left(\sum_{j\neq i}^{N} |a_{ij}^k|^2 + \sum_{j=N+1}^{\infty} |a_{ij}^k|^2 \right) \tag{3.8}$$

where $A^{k=1,2,3} = X, Y, Z$. Eqn.(4.20) clearly suggests that minimization of the objective function in Eqn.(3.4) would minimizes the first term in Eqn.(4.20), leading to minimization of the total spread. Eqn.4.20 also suggests that the total spread will reduce with increasing number of states (N) in the basis of which the first moment matrices are constructed.

We test the proposed approach first with FMMs computed in the basis of GTOs constructed for Ti with parameters from Ref..[98] In Fig.3.1 we plot the charge centres($\langle \phi | \vec{r} | \phi \rangle$) of the approximate eigen states of the first moment matrices. Evi-

(a) $sp^3, d_{x^2-y^2}, d_{z^2}$ (b) $sp^3, d_{x^2-y^2}, d_{xy}$ (c) sp^3, d_{xy}, d_{xz} (d) sp^3, d_{z^2}, d_{xz}

(e) $sp^3, d_{x^2-y^2}, d_{z^2}, d_{xy}$ (f) $sp^3, d_{z^2}, d_{xy}, d_{zx}$ (g) $sp^3, d_{z^2}, d_{yz}, d_{zx}$

(h) $sp^3, d_{x^2-y^2}, d_{xy}, d_{yz}, d_{zx}$ (i) $sp^3, d_{z^2}, d_{xy}, d_{yz}, d_{zx}$ (j) $sp^3 d^5$
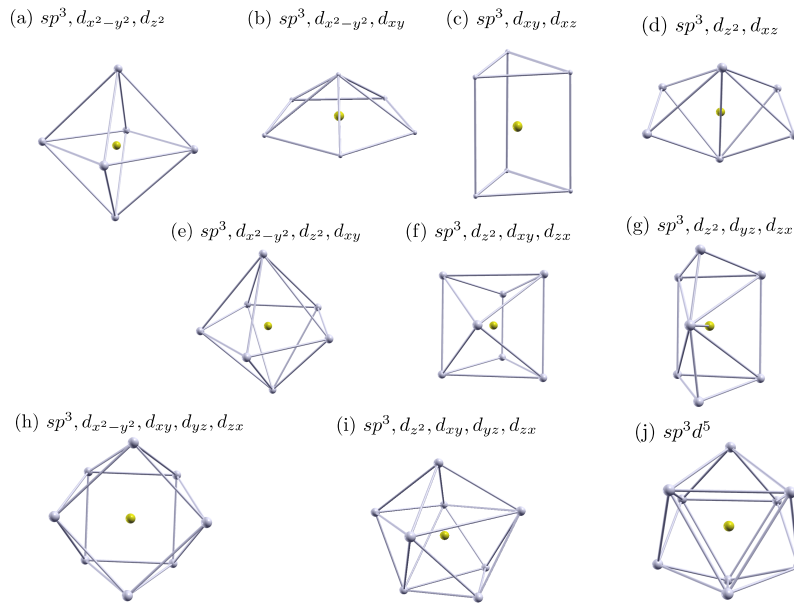
Figure 3.1: Plots of charge centres (shown in gray) of the hybrid orbitals formed by the group of GTOs representing $3s, 3p$ and $3d$ orbitals of Ti (shown in yellow) constructed as per Ref.[98] .

dently, the charge centres constitute coordination polyhedra around isolated atoms which are consistent in shape with those tabulated in Figs.6-8 in Ref..[99] This agreement confirms the identity of the resultant orbitals as the hybrid orbitals and numerically establishes the connection between maximal localization and hybridization. Such a connection between sp^3 hybridization and minimization of total quadratic spread of s and the three p orbitals has been analytically proven.[100] In this work however we do not use GTOs further and rather resort to KS states of isolated atoms. For example, for atoms of the p block, such as boron, carbon, nitrogen and silicon

dealt with in this work, if the first moment matrices are constructed in the basis
of three(four) KS states with lowest energies, namely, the one s like non-degenerate
having the lowest energy and two (three) of the three p like degenerate states above
the s like state, the approximate eigen-subspace would render three(four) $2sp^2(2sp^3)$
hybridized orbitals. Notably, for isolated systems like molecules, clusters and nano-
structures, the approximate common eigen spectrum of the FMMs computed within
the manifold of occupied KS states results into partitioning[101,102,103] of the ground
state charge density into bonding and localized orbitals.

3.2.1.1   Orientation and transfer of orbitals

Although as evident above that construction of HAOs for an isolated atom as such
do not require any pre-defined directionality, the orientation of the HAOs associated
with an atom can be nevertheless locked to their anticipated neighborhood by placing
the isolated atom within an external potential which represents the generic or exact
atomic neighborhood of the given atom in the actual system in which the HAOs
are to be used. We construct such externals potentials by placing weakly confining
spheres with small constant negative potentials inside the spheres in place of exact or
generic locations of neighboring atoms as present in the actual system. For example,
to lock sp^3 HAOs to a four coordinated tetrahedral neighborhood, a tetrahedra of
confining spheres is placed around the host C atom, leading to orientation of the
sp^3 orbitals maximally in the direction of the confining spheres as seen in Fig.3.5(a).
Typically we find confining potential amplitudes in the order of 0.01 eV and radius
0.5Åto be sufficient for the purpose. Such weak confinement in the vicinity causes
change of KS energy eigen-values of isolated atoms in the order of 0.001 eV, and
retains the shape of the lowest KS states which are used for construction of the
HAOs, effectively unaltered. For sp^3 HAOs, the tetrahedra of the confining spheres
can be an exact tetrahedra, as in case of bulk Si, or a strained tetrahedra, as in case
of cyclopropane. As evident in Fig.3.2(a) for cyclopropane, and in Fig.3.2(b-e) for
planar molecules C_nH_n, the projected charge center of the HAOs (shown in gray)
symmetrically deviate away from the C-C bonds with decreasing C-C-C angle as we

go from C_6H_6 to C_3H_3. For all of these molecules the HAOs were constructed with
the weakly confining spheres placed around the host C atom exactly as per their
nearest neighbors in the molecules, resulting into HAOs largely retaining their pure
sp^3 nature but oriented symmetrically about the directions of the confining spheres
from the host atoms. The placement of confining potential spheres thus provide a
gross directional reference for orientation of the full set of the HAOs.

Position of charge centres of the HAOs are learned in terms of the directions of the
confining spheres from the isolated host atom. Such learnings are subsequently used
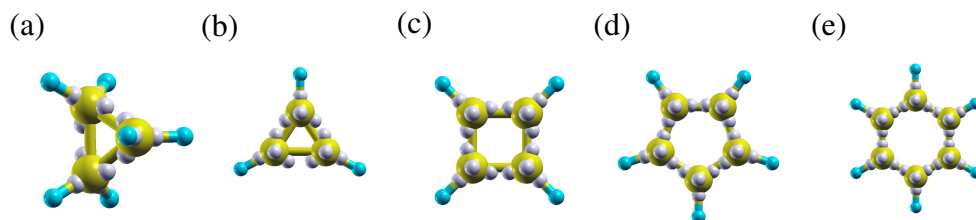
Figure 3.2: Projected charge centres of HAOs are shown by gray spheres depicting
their orientations around their host C atom shown in yellow.
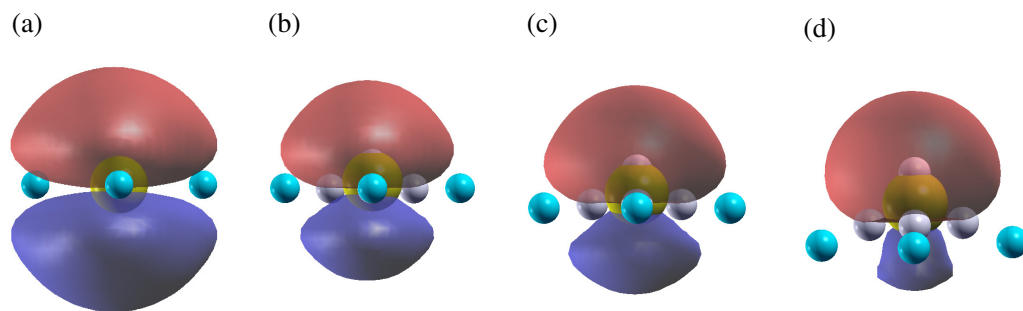
Figure 3.3: (a-d): Evolution of a pure $2p_z$ orbital[(a)] from sp^2 hybridization back-
ground, to an sp^3 hybridized orbital due to increased deviation of the centres (cyan
spheres) of the three confining potential spheres from co-planarity with the host
atom (yellow sphere). Centres of HAOs are shown by gray spheres.

in projecting centres of HAOs around the corresponding atom in a given system, as
seen for the molecules in Fig.3.2, and nano-diamonds in Fig.3.4. While transferring
HAOs from their nursery of isolated host atoms, to their matching host atoms in
a given system, HAOs are rotated such that their actual charge centres align along
the direction of their projected centers from the matching host atoms.

In addition to providing reference for orientation, the confining spheres can have an important role in deciding the level of hybridization of the HAOs. This becomes evident by noting that if we use four KS states and three confining sphere coplanar with the host atom, then instead of forming four sp^3 orbitals, the HAOs separate into three $2sp^2$ orbitals and one $2p_z$ orbital, as evident from the unhybridized shape of the $2p_z$ orbital in Fig.3.3(a). Fig.3.3(a-d) shows evolution of the $2p_z$ HAO from a pure orbital perpendicular to the plane of sp^2 hybridization, towards a $2sp^3$ hybridized orbital, with increasing non-coplanarity of the confining spheres with the host atom. HAOs with such intermediate hybridization ($2sp^{2+} + 2p_z^+$) has been used for C_{60}[Fig.5.7]. However, stronger confining potentials are found necessary to influence hybridization of KS states, typically in the order of 1eV for C atoms, such that the orbitals align along the confining spheres. The confining potentials in this case therefore does lead to minor modification of shape of the KS states, and thereby of the HAOs as well, although not quite obvious at the iso-surfaces plotted in Fig.3.3(a-d). However the values of TB parameters calculated in the basis of their Wannierized counterparts in C_{60} suggests that the overall shape of those orbitals are largely retained close to the sp^2 orbitals. Notably, we could have used stronger confinement to align the HAOs in C_3H_6, C_3H_3 or C_4H_4 as well like we did for C_{60}, but the degree of confinement would have to be much high than that used for C_{60}, which would have substantially altered the shape of the HAOs themselves, since it is obvious that with pure s, p_x, p_y, p_z orbitals it is impossible to form any set of hybrid orbitals in which two orbitals can have relative orientation less than 90°.

3.2.2   Wannier functions based on HAOs

The next step is to construct orthonormalized Wannier functions from the KS states following the HAOs transferred to a given system. The transferred HAOs constitute a non-orthogonal basis of hybridized atomic orbitals. In the general framework of periodic systems with non-zero wave-vectors ($\vec{k}$) we begin with constructing a

62

Hybrid atomic orbital basis from first principles: Bottom-up mapping of self-energy correction to large covalent systems

(a) C_3H_8

(d) $C_{84}H_{64}$

(c) $C_{26}H_{32}$

(b) $C_{10}H_{16}$
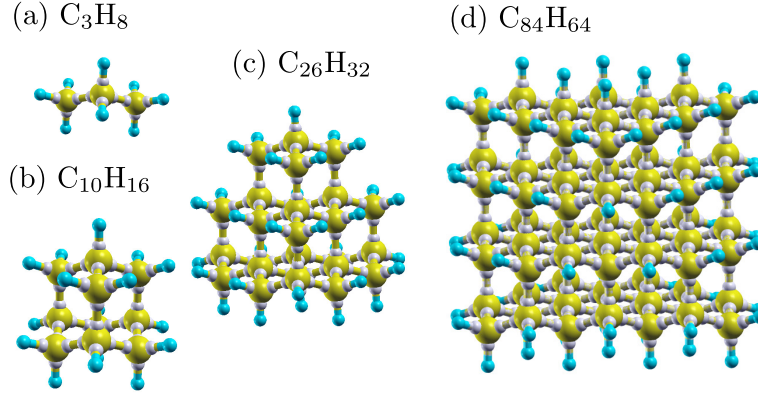
Figure 3.4: C_nH_m systems with projected charge centre of HAOs shown as gray spheres, used in this work as example of sp^3 hybridized covalent systems.

non-orthogonal set of quasi-Bloch states as:

$$\tilde{\psi}_{\vec{k},j}(\vec{r}) = \frac{1}{\sqrt{N}} \sum_{\vec{R}} e^{i\vec{k}\cdot\vec{R}} \phi_{\vec{R},j}(\vec{r}), \tag{3.9}$$

where $\phi_{\vec{R},j}(\vec{r})$ is the j-th HAO localized in the unit-cell denoted by the lattice vector $\vec{R}$ spanning over N unit-cells defining the Born-von Karman periodicity. The projections of the non-orthogonal quasi-Bloch states on the orthonormal Bloch states constructed from the KS single-particle states at all allowed $\vec{k}$, are calculated as:

$$O_{\vec{k},m,j} = \langle \psi^{KS}_{\vec{k},m} \mid \tilde{\psi}_{\vec{k},j} \rangle. \tag{3.10}$$

Elements of O thus record the representation of the HAOs within the manifold of KS bands considered. Overlaps between the non-orthogonal quasi-Bloch states within the manifold of the considered KS states are therefore calculated as:

$$S_{\vec{k},m,n} = \sum_{l} O^*_{\vec{k},l,m} O_{\vec{k},l,n}. \tag{3.11}$$

The degree of representability of HAO ϕ_n, within the set of KS states considered,

(a)   (b)   (c)
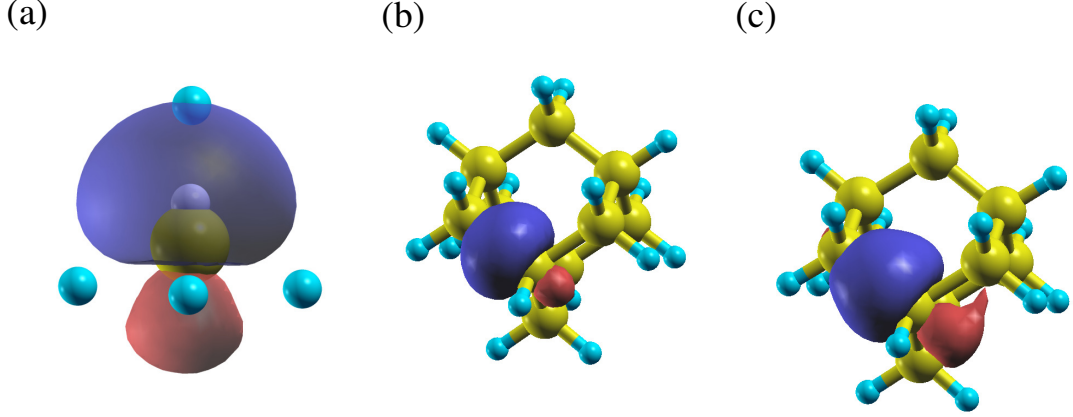
Figure 3.5: (a): HAO representing a sp^3 orbital of an isolated C atom (yellow sphere) used in this work. Charge centre of the orbital is shown in gray. Centres of the confining spheres used to determine gross orientation are shown in cyan. (b): HAO shown in (a) transfered to a C atom an adamantane($C_{10}H_{16}$) molecule, (c): the corresponding HAWO.

is guaranteed by setting a lower cutoff on individual $S_{\vec{k},n,n}$ values to be typically more than 0.85. For all the system studied in this work, the above criteria is found to be satisfied by the lower bound on the number KS states, which is set by the total number of valence orbitals of all atoms of a given system. A new set of orthonormal Bloch states from the KS single particle states are subsequently constructed using the Löwdin symmetric orthogonalization [104] scheme as:

$$\Psi_{\vec{k},n}(\vec{r}) = \sum_m S_{\vec{k},m,n}^{-\frac{1}{2}} \sum_l O_{\vec{k},l,m} \psi_{\vec{k},l}^{KS}(\vec{r}), \qquad (3.12)$$

where the sum over l spans the KS states considered and the sum over m takes care of the orthonormalization. Subsequently, a localized set of orthonormal Wannier functions are constructed as:

$$\Phi_{\vec{R}',j}(\vec{r}) = \frac{1}{\sqrt{N}} \sum_{\vec{k}} e^{-i\vec{k}\cdot\vec{R}'} \Psi_{\vec{k},j}(\vec{r}). \qquad (3.13)$$

In this process the Löwdin symmetric orthogonalization clearly provides a choice of gauge for linear combination of KS states such that the resultant Wannier functions $\left\{\Phi_{\vec{R}',j}(\vec{r})\right\}$ resemble the corresponding HAOs [$\left\{\phi_{\vec{R},j}(\vec{r})\right\}$] as much possible within

64

Hybrid atomic orbital basis from first principles: Bottom-up mapping of self-energy correction to large covalent systems

the manifold of KS states considered. Hence we refer to these Wannier functions as the hybrid atomic Wannier orbitals ("HAWO"). In Fig.3.5 we show an HAO before and after transfer to adamantane and the corresponding HAWO constructed from the KS states of adamantane. HAWOs can thus be considered as analogue of NHOs constructed from a given set of KS states with acceptable representability.
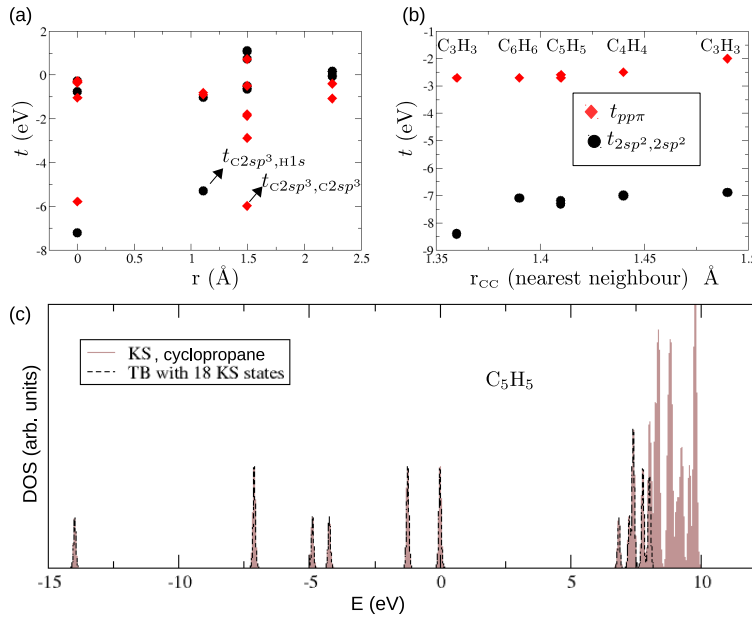
Figure 3.6: (a): TB parameter calculated for cyclopropane; (b): Nearest neighbour TB parameters between in-plane and out of plane orbitals in C_3H_3, C_4H_4, C_5H_5 and C_6H_6 molecules (shown in Fig.3.2) arranged as a function of C-C bond lengths available in the molecules. (c) DOS calculated from 50 lowest KS eigen-values, compared with DOS from eigen-values of TB Hamiltonian constructed from 18 lowest KS states, 18 being the total number of valence orbitals of cyclopropane.

Notably, following the same approach, template of bonding and lone pair orbitals made of HAOs can be used to construct localized Wannier functions rendering orbital resolved description of the valence band.[93,94] Similarly , template of anti-bonding orbitals made of HAOs can be used to extract a meaningful description of the unoccupied bands in the line of the *valence virtual orbitals*.[105]
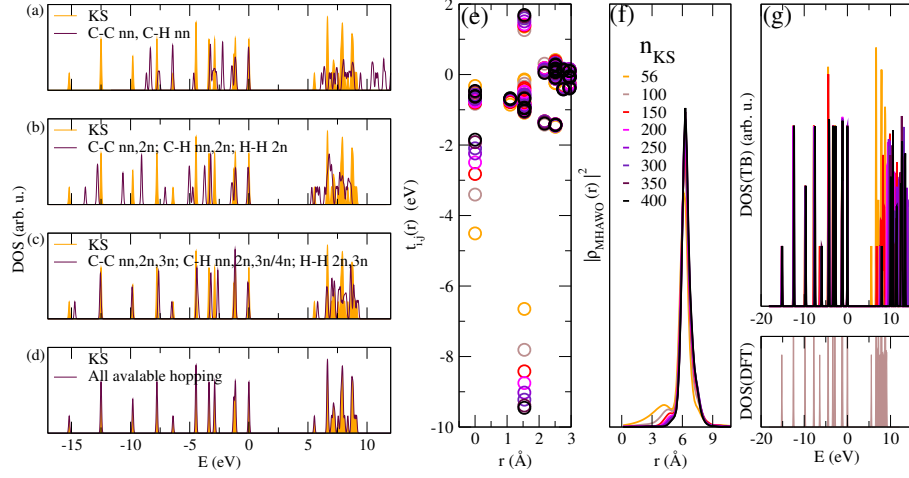
Figure 3.7: For $C_{10}H_{16}$, (a-d): Evolution of density of states(DOS) with increase in range of hopping starting from (a): the nearest neighbour (nn) to (d): all avaliable hopping graduating through hopping between second (2n) and third (3n) nearest neighbours and beyond. Convergence of (e): TB parameters and (f): spatial localization of $2sp^3$ orbitals, and (g): TB DOS, in terms of the number of KS states used in construction of HAWOs as mentioned in the legend of (f). KS DOS is shown below (g).

3.2.2.1   TB parameters in HAWO basis

TB parameters in the HAWO basis are computed from energetics of KS single particle states as:

$$t_{\vec{R}',\vec{R},i,j} = \langle \Phi_{\vec{R}',i} \mid H^{KS} \mid \Phi_{\vec{R},j} \rangle$$
$$= \sum_{\vec{k}} e^{i\vec{k}.(\vec{R}'-\vec{R})} \sum_{l} (OS^{-\frac{1}{2}})_{li}^* (OS^{-\frac{1}{2}})_{lj} E_{\vec{k},l}^{KS} \qquad (3.14)$$

Notably, similar TB parameters have been derived in the last two decade from first principles based on the either the maximally localized Wannier function[106,107,108,109,110,111] or atomic orbitals[112,113] constructed from KS states. Much effort has been reported in deriving TB parameters through projection of KS states on pseudo-atomic orbitals[114,115] as well. However, attempts to calculate TB parameters in hybrid atomic orbital basis constructed from first-principles, as proposed in this work, has been limited so far primarily to analytical models.[116,117]

In Fig.3.6(a) for cyclopropane, we plot the TB parameters calculated as per

Eqn.(4.10) for two HAOs participating dominantly in a C-C bond and a C-H bond. The t_{sp^3,sp^3} is comparable to the that in adamantane $(C_{10}H_{16})$[Fig.3.9] despite the substantial misalignment[Fig.3.2] of HAO and the C-C bond in cyclopropane while perfect alignment of the two in $C_{10}H_{16}$. The hopping parameters are obtained with 18 KS states which is same as the total number of valence orbitals of all the atoms, resulting thereby into density of states in exact agreement with that obtained from DFT [Fig.3.6(c)] as discussed above in the next paragraph. In Fig . 3.6(b) we plot hopping parameters for π and σ bonds as a function of C-C bond lengths available in planar C_3H_3 to C_6H_6 molecules. As evident in Fig.3.2, the best alignment of the HAOs along the C-C bond is possible for C_6H_6 and the worst is obviously for the shorter bond of C_3H_3 and similarly for C_3H_6. Yet, the highest in-plane hopping parameter in terms of magnitude is found for the shorter bond of C_3H_3, which is about 20 % more than that of the C-C in-plane bond of benzene, whereas the C-C bond length in benzene only about 2.2 % more than the shorter bond of C_3H_3. Similarly, the C-C nearest neighbour hoping parameter as well as the bond length in C_3H_8, both are within 1 % of those of C_3H_6, whereas in C_3H_8 the HAOs are almost perfectly aligned along the C-C bond [Fig.3.4] while in C_3H_6 they are misaligned by more than $20°$. These results can possibly be explained by the inherent bent nature the bonds[118] in C_3H_6 and C_3H_3, reflected by the symmetric misalignment of the HAOs along the two C-C bonds while maintaining perfect alignment along the C-H bonds. We plan to examine this aspect for bent bonds in details in future.

As evident in Fig.3.7(a) for $C_{10}H_{16}$ the edge of the valence band is already well described if we consider only the nearest neighbor hopping in the HAWO basis. However, as shown in Fig.3.7(b) onwards, the match of DOS from TB and DFT improves drastically with increasing extent of hopping considered up to the second nearest neigbour. This is immediately understood by noting the non-nominal positive valued of the second nearest hopping element plotted in figure Fig.3.7(e), arising due to proximity of lobes of different signs of the two HAOs. In Fig.3.7(e-g), we demonstrate evolution of the TB parameters, HAWOs, and DOS from TB, as function of number of KS states considered for construction of HAWOs. The ratio-

nale for this analysis is the possibility that the anti-bonding subspace may not be adequately represented by the unoccupied KS states if we restrict the total number of KS states to be same as the total number of HAOs associated with all the atoms, which is same as the total number of valence orbitals of all the atoms. Indeed we see clear convergence of shape of HAWO [Fig.3.7(f)] as well as the corresponding TB parameters[Fig.3.7(e)] if we consider KS states in excess of the total number of HAOs. However, the TB DOS expectedly starts deviating from the DFT DOS more in the conduction band [Fig.Fig.3.7(g)] if we include more KS states beyond the total number of HAOs, owing to the semi-unitary nature of the net transformation matrix $(OS^{\frac{1}{2}})$ implied in Eqn.(4.7) which will be rectangular in such scenarios. It is thus important to decide on the number of KS states to be considered depending on the purpose. If the aim is to represent only the valence bands through well localized HAWOs, then it may be prudent to look for convergence of HAWOs in terms of KS states. But if band-gap needs to be represented accurately by the TB parameters then the number of KS states should be kept same as the total number of valence orbitals.

3.2.3   Bottom-up mapping of TB parameters

The HAWO basis derived from the KS states offer a multi-orbital TB basis which are by construction locked to the local coordination as per the atomic neighborhood of each atom. The TB parameters derived in such a basis should therefore be transferable from one system to another with matching atomic environment. A key aim of this work is to demonstrate such transferability for effective transfer of multi-orbital TB parameters in the HAWO basis from smaller reference systems to larger target systems. The mapping of TB parameters is done in two steps.

(1) Pairs of atoms of the target system, not limited to nearest neighbors, are mapped on to pairs of atoms in the reference system based on a collection of criteria.

(2) Among the mapped pair of atoms, pair of system orbitals are mapped to pair of reference orbitals through mapping of their respective projected charge centres.

In step (1) the criteria to map pairs of atoms include matching structural parameters such as their spatial separation and their individual nearest neighborhoods characterised in terms of the type of neighboring atoms and angles made by nearest neighbors on the atoms. In particular, we use a parameter calculated as:

$$\zeta_i = \sum_j^{N_i} Z_j w(r_{i,j}) \tag{3.15}$$

where N_i is the number of neighbors of the i-th atom within a suitably chosen cutoff radius, w being a weight factor which is a function of the distance $r_{i,j}$ of the j-th neighbor of the i-th atom, and Z_i a characteristic number to be associated with each type of atom. Z_i can be chosen to be the atomic weight, as we mostly used in this work, or a similar number which can facilitate identification of a type of neighborhood or a region of the system through values of ζ. In this work we chose the weight factor w to be 1.0 within half of the cutoff radius beyond which the factor is smoothly reduced to zero using a cosine function. The choice of cutoff radius depends on the size of the reference system. It should neither be too large for variations to average out, nor should it be too small to become insensitive to morphological variations in the reference system itself. ζ allows us to map atom pairs effectively through prudent choice of values of $\{Z_i\}$ since it would allow assessment of proximity of atoms to edges, interfaces or any kind of structural inhomogeneity without any exhaustive structural relaxation.

In step 1, the minimum of the deviation:

$$|\zeta_1^{\text{target}} - \zeta_1^{\text{reference}}| + |\zeta_2^{\text{target}} - \zeta_2^{\text{reference}}|$$

obtained within a range of allowed deviation of structural parameters, is used as the criteria to choose matching pairs of atoms between target and reference systems.

Like in step 1, in step 2 as well, the mapping of one or a pair of HAOs from the reference to target systems is done based on matching structural parameters, as

well as a parameter calculated as:

$$\xi_i = \sum_{j}^{N_i} \zeta_j w^{WC}(r_{i,j}) \tag{3.16}$$

where ζ_j corresponds of the j-th atom in the neighborhood defined by w^{WC} around of the projected charge centre of the i-the HAO. Angle made by the directions of the projected charge centres of the HAOs from their respective host atoms is a key matching parameter in step 2. Additionally, if the HAOs belong to different atoms then the dihedral angle made by the centres of the HAOs through the axis connecting their host atoms, is also a key parameter. Thus in step 2, the minimum of the deviation

$$|\xi_1^{\text{target}} - \xi_1^{\text{reference}}| + |\xi_2^{\text{target}} - \xi_2^{\text{reference}}|$$

within acceptable deviations of structural parameters, defines matching pairs of HAOs.

As an example we show mapping from a small curved finite patch[Fig.5.7(a)] to C_{60}. Since C_{60} constitutes a curved surface without any edge, mapping should be done from the inner most neighborhood of the chunk. Since in C_{60}, the angles made by nearest neighbors at a given atom differ distinctly depending on whether an angle opens inside a pentagon or a hexagon, the matching parameters for mapping are mostly structural, primarily the direct and dihedral angles. The reference patch is cropped from C_{60} and passivated by H. We fix ζ tolerance to zero which implies that C_{60} is getting mapped from only six C atoms of the patch [Fig.5.7(a)] having all C neighbors. Given the curvature of C_{60}, we chose to use confining spheres to influence the hybridization of sp^2 HAOs in order to break their co-planarity and align them along nearest neighbor C-C bonds, as shown in Fig.3.3(c) where the placement of confining potential spheres are as per the nearest neighborhood in C_{60}. The projected charge centres of HAOs with intermediate hybridization $(2sp^{2+}+2p_z^+)$ between (sp^2+p_z) and sp^3 shown in Fig.5.7(c), is used to map from that of the

Hybrid atomic orbital basis from first principles: Bottom-up mapping of self-energy correction to large covalent systems

70

reference shown in Fig.5.7(b). TB parameters $t_{2sp^{2+},2sp^{2+}}$ for the shorter and longer C-C bonds are about -6.9 eV and -6.5 eV, whereas $t_{2p_z^+,2p_z^+}$ are about -2.36 eV and -2.0eV. The match of the DFT DOS with the DOS from TB parameters mapped from the reference system is shown in Fig.5.7(d), which can be further improved beyond the valence bond by considering HAOs for excited states, which will be taken up in a subsequent work on optical properties.
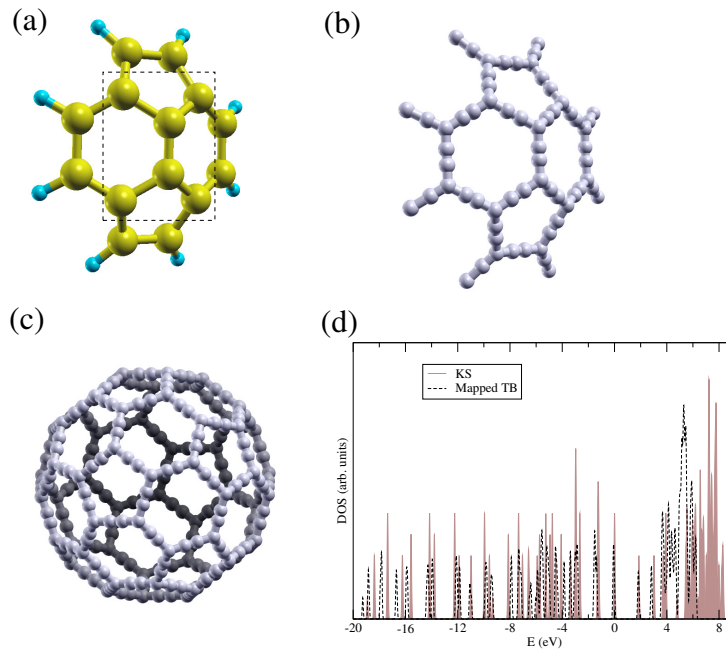
Figure 3.8: (a): Structure of reference system, and (b): the corresponding charge centres of HAOs with intermediate hybridization $(2sp^{2+}+2p_z^+)$ between sp^2 and sp^3. (c): Projected charge centre with similar hybridization for C_{60}. (d): Corresponding matches of DFT DOS with TB DOS with parameters mapped from the reference system.

3.2.4 Self-energy correction of TB parameters

Self-energy corrected TB parameters $\left\{t^{QP}_{\vec{R'},\vec{R},i,j}\right\}$ in the HAWO basis are calculated by substituting $E^{KS}_{\vec{k},n}$ in Eqn.(4.10) by quasiparticle energies $E^{QP}_{\vec{k},n}$ obtained at the G_0W_0 level which is the first order non-self-consistent GW approximation of MBPT[61].[5]

Within the GW approximation, the quasi-particle energies are approximated as:

$$E_{\vec{k},n}^{QP} = E_{\vec{k},n}^{KS} + \langle \psi_{\vec{k},n}^{KS} \mid \Sigma - V_{xc}^{KS} \mid \psi_{\vec{k},n}^{KS} \rangle, \qquad (3.17)$$

where V_{xc}^{KS} is the mean-field exchange-correlation potential and Σ^{15} is the self-energy operator derived by considering the many-electron effects as perturbation treated within a self-consistent framework of Dyson's equation formulated in terms of the one-particle dynamic non-local Green's function constructed from the KS states. Similar efforts have been reported in recent years on incorporating SEC in TB parameters computed in terms of the MLWFs.[119,120,121]Incorporation of SEC in TB parameters has also been attempted through matching specific bands of the QP structure.[122,123,124]

3.3   Computational Details

Electronic structures of the ground states of all the systems considered in this work are calculated using the Quantum Espresso (QE) code[125] which is a plane wave based implementation of DFT. We have used norm conserving pseudo-potentials with the Perdew-Zunger (LDA) exchange-correlation[126] functional and a plane wave cutoff of 60 Rydberg for wave-functions and commensurately more for charge density and potential. Self-energy correction to single particle levels have been estimated at the non-self-consistent G_0W_0 level of GW approximation implemented in the BerkeleyGW code.[127] To calculate the static dielectric matrix required for computation of the self-energy operator, the generalized plasmon-pole model[15] is used to extend the static dielectric matrix in the finite frequencies. For all the nanoribbons parameters are chosen from Ref..[128] In house implementation interfaced with the QE code is used for generation of HAOs, HAWOs from KS states, calculation of TB parameters in the HAWO basis, and mapping of TB parameters from reference to target systems.

3.3.1 Mapping self-energy corrected TB parameters in HAWO basis
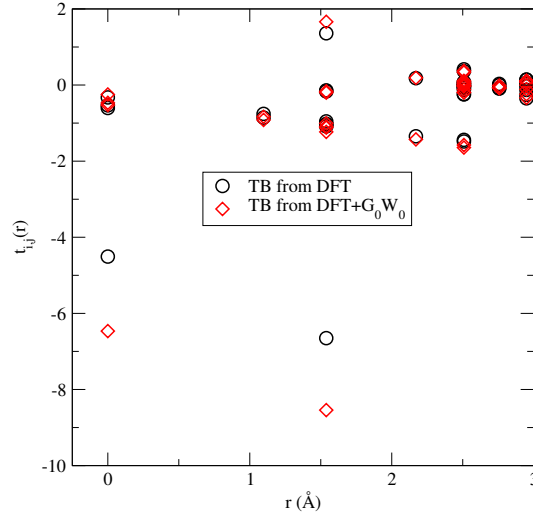
Figure 3.9: TB parameters involving a C atom in $C_{10}H_{16}$ with three C neighbors, computed using 56 KS states with and without SEC at the G_0W_0 level, and plotted as a function of distance from the atom. TB parameters from DFT are same as those plotted in Fig.3.7(e).

Fig.3.9 suggests that the extent of SEC to TB parameters are spatially limited mostly within the third nearest neighborhood, implying possible transferability of SE corrected TB parameters to large covalent systems from smaller reference systems of which are large enough to accommodate the full spatial range of non-nominal SEC to TB parameters. Accordingly, mapping in nano-diamonds is demonstrated with C_3H_8 and $C_{10}H_{16}$ (adamatane) as reference systems to map to nano-diamonds $C_{26}H_{32}$ (pentamantane) and $C_{84}H_{64}$.

We start with attempts to map $C_{10}H_{16}$, $C_{26}H_{32}$ and $C_{84}H_{64}$ targets from C_3H_8 reference in sp^3 HAO basis. The mapping process starts with plotting the distance of atom pairs (C-H, C-C, H-H) for target and reference systems. As seen in Fig.3.10(a) there is one-to-one correspondence of C-C bonds between C_3H_8 and all targets up to approximately 2.5Å, which is the second nearest C-C distance. For C-H and H-H pairs, such correspondence exists up to about 3Å and 3.75Å respectively. These correspondences decide the range of hopping parameters to be mapped. Notably,
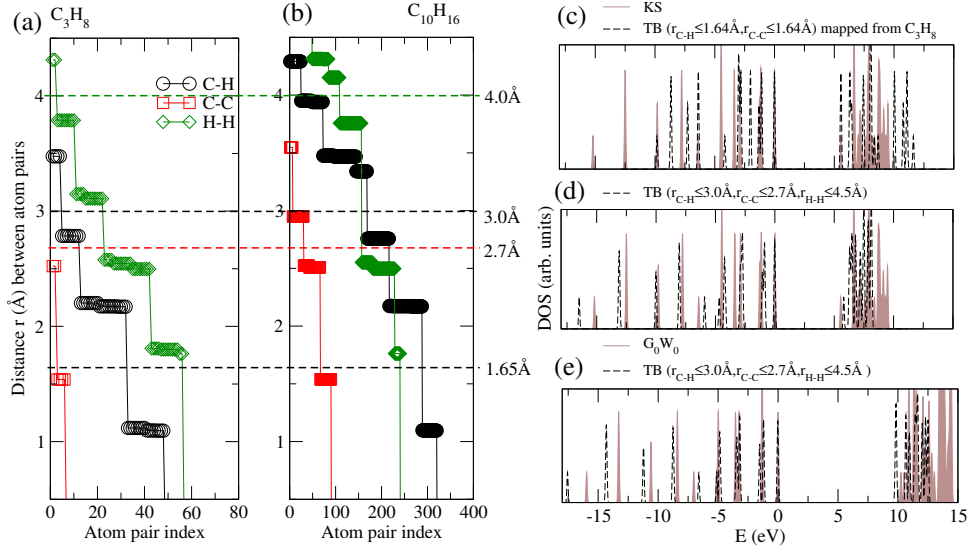
Figure 3.10: Distribution of distance between pairs of atoms in (a): reference (C_3H_8) and (b): target ($C_{10}H_{16}$) systems. (c-d) Match between DFT DOS and mapped TB DOS as demonstrated of efficacy of mapping of TB parameters from C_3H_8 to $C_{10}H_{16}$ with increasing spatial range of neighborhood considered for mapping. (e) Match between DFT+G_0W_0 DOS and mapped self-energy corrected TB DOS.
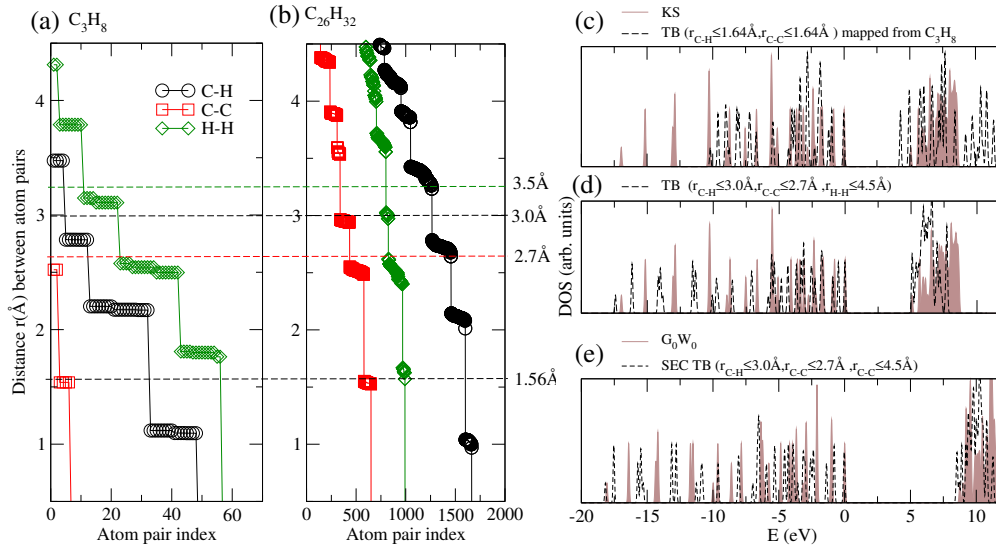
Figure 3.11: Distribution of distance between pairs of atoms in (a): reference (C_3H_8) and (b): target ($C_{26}H_{32}$) systems. (c-d): Match between DFT DOS and mapped TB DOS as with an increasing spatial range of neighborhood considered for mapping. (e): Match between DFT+G_0W_0 DOS and mapped self-energy corrected TB DOS.

C_3H_8 has two varieties of C atoms - one with two(two) C(H) neighbors, and the other with one(three) C(H) nearest neighbors, whereas, $C_{10}H_{16}$ has C atoms with three(one) C(H) neighbors and two(two) C(H) neighbors. Additionally, $C_{26}H_{32}$ and

$C_{84}H_{64}$ have C atoms with all C nearest neighbors(nn). Exact match of ζ between all atoms of reference and target systems is thus impossible in these examples. Matching ζ and ξ will therefore be less effective in mapping from C_3H_8. Also, since there is only one C atom with two(two) C(H) neighbors in C_3H_8, matching ζ can be restrictive in terms the variety of orientations. We thus opt for matching structural parameters within a tolerance for ζ set to the minimum difference of ζ values between similar type of atoms in reference and target systems to ensure maximal matching of ζ besides finer matching of structural parameters. As obvious, a better choice of reference system than C_3H_8 with C atoms having all varieties of neighborhood can be easily made. However, we deliberately chose to test mapping from C_3H_8 which is the smallest possible reference system with just one C atom with two(two) C(H) neighbors, since such C atoms dominates the surfaces of the nano diamonds and are thereby expected to host the states at the edges of the valence and conduction bands. Surprisingly, as evident in Fig.3.10(c), with mapping of only the nn-hopping terms from C_3H_8 to $C_{10}H_{16}$, the mapped TB DOS already matches reasonable well with DFT DOS of $C_{10}H_{16}$ in terms of the band-gap and DOS around band edges. With increase in range of hopping to 2.7Å(nn,2n), 3Å(nn,2n,3n) and 4Å(2n,3n,4n)) for C-C, C-H and H-H pairs based on availability of one-to-one mapping[Fig.3.10(a,b)] the match of mapped TB DOS and DFT DOS[Fig.3.10(d)] extends deeper into the valence band. The quality of match improves further with additional mapping of C-H and H-H atom pairs up to 4.5Å [Fig.3.10(e)] without compromising on tolerance factors. Notably, the range of hopping of C-H and H-H, although more than that of C-C, are actually consistent with the range of C-C hopping, since the farthest H atoms considered are associated with two second nearest C atoms. The same mapping parameters are then used to map self-energy corrected TB (SEC-TB) parameters of C_3H_8 to $C_{10}H_{16}$ leading to a good match of not only the SEC-TB mapped band-gap and the QP band-gap calculated at the G_0W_0 level, but also the SE corrected DOS of the valence band[Fig.3.10(f)].

Next we attempt mapping $C_{26}H_{32}$ from smaller references, starting with mapping from C_3H_8 to $C_{26}H_{32}$, which is about five times increase in system size.Mapping of

only nearest neighbor C-C and C-H hopping underestimates band-gap by about 15%[Fig.3.11(c)]. Mapping all hopping parameters up to upto 4.5Å which is the maximum range of hopping available in the reference, drastically improves overall match of not only mapped TB DOS and DFT DOS[Fig.3.11(d,e)] but also mapped SEC-TB DOS and DFT+G_0W_0 DOS[Fig.3.11(f)], as is seen in case of mapping $C_{10}H_{16}$ from C_3H_8.
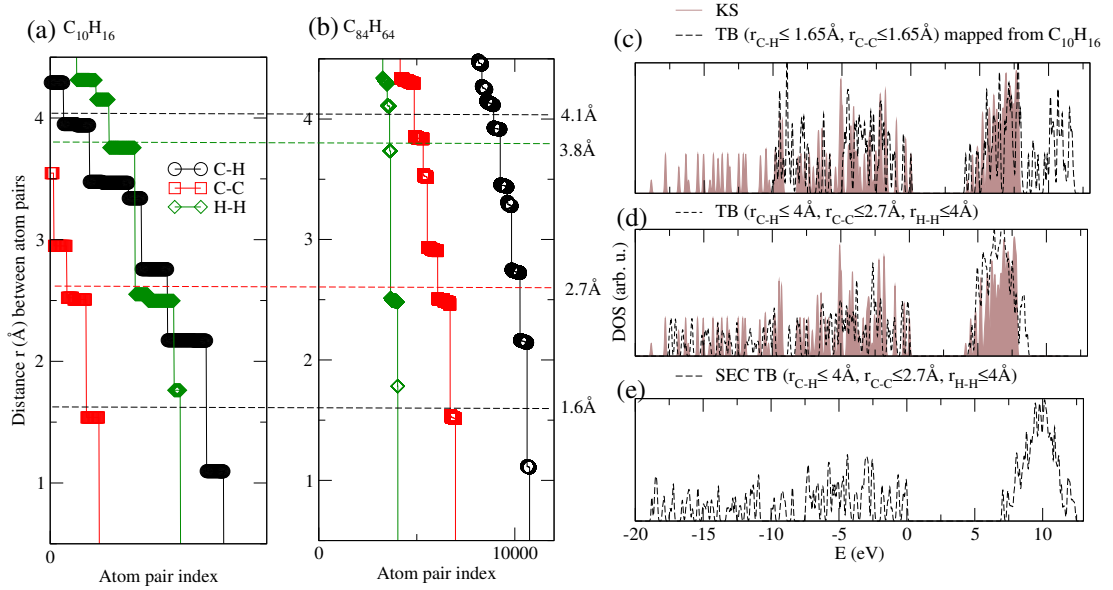
Figure 3.12: Distribution of distance between pairs of atoms in (a): reference ($C_{10}H_{16}$) and (b): target ($C_{84}H_{64}$) systems. (c-d): Match between DFT DOS and mapped TB DOS as with an increasing spatial range of neighborhood considered for mapping. (e): Match between DFT+G_0W_0 DOS and mapped self-energy corrected TB DOS.

Finally we demonstrate mapping to $C_{84}H_{64}$ from $C_{10}H_{16}$, which is about six time enhancement in system size. Mapping of only the nearest neighbor C-C and C-H bonds results into good match of the mapped TB band-gap[Fig.3.12(c)] with the DFT band-gap. With further mapping of hopping parameters upto 2.75Å(nn,2n), 4Å (nn,2n+) and 4Å (2n,3n+)[Fig.3.12(a,b)] for C-C, C-H and H-H pairs, satisfactory match of the entire valence band and a good match[Fig.3.12(d)] of the band-gap is achieved. Mapping of SEC of TB parameters from $C_{10}H_{16}$ to $C_{84}H_{64}$ results into a QP band-gap of about 7.2 eV which is within 5% deviation from the QP band-gap implied in literature.[129,130,131,132]

76

Hybrid atomic orbital basis from first principles: Bottom-up mapping of self-energy correction to large covalent systems

In Fig.3.13 we show similar mapping of TB parameters at the DFT and DFT+G_0W_0 levels for Si based nano-diamonds. Like in case of nano-diamonds, mapping of hopping up to second nearest Si neighbours and H atoms associated with them from Si_3H_8, renders good match of the SEC-TB band-gap with the explicitly estimated DFT+G_0W_0 band-gap almost up to six times escalation of system size. These results imply consistency in transferability of SEC corrected TB parameters with increasing principal quantum number of valence orbitals.
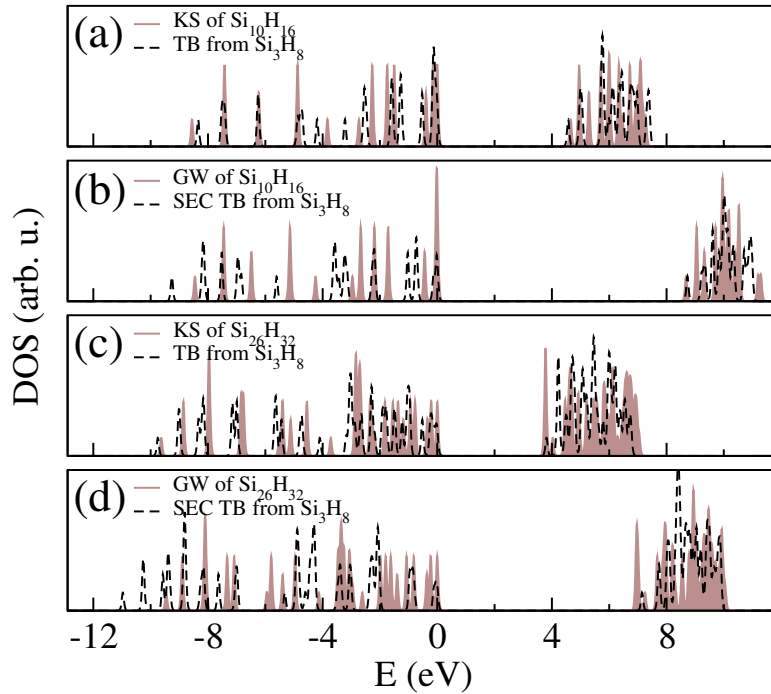
Figure 3.13: (a,c): Match between DFT DOS and TB DOS with parameters mapped from Si_3H_8. (b,d): Match between DFT+G_0W_0 DOS and SEC-TB DOS using mapped self-energy corrected TB parameters from Si_3H_8.

3.4   Conclusion

In conclusion, construction of naturalized hybrid atomic orbitals(HAO) is proposed as the common eigen-states of the non-commuting set of finite first-moment matrices corresponding to the orthogonal directions. Hybridization and orientations of HAOs are numerically naturalized as per their anticipated immediate atomic

neighborhood. Choice of gauge based on the HAOs leads to the construction of the hybrid atomic Wannier orbitals (HAWO) from Kohn-Sham(KS) single particle states, rendering a multi-orbital orthonormal tight-binding(TB) basis locked to the nearest neighborhood. HAWO basis allows calculation of single TB parameters per bond from first principles, and facilitate their easy transfer across iso-structural systems through mapping of immediate atomic neighborhoods and projection of charge centres learned in the process of naturalization of the HAOs. The mapping allow effective bottom-up transfer of self-energy corrected TB parameters estimated within the GW approximation of many-body perturbation theory in HAWO basis, from smaller reference systems to much larger target systems having similar covalent atomic neighborhoods, suggesting a possible route towards computationally inexpensive estimation of quasi-particle structures of large covalent systems within acceptable range of accuracy, with extra computational cost scaling as N^2, beyond the explicit computation of self-energy correction for smaller reference systems which typically scale as N^4. Demonstrated in nano-diamond systems, the transferability of self-energy corrected multi-orbital TB parameters in HAWO basis, is rooted at the spatial localization of the extent of self-energy correction predominantly within the third nearest neighborhood.

Chapter 4

Maximally valent orbitals in systems with non-ideal bond-angles: Atomic Wannier orbitals guided by Mayer bond order

In the previous chapter we described the construction of the hybrid atomic Wannier orbital (HAWO) based on the template of de-generate hybrid orbitals, which by construction are directed towards the nearest coordination in the system with ideal bond angle.

In this chapter we focused on system with non ideal bond angle. In search of an optimally directed minimal set of basis for such systems, in the work presented in this chapter we find the exact orientation of the major overlapping orbitals along the nearest neighboring coordination segments in a given systems such that they maximally represent the covalent interactions through out the system. We compute Mayer's bond order, akin to the Wiberg's bond index, in the basis of atomic Wannier

orbitals with customizable non-degenerate hybridization leading to variable orientations, constructed from first principles, in a representative variety of molecules. We put them in perspective with unbiased maximally localized descriptions of bonding and non-bonding orbitals, and energetics to tunneling of electrons through them between nearest neighbors, to describe the different physical aspects of covalent interactions, which are not necessarily represented by a single unique set of atomic or bonding orbitals.

4.1 Introduction

To represent the electronic structure of a given covalent system with minimal tight-binding parameters it is preferable to resort to a directed localized basis[66,85,86,133] such that the basis orbitals maximally represent the dominant covalent interactions in the system. At a fundamental level the problem is essentially that of finding the orientation of the atomic orbitals such that a minimum number of them facilitate maximum sharing or tunneling of electrons between neighboring atoms. An associated problem is to partition the electrons in a covalent system among atoms and bonds[134] such that the population of bonds are contributed by a minimum number of orbitals. Solutions are rather straightforward for systems with ideal bond-angles corresponding to degenerate hybridizations like $sp^{2,3}$. Complication arises with non-ideal bond angles, since for such systems, as we show in this work, making a choice becomes difficult, as different facets of covalent interactions are represented by different sets of orbitals for the same coordination. In fact, "bent bonds"[118] have been long suggested in such systems, indicating deviation of orientation of atomic orbitals from the direction of coordination, as they take part in such covalent bonds.

Hybrid orbitals have been central to description of covalent bonding since their introduction[65,66] almost a century ago. Molecular orbitals theory based methodologies for construction of hybrid orbitals,[68,70,72,73,74,75] predating the advent of the Kohn-Sham(KS) density functional theory(DFT)[9,27] based framework, have been grossly based on the maximum overlap condition, wherein either the overlap ma-

trix[68,70] or the first-order density matrices,[74,76] calculated typically in the basis of Slater[77] or the Gaussian[78,79] type orbitals, are transformed into block diagonal forms, where each blocks are spanned by orbitals centered on a pair of nearest neighbouring atoms. The resultant variants of the hybrid orbitals like the *natural hybrid orbitals*,[76] the *effective atomic orbital*,[75] the *generalized hybrid orbitals*,[85,86] the *oriented quasi-atomic orbitals*,[81] or the ones constructed using the *maximal orbital analysis*[82] approach, constituted the bedrock for understanding chemical bonding in molecules, although limited or biased by the selection of the semi-analytic basis states with adjustable parameters. With the advent of DFT[27] based computation of electronic structure from first principles, attempts to construct localized description of electronic structure in the basis of the KS single particle states, has been primarily undertaken in terms of the spatially localized Wannier functions(WF),[8] which rendered bonding and non-bonding orbitals if constructed from the occupied KS states. Since WFs cannot be uniquely localized in more that one direction simultaneously unless facilitated by symmetry, template based construction of WFs with numerically chosen gauge for the KS states to ensure maximal localization,[93,135] has been the mainstay. However with only Γ point, as is the case for finite systems and acceptable for large super-cells, the maximally localized WFs can be constructed without using any template,[102,135,136] as done in this work.

Methodologically, in this work we introduce the notion of maximally valent orbitals (MVO), which are essentially a selection of major overlapping orbitals along coordinations, oriented such that a minimal of them maximally account for sum of bond-orders along coordinations across the system, at the level of nearest neighborhoods or beyond. Wannier function based on the template of MVOs thus constitute the maximally covalent Wannier functions(MCWF). We demonstrate search of MVOs within the sets of orthonormal Wannierized counterparts of non-degenerate sp^2 and sp^3 orbitals, referred here onwards as the n-sp^2 and n-sp^3 orbitals, with customizable orientation, constructed from first principles. The n-sp^2 and n-sp^3 orbitals are the custom hybridized atomic orbitals(CHAO) with tunable hybridization as per the geometry of nearest neighbor coordination around atoms in systems with non-

ideal bond angles. CHAOs are generalization of degenerate HAOs constructed from KS states of isolated atoms as demonstrated in Ref..[10] Wannierization of CHAOs in the basis of the KS states of a given system renders the custom hybridized atomic Wannier orbitals(CHAWO), which constitute a set of orthonormal localized basis which incorporates effects of local environment of a given atom in the system, notionally similar to the quasi atomic orbitals.[133,137] At the heart of the search of MVOs is the formulation and computation of bond-order in the basis of CHAWOs, as defined by Mayer[138] and found analogous to the Wiberg's bond index[139] priorly introduced. Mayer bond order, known to formally render values discernible as per the classical definition of bond order,[140,141,142] has been a powerful tool in probing and quantifying the quantum nature of interaction between atoms in general.[143,144,145]

We further calculate energetics and tight-binding parameters in the basis of CHAWOs, and calculate their projection on maximally localized WFs constructed without any template of CHAOs, in order to compare MVOs and MCWFs with other possible descriptions of atomic and bonding orbitals representing different aspects of covalent interactions. Results have been demonstrated in a wide range of systems starting with cyclopropane which has the smallest C-C-C bond angle, to cyclobutadiene, diborane, ammonia and water, and finally fullerene, all with bond angles different from that of degenerate sp^2or sp^3coordination.

4.2   Methodological details

In this section first we briefly outline the construction of the template free maximally localized WFs used in this work, and the HAOs, following similar approach. Next we describe construction of CHAOs from HAOs and their Wannierization, followed by formulation of bond-order in terms of the Wannierized CHAO, that is, the CHAWOs. Finally we introduce MVOs as a particular choice of CHAWOs, and MCWOs.

The construction of the template free variant of the maximally localized Wannier functions (MLWF)[102,136] to describe bonding and non-bonding orbitals in isolated systems, is precursor to the construction of HAOs,[10] in terms of the technique for

spatial localization. The only difference is that the MLWFs are constructed exclusively within the subspace of the occupied KS states of a given system, while the HAOs are constructed within an extended sub-space beyond the occupied sub-space of an isolated atom. The localization scheme in both cases is based on maximal joint diagonalization of the generally non-commuting set of the first moment matrices(FMM) which are the representation of the three position operators $\hat{x}, \hat{y}, \hat{z}$ within a finite sub-space of basis states. The procedure follows from the fact that the total spread of a set of finite (N) number of orbitals along $\hat{x}$, given by:

$$\Omega_x = \sum_{i=1,N} \left[\langle \phi_i | x^2 | \phi_i \rangle - |\langle \phi_i | x | \phi_i \rangle|^2 \right], \tag{4.1}$$

can be expressed as:

$$\Omega_x = \sum_{i=1,N} \left(\sum_{j \neq i}^{N} |X_{ij}|^2 + \sum_{j=N+1}^{\infty} |X_{ij}|^2 \right). \tag{4.2}$$

where $X_{ij} = \langle \phi_i \mid x \mid \phi_j \rangle$. The off-diagonal elements of the FMM in the first term in the RHS of Eqn.4.2 are simultaneously minimized through an iterative scheme based on the Jacobi method of matrix diagonalization, wherein the off-diagonal elements of a single or a commuting set of matrices are set to zero through successive application of two dimensional rotation. In case of a set of non-commuting matrices, a choice of rotation matrices which will maximally diagonalize the non-commuting matrices has been derived in Ref..[95] The same has been used in this work, as well as for construction of HAOs described in Ref.,[10] which may be refer for relevant details of computation of the rotation matrices.

Construction of CHAOs from HAOs involve two steps - (1) Reconstruction of unhybridized atomic orbitals(UAO) from degenerate HAOs, and (2) Re-hybridization of UAOs to construct CHAOs. In step 1, for a given element, linear combination of HAOs render UAO aligned perfectly as per a preferred Cartesian system of axes, with the variation of the radial part determined by the pseudo-potential used. In principle this process is straightforward since the analytic hybridization matrix

for degenerate $sp^m d^n$ hybridization is known. Surmountable technical complication arises with the arbitrary overall orientation of the set of degenerate HAOs. Notably, up to $n = 2$, UAOs obtained this way are essentially the rotated KS states, since for elements with $2s$ and $2p$ valence electrons, the lowest three degenerate block of KS states are the three orthonormal $2p$ states in random orientation. However, for $n > 2$ arbitrary mixing of degenerate KS states of the valence shells makes it impossible to directly use them individually as pure atomic orbitals after simple rotation. UAOs obtained from the HAOs, which are maximally localized by construction, are thus assured to render the most localized form of pure orbitals aligned along any preferred set of Cartesian axes as per the pseudo-potential used.

Re-hybridization of UAOs to n-sp^2 or n-sp^3 CHAOs are performed using hybridization matrices specific to symmetries as per that of the nearest neighborhoods. For example, for CHAOs of the nitrogen atom in NH_3 we use a hybridization of form

$$\begin{pmatrix} a & b & b & c \\ a & c & b & b \\ a & b & c & b \\ d & e & e & e \end{pmatrix} \begin{pmatrix} s \\ p_x \\ p_y \\ p_z \end{pmatrix}. \tag{4.3}$$

The unitarity of the matrix allows one independent parameter and if we choose it to be c then the other parameters can be calculated as: $a = \sqrt{-1 - 3c^2 + 4c}$, $b = c - 1$, $e = a$, $d = \sqrt{1 - 3a^2}$. More generally, an irregular tetrahedral orientation of orbitals can be assigned with hybridization matrix of form:

$$\begin{pmatrix} a & \frac{1}{\sqrt{2}} & \sqrt{\frac{1}{2} - a^2} & 0 \\ a & -\frac{1}{\sqrt{2}} & \sqrt{\frac{1}{2} - a^2} & 0 \\ b\sqrt{\frac{1}{2} - a^2} & 0 & -ab & -\sqrt{1 - \frac{b^2}{2}} \\ \sqrt{2 - b^2}\sqrt{\frac{1}{2} - a^2} & 0 & -a\sqrt{2 - b^2} & \frac{b}{\sqrt{2}} \end{pmatrix} \tag{4.4}$$

with two independent parameters a and b representing the two angles which complete

the assignment of four orthonormal orbitals. As evident in the matrix, we consider two of the orbitals, the first two, oriented in xy plane symmetrically about the y axis, while the other two orbitals are in the yz plane. The third and fourth orbitals can also be chosen to be symmetric about the y axis, which reduces the number of independent parameters to one, and geometrically akin to the majority of tetrahedral coordination, like those of C in C_nH_{2+2n}.

Given a system of atoms, we construct separate sets of CHAOs for atoms of different elements and relative orientation of nearest neighbors(nn) around them. Through choice of parameters in the hybridization matrix we can orient the CHAOs exactly along the direction of coordinations, or in any systematic variation expressible in terms of those directions. Sets of CHAOs constructed for each such types of atoms are then transferred from their atomic nurseries to the given system and oriented according to nn coordinations around each atom, to constitute a set of localized non-orthogonal basis made of transferred CHAOs with intra-atomic orthogonality.

Wannierization of the transferred CHAOs, say N in number, in the basis of $N_{KS}(\geq N)$ number of KS states, starts with construction of a set of quasi-Bloch states $\left\{ \tilde{\psi}_{\vec{k},j}(\vec{r}) \right\}$ from CHAOs, and subsequently projecting them on the orthonormal Bloch states constructed from the KS single-particle states:

$$O(\vec{k})_{m,j} = \langle \psi_{\vec{k},m}^{KS} \mid \tilde{\psi}_{\vec{k},j} \rangle. \tag{4.5}$$

Overlaps between the non-orthogonal quasi-Bloch states are calculated within the manifold of the considered KS states as:

$$S(\vec{k})_{m,n} = \sum_{l}^{N_{KS}} O(\vec{k})_{l,m}^{*} O(\vec{k})_{l,n}. \tag{4.6}$$

Values of $\sum_{\vec{k}} |S(\vec{k})_{n,n}|^2 / N_k$ implies representability of the n-th CHAO within the set of KS states considered, and should be typically above 0.85 for good agreement of KS band-gap and valence band width, with those calculated with the resultant tight-

binding parameters, in the covalent systems made of p-block elements as mostly studies in this work.

Through Löwdin symmetric orthogonalization(LSO)[104] a new set of orthonormal Bloch states can be constructed as:

$$\Psi_{\vec{k},n}(\vec{r}) = \sum_m^N S(\vec{k})_{m,n}^{-\frac{1}{2}} \sum_l^{N_{KS}} O(\vec{k})_{l,m} \psi_{\vec{k},l}^{KS}(\vec{r}), \tag{4.7}$$

which can be used to construct an orthonormal set of localized Wannier functions referred in this paper as the custom hybrid atomic Wannier orbitals (CHAWO):

$$\Phi_{\vec{R'},j}(\vec{r}) = \frac{1}{\sqrt{N_k}} \sum_{\vec{k}} e^{-i\vec{k}\cdot\vec{R'}} \sum_l^{N_{KS}} U(\vec{k})_{lj} \psi_{\vec{k},j}^{KS}(\vec{r}). \tag{4.8}$$

where

$$U(\vec{k}) = O(\vec{k})S(\vec{k})^{-\frac{1}{2}}. \tag{4.9}$$

LSO chooses the appropriate linear combination of KS states such that resultant CHAWOs are orthonormal yet substantially resemble the template of transferred CHAOs. TB parameters in CHAWO basis is straightforwardly calculated as:

$$t_{\vec{R'},\vec{R},i,j} = \langle \Phi_{\vec{R'},i} \mid H^{KS} \mid \Phi_{\vec{R},j} \rangle$$
$$= \frac{1}{N_k} \sum_{\vec{k}}^{BZ} e^{i\vec{k}\cdot(\vec{R'}-\vec{R})} \sum_l^{N_{KS}} U(\vec{k})_{li}^* U(\vec{k})_{lj} E_{\vec{k},l}^{KS}. \tag{4.10}$$

where $\left\{ E_{\vec{k},l}^{KS} \right\}$ are KS energy eigenvalues. With $N_{KS} > N$, $U(\vec{k})$ becomes semi-unitary, and spatial localization of CHAWOs enhances and eventually converges with N_{KS}. However for this work we have restricted $N_{KS} = N$ so that $U(\vec{k})$ is square matrix whose inverse can be unambiguously invoked in order to expand KS states completely in terms of CHAWOs.

Notably, representability of the UAOs or HAOs or CHAOs in the KS states of the given system where they are to be Wannierized, can be maximized by choosing

to construct them using the same pseudo-potentials which are used to compute the KS states of the given system. High degree of representability ensures consolidation of the O matrix [Eqn.(4.5)] over fewer bands of KS states, which in turn consolidates localization of the Wannierized orbitals. In principle, for a given system we could also directly Wannierize a template of analytic or semi-analytic orbitals such as the hydrogenic, Slater or Gaussian type orbitals, or their hybrids, instead of the UAOs or the HAOs or CHAOs which are purely numerical in nature. However, unlike the numerical ones which can be chosen to have maximum representability by construction, the enhancement of representability of the analytic orbitals require numerical optimization of parameters used in defining those orbitals.

4.2.1 Bond-order in CHAWO basis

To derive an expression of bond-order(BO) similar to that proposed by Mayer[13,138] , we start with the traditional or classical definition of BO involving the i-th and j-th atomic orbitals for a given spin:

$$\mathrm{B}_{\vec{R}'\vec{R},ij} = \frac{n^{+}_{\vec{R}'\vec{R},ij} - n^{-}_{\vec{R}'\vec{R},ij}}{2},$$

$n^{\pm}_{\vec{R}'\vec{R},ij}$ being the occupation of the bonding(+) and anti-bonding(-) orbitals considered in the CHAWO basis as:

$$\phi^{\pm}_{\vec{R}'\vec{R},ij} = \frac{1}{\sqrt{2}}\left(\Phi_{\vec{R}',i} \pm \Phi_{\vec{R},j}\right),$$

Within the subspace of KS states:

$$\mathrm{B}_{\vec{R}'\vec{R},ij} = \mathrm{Re}[\langle\Phi_{\vec{R}',i} \mid \hat{P} \mid \Phi_{\vec{R},j}\rangle]$$
$$= \sum_{\vec{k}}^{BZ}\sum_{l}^{N_{KS}}\frac{f_{\vec{k},l}}{N_k}\mathrm{Re}[e^{i\vec{k}.(\vec{R}'-\vec{R})}U(\vec{k})^{*}_{li}U(\vec{k})_{lj}] \qquad (4.11)$$

where $\hat{P}$ is the projection operator for a given spin:

$$\hat{P} = \sum_{\vec{k}}^{BZ} \sum_{l}^{N_{KS}} \mid \psi_{\vec{k},l}^{KS} \rangle f_{\vec{k},l} \langle \psi_{\vec{k},l}^{KS} \mid$$

$f_{\vec{k},l}$ being the occupancy of the l-th KS state with wave-vector $\vec{k}$. $B_{\vec{R}'\vec{R},ij}$ in (4.11) is essentially the Coulson's bond order(CBO),[146] used primarily in case of a single orbital per atom, where i and j effectively become the atom indexes. For a given covalent bond, CBO values, as evaluated in (4.11), can be positive or negative depending on the relative phase of the two orbitals involved. This indicates that CBO values can not be associated with any form of electron population. In fact, the total number of electrons for a given spin:

$$
\begin{aligned}
N_e &= \frac{1}{N_k} \sum_{\vec{k}}^{BZ} \sum_{l}^{N_{KS}} \langle \psi_{\vec{k},l}^{KS} \mid \hat{P} \mid \psi_{\vec{k},l}^{KS} \rangle \\
&= \frac{1}{N_k} \sum_{\vec{R}} \sum_{j}^{N} \langle \Phi_{\vec{R},j} \mid \hat{P} \mid \Phi_{\vec{R},j} \rangle \\
&= \frac{1}{N_k} \sum_{\vec{R}} \sum_{j} B_{\vec{R}\vec{R},jj} \\
&= \sum_{A} \sum_{j \in A} B_{00,jj} = \sum_{A} Q_A
\end{aligned}
\tag{4.12}
$$

Q_A being the number of electrons which can be associated with atom A. Notably, Q_A is analogous to the Mulliken's *gross atomic population*,[147] which is same as the *net atomic population* in case of orthonormal basis, like the CHAWOs, since the *overlap population* vanishes due to the orthonormality of the basis in the Mulliken's population analysis scheme. Eqn.(4.12) also reiterates that the CBO values can not be used in partitioning of electrons into atoms or bonds since they do not contribute to the total number of electrons, whereas, the general classical notion of bond-order is that it is half the total number of electrons shared in a covalent bond including both the spins.

However, using the indempotency of $\hat{P}$ for integral occupancy of states for a

given spin, we can write:

$$
\begin{aligned}
N_e &= \frac{1}{N_k} \sum_{\vec{k}}^{BZ} \sum_{l}^{N_{KS}} \langle \psi_{\vec{k},l}^{KS} \mid \hat{P}\hat{P} \mid \psi_{\vec{k},l}^{KS} \rangle \\
&= \frac{1}{N_k} \sum_{\vec{R}} \sum_{j}^{N} \langle \Phi_{\vec{R},j} \mid \hat{P}\hat{P} \mid \Phi_{\vec{R},j} \rangle
\end{aligned}
\tag{4.13}
$$

Inserting $\sum_{\vec{R}} \sum_{l}^{N} \mid \Phi_{\vec{R},l} \rangle \langle \Phi_{\vec{R},l} \mid$ between the two $\hat{P}$ in (4.13) we obtain:

$$
\begin{aligned}
N_e &= \frac{1}{N_k} \sum_{\vec{R}} \sum_{j}^{N} \sum_{\vec{R}'} \sum_{l}^{N} B_{\vec{R}\vec{R}',jl} B_{\vec{R}'\vec{R},lj} \\
&= \sum_{j}^{N} \sum_{\vec{R}'} \sum_{l}^{N} B_{0\vec{R}',jl} B_{\vec{R}'0,lj}
\end{aligned}
\tag{4.14}
$$

using (4.11). In (4.14), for an atom in the 0-th unit-cell, all other atoms in the 0-th or in any other unit-cell($\vec{R}'$) can be generalized as neighbors. Therefore we can generalize (4.14) and partition N_e as:

$$
\begin{aligned}
N_e &= \sum_{j}^{N} \sum_{l}^{N \times N_k} B_{jl} B_{lj} \\
&= \sum_{A}^{N_{atom}} \left[\sum_{j \in A} \sum_{l}^{N \times N_k} B_{jl} B_{lj} \right] \\
&= \sum_{A}^{N_{atom}} \left[\sum_{j \in A} \left[\sum_{l \in A} B_{jl} B_{lj} + \sum_{l \notin A}^{N \times N_k} B_{jl} B_{lj} \right] \right] \\
&= \sum_{A}^{N_{atom}} \left[\sum_{j \in A} \sum_{l \in A} B_{jl} B_{lj} + \sum_{j \in A} \left(\sum_{B(\neq A)}^{N_k N_{atom}} \sum_{l \in B} B_{jl} B_{lj} \right) \right] \\
&= \sum_{A}^{N_{atom}} \left[\sum_{j \in A} \sum_{l \in A} B_{jl} B_{lj} + \sum_{B(\neq A)}^{N_k N_{atom}} \left(\sum_{j \in A} \sum_{l \in B} B_{jl} B_{lj} \right) \right] \\
&= \sum_{A}^{N_{atom}} \left[Q_{AA} + \sum_{B(\neq A)}^{N_k N_{atom}} Q_{AB} \right]
\end{aligned}
\tag{4.15}
$$

where Q_{AA} is the *net atomic population* of atom A and the Q_{AB} is the *overlap*

population between atoms A and B, as defined by Mayer[134]. Note that this version of overlap population is different from the Mulliken's overlap population since the later is zero for orthonormal basis. Therefore for an isolated molecule ($N_k = 1$):

$$
\begin{aligned}
N_e &= \sum_A^{N_{atom}} Q_{AA} + \sum_A^{N_{atom}} \sum_{B(\neq A)}^{N_{atom}} Q_{AB} \\
&= \sum_A^{N_{atom}} Q_{AA} + \sum_{\substack{\text{unique} \\ \text{atom pairs}}}^{N_{atom}(N_{atom}-1)/2} 2Q_{AB},
\end{aligned}
$$

(4.16)

since $Q_{AB} = Q_{BA}$. For periodic systems with N_{atom} number of atoms inside an unitcell:

$$
\begin{aligned}
N_e &= \sum_A^{N_{atom}} Q_{AA} + \sum_{\substack{\text{unique} \\ \text{atom pairs} \\ \text{within unitcell}}}^{N_{atom}(N_{atom}-1)/2} 2Q_{AB} \\
&\quad + \sum_A^{N_{atom}} \sum_B^{(N_k-1)N_{atom}} Q_{AB},
\end{aligned}
$$

(4.17)

The quantity Q_{AB} was originally introduced as a bond-index[139] following Wiberg's interpretation of *covalent bonding capacity* of a basis orbital, say Φ_j, as:

$$
b_j = 2P_{jj} - P_{jj}^2
$$

(4.18)

where $P = \sum_\sigma P^\sigma$. As easily seen, b_j will be 1 if Φ_j takes part in a bonding orbital,

and 0 if it is one in a lone-pair. Using the indempotency property of $\hat{P}$ again,

$$b_j = P_{jj}^2$$

which implies

$$b_j = \sum_{l \in A} P_{jl} P_{lj} + \sum_{l \notin A} P_{jl} P_{lj}$$

with more than one orbitals per atom. Noting $P_{ij} = B_{ij}$ shown in Eqn.(4.11), we can therefore write for atom A if $j \in A$:

$$\sum_{j \in A} b_j = Q_{AA} + \sum_{B \neq A} Q_{AB},$$

where

$$Q_{AB} = \sum_{j \in A} \sum_{i \in B} q_{AB,ij},$$

with

$$q_{AB,ij} = P_{ji} P_{ij} \mid_{i \in B, j \in A} .$$

Thus with more than one basis orbitals centred on A, the net *covalent bonding capacity* or the valency V_A of atom A is assessed after subtracting the intra-atomic term Q_{AA} from the net $\sum_{j \in A} b_j$:

$$V_A = \sum_{j \in A} b_j - Q_{AA} = \sum_{B \neq A} Q_{AB}. \tag{4.19}$$

This notionally identifies $2Q_{AB}$, which is the net overlap population between A and B, as the bond order in agreement with Eqn.43-44 in Ref.[134], in the classical sense of valency of an atom in a covalent system.

In this work we calculated bond orders as defined by $2Q_{AB}$ and their decomposition in orbital pairs, as a function of orientation of the CHAWOs, in order to pin point the orientation which maximises the BO contribution from the dominant orbital pairs for a given pair of nearest neighboring atoms. Since the net BO remains

largely constant over different orientations [Fig.4.1] the dominant contribution can be numerically traced as the maxima of the variance of contributions from different pairs for a given coordination. In fact, the set of CHAWOs which maximizes the sum of standard deviation of BO contributions of all the coordinations in a given system should in principle pin point to the orientation of CHAOs which would render CHAWOs such that a minimum of them would maximally incorporate covalent interaction along all coordinations, led by the nn coordinations. We therefore propose to seek the maxima of:

$$\Omega = \sum_A \sum_{B \neq A} \sum_{i \in A} \sum_{j \in B} \frac{(\bar{q}_{AB} - q_{AB,ij})^2}{n_A n_B}, \tag{4.20}$$

where

$$\bar{q}_{AB} = \sum_{i \in A} \sum_{j \in B \neq A} \frac{q_{AB,ij}}{n_A n_B},$$

n_A and n_B being number of orbitals centered on atoms A and B respectively. CHAOs corresponding to the maxima of Ω can thus be referred as *maximally valent hybrid atomic orbitals*(MVHAO). Correspondingly, WFs constructed using the template of MVHAOs can thus be referred as the *maximally covalent Wannier functions*(MCWF).

Notably, for systems with inequivalent atoms, finding Ω is in principle a multi-variable maximization problem. In this work however we have restricted to systems where single variable maximization of Ω is sufficient or effectively so. For example, the symmetry of cyclopropane, diborane and water molecules allow us to vary a single angle α marked in Fig.4.1(1a,3a) and Fig.4.2(4a). Different sets of non-degenerate sp^3CHAOs are constructed using UAOs following the hybridization matrix given in Eqn.(4.4) with $a = b$. A 3×3 variant of the same hybridization matrix is used to construct non-degenerate sp^2CHAOs for cyclobutadiene. Notably, when the CHAOs are transferred to any given system from their atomic nurseries they are oriented such that they maintain their intra-atomic orthonormality. In case of cyclopropane, diborane and water molecules the principal symmetry axis of the

transferred CHAOs coincides with the axis bisecting the HCH, HBH or HOH angles. For ammonia, we have used the hybridization matrix given in Eqn.(4.3). The orientation of the CHAWOs remain practically unaltered compared to the corresponding CHAOs.

4.3   Computational details

All the ground state geometries as well as ground state electronic structures are calculated using the Quantum Espresso (QE) code[125] which is a plane wave based implementation of density functional theory (DFT).[9,27] The BFGS scheme has been used to obtain the relaxed structures within the pseudo-potential used. The KS ground states are calculated within the Perdew-Burke-Ernzerhof (PBE)[148] approximation of the exchange-correlation functional. Plane wave basis with kinetic energy cutoff of of 60 Rydberg has been used for all systems considered in this work.

For construction of WFs, CHAWOs and calculation of TB parameters and BO, we use our in-house implementation which used the KS states computed by the QE code. Towards construction of n-sp^2 and n-sp^3 CHAOs, the sp^3 HAOs for $n = 2$ are constructed in this work for B, C, N, O using the lowest four KS states which include a triply degenerate block.

4.4   Results and discussion

To choose the criteria of seeking optimal orientation of CHAOs as they take part in covalent bonding, we can in principle take recourse to the different descriptions of covalent bond based on different physical aspects of covalent interaction, for the same coordination. Different choices of bonding orbital along a nn coordination, can differ on the degree of sharing of electrons between atoms, or the degree of spatial localization of electrons participating in the bond, besides the energetics of the orbitals. Similarly, different choices of orientations of CHAOs would differ not only on the degree of sharing of electrons they facilitate between atoms, but also on

Cyclopropane:
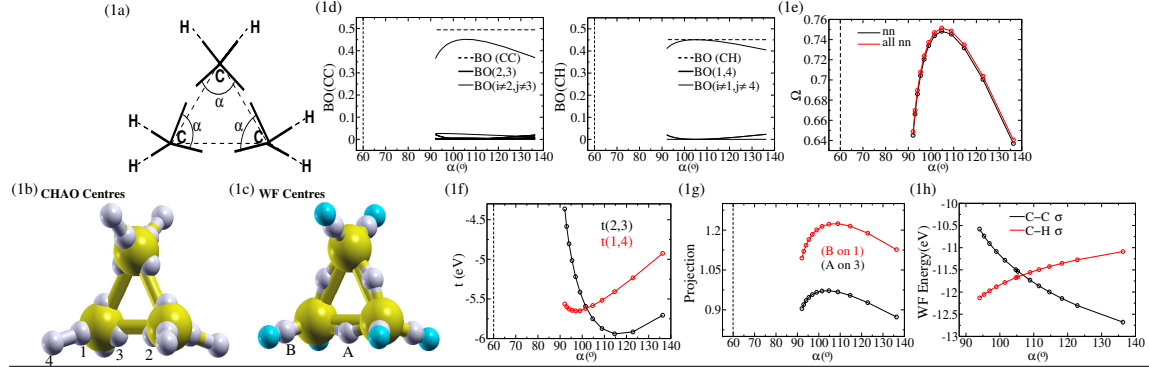
Cyclobutadiene:
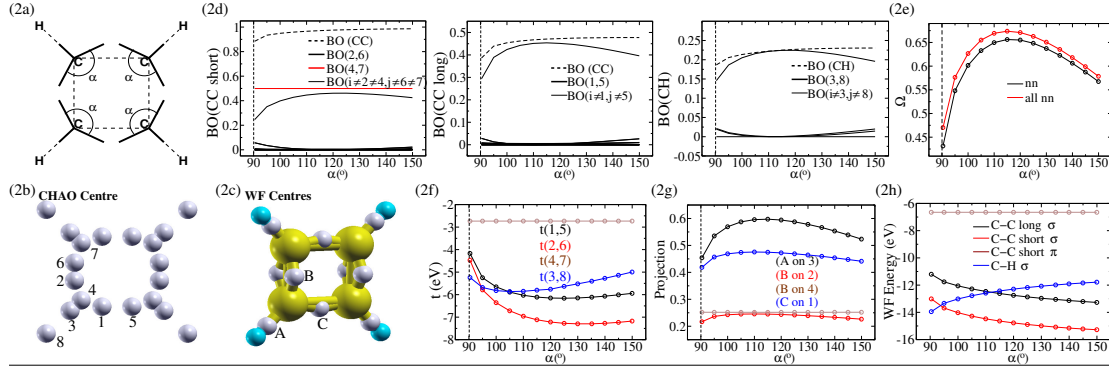
Diborane:
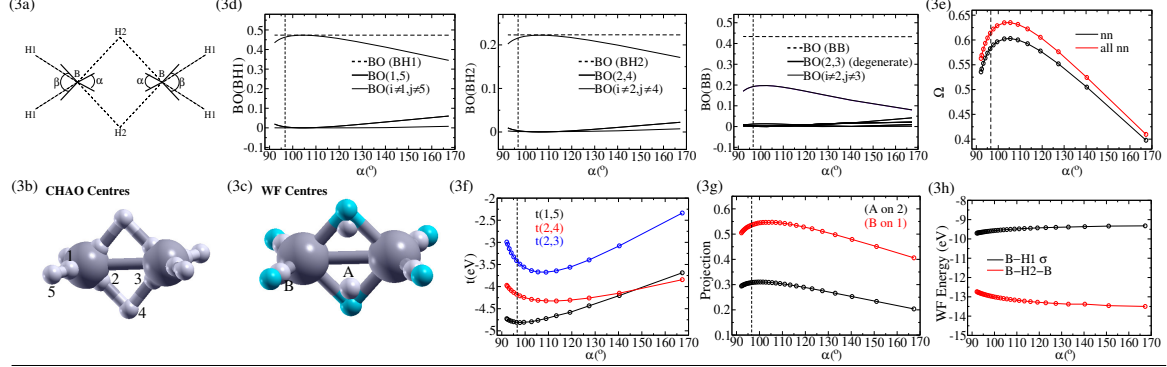
Figure 4.1: Plotted as function of relative angle α[(a)] between CHAOs, variations of: (d) net BO and BO contributions from CHAWO pairs (whose charge centres are marked in (b)), (e) Ω[Eqn.(4.20)], (f) hopping parameter between the major overlapping CHAWOs, (g) projection of template free WFs (whose charge centres are marked as in (c)) on CHAWOs marked in (b), (h) energetics of WFs made with template of CHAOs.

energetics of hopping of electrons through them, which has bearing on the strength of the covalent interaction they would support.

Since systems with non-ideal bond angles have been reported to have bent

bonds,[118] making a choice of an optimal orientation would also thus amount to substantiating the bent nature from the deferent perspectives of covalent interaction. For a given nn coordination, we therefore first look for the peak for Ω [Eqn.4.20]to find the orientation of the CHAOs which maximally hosts the covalent interactions as described by BO. Secondly, the maxima of projection of the template free maximally localized bonding WFs on CHAWOs, with the aim of seeking the CHAOs which would lead to the most localized description of the covalent interaction pointing arguably to the shortest path of tunneling of electrons. And thirdly the maxima of the magnitude of the hopping parameter(t) between the two major overlapping CHAWOs to find the energetically most favourable route of tunneling of electron for the given coordination. Symmetry of cyclopropane allows a single variable maximization of Ω with one independent parameter in the hybridization matrix. As evident in Fig.4.1(1d), the relative angle α_{BO}, which is the α where the dominant BO contribution maximize for a given coordination, are close for C-C and C-H coordinations, and thus coincide with α_Ω which is where the Ω [(1e)] maximizes.

The value of α_{WF}, which is the α where the dominant projection of the template free MLWF on CHAWOs maximize[Fig.4.1(1g)], for both the coordinations, is also close to α_Ω - at around 105°. Thus the CHAWOs of C at α_Ω, namely, the MVHAOs of C as defined above, as well as the CHAWOs of C which have maximum overlap with the MLWFs representing the bonds, both have similar orientation and deviate from the directions of C-C and C-H by about 22.5° and 0.4° respectively. Therefore for cyclopropane both the kinds of bonding orbitals - MLWFs as well as MCWFs, are essentially same. Such identical nature of MLWFs and MCWFs can be attributed to the fact that the charge density between the C atoms in this case in effect completely deviate away from the direction of coordination. In fact, the similarity of MLWFs and MCWFs exhaustively substantiate the strictly bent nature of the C-C sigma bonds. Interestingly, while the values of α_{BO} and α_{WF} coincides with α_Ω, the values of α_t, which is the α where $|t|$ maximizes[Fig.4.1(1f)] for the major overlapping CHAWOs, occur respectively at lower and higher angles than α_Ω for the C-H and C-C coordinations. Such a trends of α_t values is consistent with the fact that the

Water:
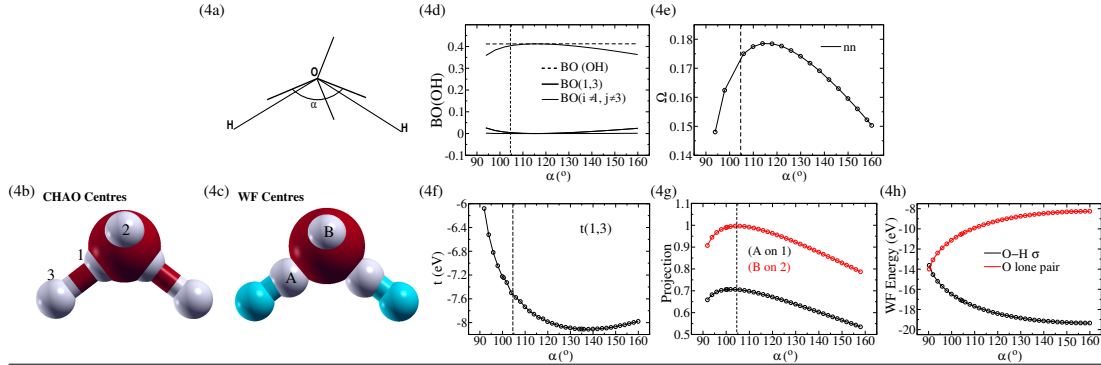
Ammonia:
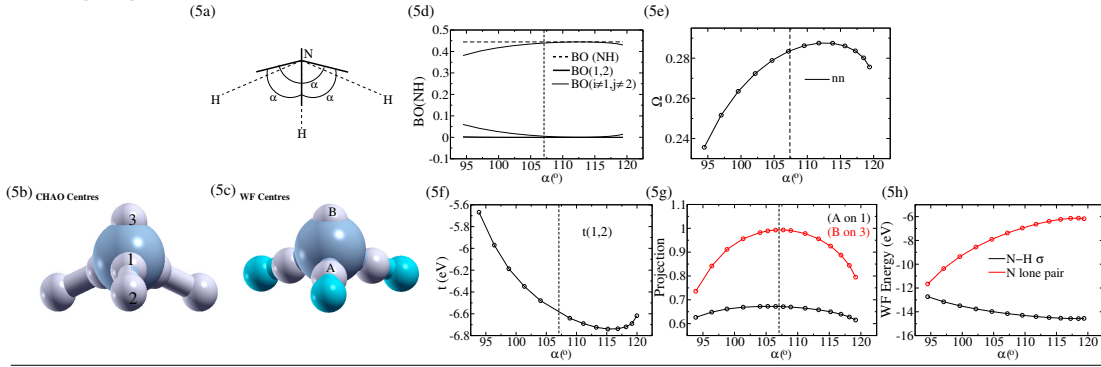
Figure 4.2: Similar to Fig.4.1, Plotted as function of α[(a)], variations of: (d) net BO and BO contributions from CHAWO pairs marked in (b), (e) Ω, (f) hopping parameter between the major overlapping CHAWOs, (g) projection of template free WFs marked as in (c), on CHAWOs marked in (b), (h) energetics of WFs made with template of CHAOs.

energies of the C-Hσ and C-Cσ WFs constructed based on template made of CHAOs, show a crossing[Fig.4.1(1h)] around α_Ω, with the C-C(C-H)σ being lower in energy below(above) α_Ω. These trends clearly suggest a competing preference of the two bonds, to deviation or "bending" from their respective directions of coordinations, above and below α_Ω.

In case of cyclobutadiene, the optimization of CHAWOs of C atoms is essentially a problem of two variable maximization of Ω owing to the lack of symmetry about C due to the inequivalent C-C bonds. However, motivated by the small deviation of MVHAOs from the C-H coordination in cyclopropane, we limit optimization of CHAOs for cyclobutadiene to their symmetric orientations about the C-H coordination, as evident in Fig.4.1(2a). Within such a constraint, the dominant BO

contributors for the C-H and the longer C-C coordination occurs between 110° and 115° [Fig.4.1(2d)], while it is about 120° for the shorter C-C coordination, leading to an α_Ω arond 115°, implying a deviation of MVHAOs from both the shorter and longer C-C coordinations by about 12°.

Similar to cyclopropane, firstly, the values of α_{WF} [Fig.4.1(2g)] in this case are also close to the respective values of α_{BO}, and secondly, the values of α_t [Fig.4.1(2f)] for C-H σ and both the C-Cσ bonds, are respectively lower and higher than the α_Ω value. Competing preference to deviation from direction of coordination, as seen in cyclopropane, is also evident in cyclobutadiene from the variation of energetics of the C-H σ and the C-Cσ bonds [Fig.4.1(2h)] with α.

Next we calculate CHAWOs for diborane molecule well known for the B-H-B three centre two electron bond, which in this work is marked by the BO values of B-B and B-H2 [Fig.4.1(3f)] of about 0.85 and 0.45 per spin, implying a total of about $(0.85 + 2 \times 0.45) = 1.75$ electrons per spin for each of the two B-H-B bonds. Symmetry of diborane allows single parameter maximization of Ω . Values of α_{BO} [Fig.4.1((3d))], although are generally close to α_0, are larger for the B-H1 and B-H2 coordinations than that for the B-B coordination, leading to an intermediate value of α_Ω [(3e)] close to α_0, implying a deviation of MVHAOs by about 4° from both the B-H1 and B-H2 coordinations. Deviation of the α_{WF} values[Fig.4.1(3g)] from α_0 for the B-H2-B and B-H1 WFs are similar to those of the respective α_{BO} values. Thus in this case also the MLWFs and the MCWFs suggest similar deviations of the B-H2-B and B-H1 bonds from the directions of B-H2 and B-H1 coordinations. Among the hopping parameters, like we saw in case of cyclopropane and cyclobutadiene, the deviation of α_t [Fig.4.1(3f)] of the B-H1, which is B-H σ in this case, is the least, which is also corroborated by the energetics[(3h)] of the template based WFs, as it shows that the B-H1 bonds do not prefer deviation, while the B-H2-B three centre bonds do. Thus the competing energetics of B-B covalent interaction mediated by the H, and that of the C-H σ bonding, with the latter dominating over the former due to multiplicity, determines the structure of diborane.

Deviation of angle(α_Ω) between MVHAOs in cyclopropane, and diborane, from
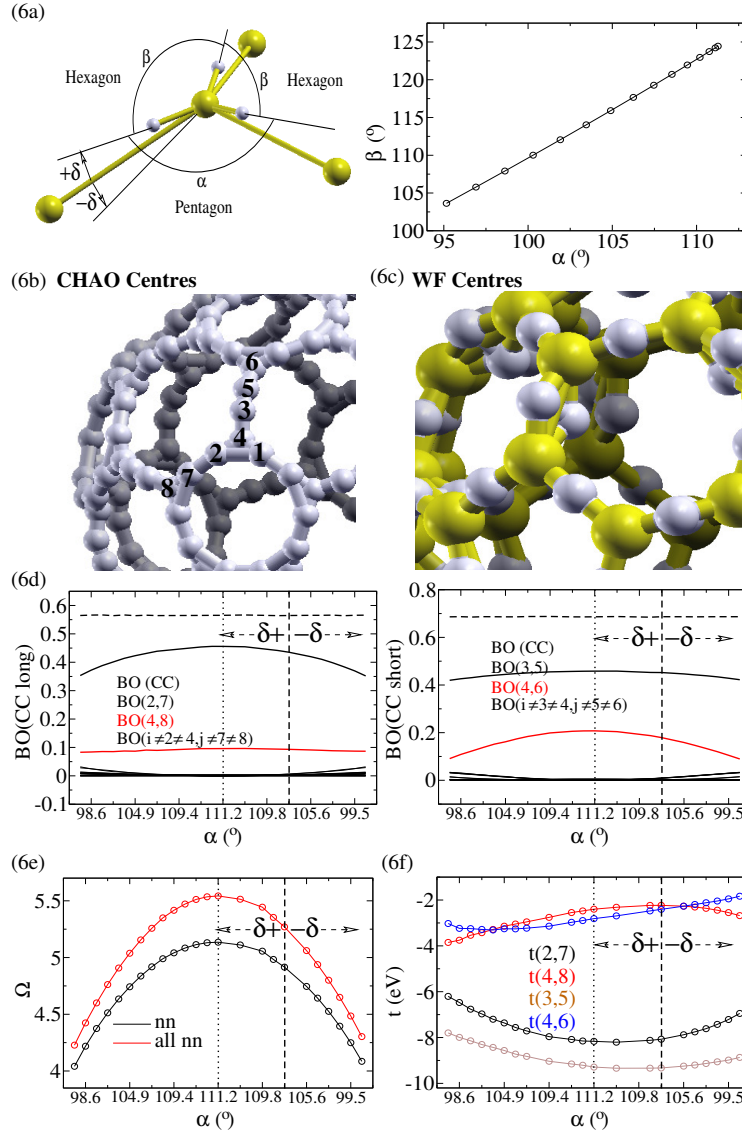
Figure 4.3: Plotted as function of α as shown in (6a) - (6d) net BO and BO contributions from the Wannierized pair of CHAOs marked in (6b), (6e) Ω, (6f) hopping parameter between the major overlapping CHAWOs. Charge centres of template free MLWFs are shown in (6c). Note that same values of α recurs about the dotted line which corresponds to co-planarity of α and β : $\alpha + 2\beta = 360°$. The (α, β) trajectory considered is plotted in 6a.

109° of ideal tetrahedra, is indicative of the fact that the lowering of kinetic energy due to formation of a σ bonding orbital is competing with the lowering of electron repulsion at each C atom. The same can be seen in case of cyclobutadiene as well, where α_Ω is between 110 degrees and 120 degrees. Whereas in case of a perfect tetrahedral or honeycomb coordinations minimizations of kinetic energy in the di-

rection of coordination and potential energy in the vicinity of atoms will cooperate with each other to consolidate tetrahedral coordination leading to robust crystal structures.

For molecules of water and ammonia[Fig.4.2], each with only one kind of coordination, α_{BO} [Fig.4.2(4d,5d)] and α_{Ω} [(4e,5e)] are same, and are clearly higher than their corresponding α_{WF} values [(4g,5g)], which interestingly almost coincides with the actual bond angles α_0 for both the molecules. Therefore, while the template free MLWFs suggest no deviation in effect, the MCWFs would suggest deviations of about 10° and 5° respectively from directions of of O-H and N-H coordinations. Such substantial deviation between MLWF and MCWF can be attributed to the fact that in these molecules the charge density exists along the direction of coordinations as well as with modest deviation from it, allowing the MLWFs and MCWFs to consolidate using different sets of states as majority contributors. Values of α_t [Fig.4.2(4f,5f)]for both the O-H and N-H σ bonds clearly suggest even larger deviations, which is consistent with the energetics[Fig.4.2(4h,5h)] of the template based WFs for both the molecules, since in both cases the bonding WFs energetically prefers deviation which is opposed by the lone pairs.

In C_{60} the two different C-C bonds - the shorter ones shared by two adjacent hexagons, and the longer ones shared by hexagons with adjacent pentagons, demand a two parameter maximization of Ω in terms of α and β [Fig.4.3(6a)]. In this work however we restrict effectively to a one parameter optimization by seeking maxima of Ω along the (α, β) trajectory plotted in Fig.4.3(6a), which nevertheless brings out the key aspect about the true nature of the MVHAOs. For both the C-C bonds the α_{BO} [Fig.4.3(6d)] and α_{Ω} [(6e)] occur at around 111° where the three n-sp^3orbitals in effect become co-planar n-sp^2 and the fourth one becomes pure p_z implying a $+\delta$ deviation of MVHAOs by about 13° and 11° from the direction of longer and shorter C-C coordination respectively. Although the MLWFs [Fig.4.3(6c)] in this case renders the π bond exclusively along the shorter C-C coordination since the longer C-C bonds make pentagons, comparable BO contribution exists between $p_z$orbitals along the longer C-C [(6d)] coordination as well. In fact the BO values

along the two C-C coordinations are much comparable, in exception to that implied by MLWFs. Notably, for both the C-C, α_t for $t(2,7)$ and $t(5,3)$ suggests strongest σbond with similar or marginally less $+\delta$ deviation of participating CHOAs from the C-C coordinations, compared to that implied by α_Ω. However, for the shorter C-C, the value of α_t [Fig.4.3(6f)] for $t(4,6)$ suggests stronger πbond due to much larger $+\delta$ deviation from C-C coordination than that implied by α_Ω, which would push the major lobe of the unpaired n-sp^3orbital inside the fullerene cage. Thus the α_Ω allows strong enough σbonds but a weaker π-bond, reiterating that it is primarily the C-C σbonds constituting the pentagons which are responsible for the curved nature surfaces made of three coordinated carbon atoms with pentagon surrounded by hexagons.
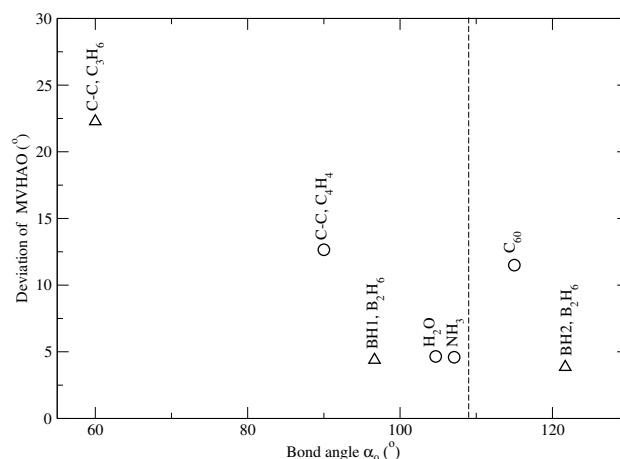
Figure 4.4: Plotted as a function of α_0, the deviation of the MVHAOs from the coordination segment mentioned above the data points. The dashed line is at the ideal bond-angle for tetrahedral coordination.

The deviation of MVHAOs from the direction of coordinations found in all the systems studied in this work is summarized in Fig.4.4, where the deviations of MVHAOs centred on four(three)-coordinated sites, are shown by up-traingles(circles). Deviations of such MVHAOs increases in effect linearly with the degree of lowering of bond angle from the ideal tetrahedral bond-angle, with clear pinch-off at the ideal bond-angle. Deviations of MVHAOs centred on three coordinated sites also appears to approach pinch-off at the ideal tetrahedral bond-angle with increasing tetrahedrality of the three nn coordinations and the lone-pair. Substantial deviations in

case of cyclobutadiene and C_{60} are rooted at substantial differences among their bond-angles. As obvious, the effectiveness of MVHAOs as minimal basis increases with their increasing deviation from nn coordinations.

4.5 Conclusion

In search of an optimally directed basis, we begin this work with construction of non-degenerate *custom hybridized atomic orbitals*(CHAO) with variable orientation, from the degenerate set of hybridized atomic orbitals, in the basis of KS states of isolated atoms. We next formulate Mayer's bond order in the basis of the Wannierized counterparts of the CHAO, constructed from the KS states of a given system, and introduce the *maximally valent hybrid atomic orbitals* (MVHAO) and the corresponding template based WFs as the *maximally covalent Wannier functions* (MCWF), and use them to substantiate the deviation of hybrid atomic orbitals from directions of coordinations as they participate in covalent bonding, as summarized in Fig.4.4, leading to the bent nature of such bonds, in a host of molecules with non-ideal bond angles. Through comparison of bond-order(BO) contributions and hopping parameters from the Wannierized pairs of CHAOs, and their overlap with template free maximally localized Wannier functions(MLWF), we point out how maximally covalent representation of a given coordination can differ from its maximally localized, and energetically favourable representations of covalent interactions in these systems, shedding light on different perspectives of inter-atomic sharing of electrons in general.

Chapter 5

Optical excitation from anti-causally corrected real-time dynamics in a minimal tight binding framework

In this chapter, we demonstrate workably accurate estimation of optical excitation threshold for large systems comprising of hundreds of atoms through an anti-causally corrected(ACC) real-time dynamics(RTD) approach implemented in a minimal tight-binding basis constituted by the directed hybrid atomic Wannier orbitals. A correction to the Hamiltonian is applied anti-causally at all time steps to account for electron-hole interaction using the density-density response function. Minimality of basis and ease of transferability of parameters to large systems arises from the directed nature of the Wannierized hybrid basis orbitals used. With self-energy corrected TB parameters evaluated at the $DFT + G_0W_0$ level, the proposed ACC-RTD scheme can be systematically parametrized to render optical excitation threshold for systems of experimentally realizable length-scales through inexpensive computation.

5.1   Introduction

Over the last few decades a key motivation to study nano-structures of a different
size and shape[149,150] primarily of elemental or compound semi-conducting materi-
als, has been to manipulate light-matter interaction aimed at applications ranging
from controlled absorption, emission and harvesting of light.[151,152] In this direc-
tion elements of the p-block having valence electrons in $2p, 3p$ and $4p$ orbitals, have
been in the forefront.[18] Effective theoretical prediction of new device possibilities in
this direction thus crucially depends on accurate estimation of optical-gap of nano-
structures.[20,21,153,154] However, they still consists of few hundreds to thousands of
atoms which makes it a considerable computational challenge to compute optical
excitations accurately.

Time dependent density functional theory(TDDFT) using the LDA exchange-
correlation (xc) has been traditionally used to compute optical excitation in extended
systems.[20,153] However as system size shrinks, a more structured correlation among
electrons causes loss of accuracy of the ground-state calculation and also the de-
scription of electron-hole interaction with static local xc functionals used in DFT.
While the ground-state energetics can be improved using hybrid pseudo-potentials,[50]
the most accurate computation of the energetics of the ground-state starting with
the KS single particle levels, is obtained perturbatively as their self-energy correc-
tions due to a non-local and dynamic self-energy operator derived within the GW
approximation of the many-body perturbation theory.[15,61,155] DFT+GW compu-
tation however is expensive due to convergence of the dielectric function and the
self-energy operator, with respect to unoccupied states, typically requiring in thou-
sands. Subsequently, TDLDA calculation with scissor correction as per the shift in
single particle levels as per their self-energy corrections, has been shown to render
correct optical gap for smaller carbon nano-diamonds.[20] Scissor correction has also
been extended to the real time TDDFT[156] to account for the band-gap problem
in optical excitation. For extended systems a long-range correction has been pro-
posed[157] to approximately account for the inherent non-locality of screening, which

however considerable increases the cost of computation. The most accurate estimation of linear optical excitation is possible through solution of the Bethe-Salpeter equation(BSE)[64] in the basis of exciton amplitudes considered as products of KS single particle levels from the valence and conduction bands. The high computational cost of BSE calculation stems from convergence of the interaction kernel and the exciton amplitude with respect unoccupied states. In particular for the large nano-diamond systems considered in this work, DFT+GW and subsequent BSE calculations become computationally impossibly expensive.

In this work we propose a computationally much inexpensive alternate route to estimate optical absorption spectra, primarily the threshold up to workable accuracy, using the real time dynamics(RTD) approach, in a minimal tight-binding basis constructed from first principles. The minimal nature of the basis stems from the fact that the optimally directed hybrid orbitals,[11] maximally incorporate all covalent interactions prevalent in the system and thus represent nearest neighbor covalent bonds predominantly by a single off-diagonal element. However given the ideal nature of the bond angles in the systems consider in this work the degenerate hybrid orbitals[10] constitute the minimal basis. We have recently demonstrated effective transfer of self-energy correction from smaller reference system to much larger isomorphic systems in the basis of such directed hybrid atomic Wannier orbitals (HAWO), to render estimates for quasi-particle band-gap[10,158] of the large systems with over 90% accuracy. In this work we use self-energy corrected tight-binding parameters in the HAWO basis and introduce a justifiably parametrizable anti-causal correction to RTD which indirectly accounts for the presence of excitons in the Hamiltonian to render absorption threshold of large systems with workable accuracy comparable to GW-BSE estimates.

5.2   Methodology

First we briefly sketch the construction of the tight-binding Hamiltonian from first principles in the basis of HAWOs [10], which are constructed from the KS states of

the given system as:

$$\Phi_j(\vec{r}) = \sum_{\vec{k}} e^{i\vec{k}\cdot\vec{r}} \sum_l U_{jl} \Psi^{KS}_{\vec{k},l}(\vec{r}) \tag{5.1}$$

where the choice of gauge (U) is obtain though Lowdin symmetric orthogonalization of the template made of hybrid atomic orbitals (HAO) projected on the KS states. The four sp^3 HAOs of C or Si atoms are obtained through maximal joint diagonalization[95] of the first moment matrices corresponding to the three orthogonal direction in the basis of the lowest four KS states generated for an isolated atom using the same pseudo potential used for the nano-diamond systems. HAWOs being directed toward nearest neighbor coordination, TB parameters derived in such a basis are therefore easily transferable from smaller to larger nano-diamond systems through mapping of neighborhood. Self-energy corrected TB parameters for smaller reference systems are obtained in the HAWO basis using quasi-particle levels computed at the G_0W_0 level.[61,159]

For time dynamics we use the standard Crank-Nicholson[160] approach where the time evolution operator is approximated as:

$$\hat{U}(t+\delta t, t) = \frac{1 - i\hat{H}(\delta t/2)}{1 + i\hat{H}(\delta t/2)} \tag{5.2}$$

which is exact up to δt^2 and assumes $\hat{H}$ to remain constant over the time interval δt. In our implementation we have used a higher order formulation[160] of $\hat{U}(t+\delta t, t)$:

$$\hat{U}(t+\delta t, t) = \frac{\left(I - \frac{i\delta t}{2\hbar}H - 1/2(H\delta t/2)^2 + i1/6(H\delta t/2)^3\right)}{\left(I + \frac{i\delta t}{2\hbar}H - 1/2(H\delta t/2)^2 - i1/2(H\delta t/2)^3\right)} \tag{5.3}$$

We apply a small constant electric field across the system[161] $\vec{E}(\vec{r},t) = \vec{I}\delta(t)$ in the first time-step and revert back to the original unperturbed $\hat{H}$ from the second time-step onwards. If the $\hat{H}$ is retained unchanged for all successive steps then the absorption spectra obtained from the time evolved occupied states can be compared to the spectra obtained at the independent particle level within linear response, as demonstrated in Fig.5.1.

Photo-absorption cross-section relevant to the direction μ is calculated as:

$$\sigma_{\mu\mu}(\omega) = \frac{4\pi\omega}{c}\Im[\alpha_{\mu\mu}(\omega)] \tag{5.4}$$

where the polarizability $\alpha_{\mu\mu}(\omega)$ is calculated from the μ-th component of the time evolved net dipole-moment $\vec{p}(t)$, as:

$$\alpha_{\mu\mu}(\omega) = \frac{1}{\tilde{E}_\mu(\omega)}\int dt e^{i\omega t}p_\mu(t), \tag{5.5}$$

$\tilde{E}_\mu(\omega)$ being the Fourier transform of the applied electric field component $E_\mu(\vec{r},t)$. In effect $\tilde{E}_\mu$ is constant in ω given the pulsed nature of the applied field. The net dipole moment from the time evolved occupied states is calculated approximately as:

$$\vec{p}(t) = -e\sum_i^{occ}\sum_j \mid C_{ij}(t)\mid^2 \vec{r}_j \tag{5.6}$$

$\{\vec{r}_j\}$ being the charge centers of the directed hybrid orbital basis $\{\phi_j\}$, and the time evolved states in effect being $\left\{\psi_i(r,t) = \sum_j C_{ij}(t)\phi_j(r)\right\}$. Such a simultaneity is prevented by the inherent non-commuting nature of more than one orthogonal position operators if projected within a finite subspace. In Fig.5.1, we find good agreement of threshold and initial peaks between the IP level spectra obtained within linear response from the KS states and the RTD spectra rendered by the time evolved occupied states in the HAWO basis.

In order to compute spectra beyond the independent particle level we invoke an anti-causal correction, where Hamiltonian is updated at each time step as per the evolution of the charge density in the previous step. A correction $\{\delta V_j\}$ is added to the on-site terms of the unperturbed Hamiltonian H_0 such that the eigenstate of the modified Hamiltonian renders to charge density of the previous time step. The applied correction is anti-causal since it is derived back from $\{\delta\rho_j\}(t-\delta t)$. The $\hat{H}(t)$ is thus updated such that the instantaneous charge density will become increasingly
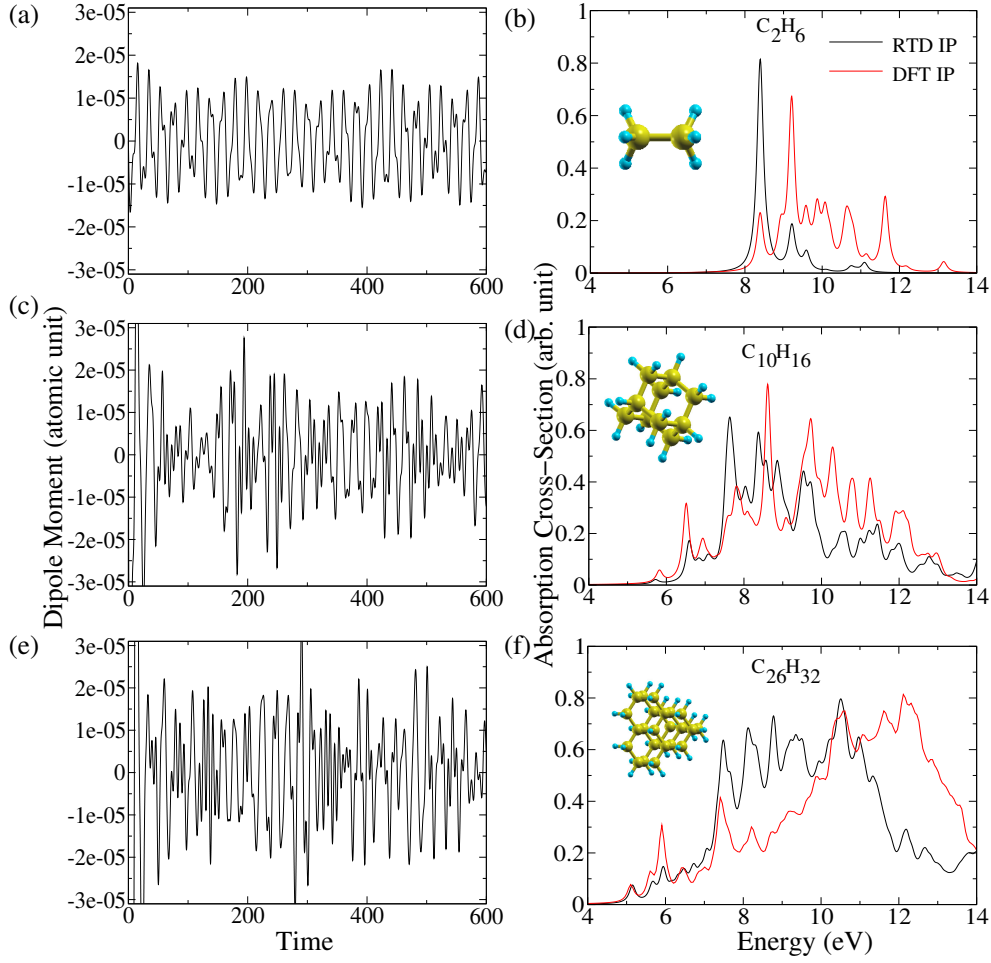
Figure 5.1: RTD(IP) polarization in the directed TB basis without anti-causal correction, for :(a) C_2H_6, (c) Adamantane, (e) Pentamantane. The corresponding RTD spectra for longer time, and the spectra obtained from the LR density-density response function computed from the KS single-particle states, for he same systems (b,d,f respectively).

similar to that of the previous step as time progresses, as we see in Fig.5.2(a). In our implementation we compare the evolving charge density at each time step to that of the ground state and use density-density response function or the dielectric susceptibility (χ) computed from the ground state wave functions in the HAWO basis.

At the outset, $\delta V(\vec{r})$ can be connected to $\delta \rho(\vec{r'})$ through χ^{-1} as

$$\delta V(\vec{r}) = \int d\vec{r'} \chi^{-1}(\vec{r}, \vec{r'}) \delta \rho(\vec{r'}).$$

With $\delta\rho(\vec{r'}) = \sum_j \delta\rho_j(\vec{r'})$, j being orbital index. We can notionally discretized $\chi^{-1}(\vec{r},\vec{r'})$ as $\chi_{ij}^{-1}\Theta(\vec{r}-\vec{r_i})\Theta(\vec{r'}-\vec{r_j})$ using non-intersecting step-functions (Θ) centered at orbital charge centers $\{r_i\}$, leading to :

$$\delta V_i(\vec{r}) = \int d\vec{r'} \sum_j [\chi_{ij}^{-1}\Theta(\vec{r}-\vec{r_i})\Theta(\vec{r'}-\vec{r_j})]\delta\rho_j(\vec{r'})$$
$$= \Theta(\vec{r}-\vec{r_i})\sum_j \chi_{ij}^{-1} \int d\vec{r'}[\Theta(\vec{r'}-\vec{r_j})]\delta\rho_j(\vec{r'}), \qquad (5.7)$$

which implies

$$\delta V_i = \sum_j \chi_{ij}^{-1}\rho_j, \qquad (5.8)$$

where $\delta V_i(\vec{r}) = \delta V_i\Theta(\vec{r}-\vec{r_i})$ and $\rho_j = \int d\vec{r'}[\Theta(\vec{r'}-\vec{r_j})]\delta\rho_j(\vec{r'})$. In our case we obtain:

$$\delta\rho_j(t) = \sum_i^{occ}(\mid C_{ij}(t)\mid^2 - \mid C_{ij}^0\mid^2, \qquad (5.9)$$

where $\{C_{ij}\}$ are the elements of the i-th wave function, which are also used to estimate χ in the static limit within linear response as:

$$\chi(i,j) = \sum_{kl}^N (f_k^0 - f_l^0)\frac{C_{li}^0 C_{ki}^{0*} C_{lj}^{0*} C_{kj}^0}{E_k^0 - E_j^0 + i\eta}, \qquad (5.10)$$

where f_i^0 and E_i^0 respectively are the occupation and energy of the i-th level in the ground state, and η is a broadening parameter.

Although partitioning the unit-cell into such non-intersecting domains around the centers of each orbitals should in-principle possible, it would also results into sharp changes in values of χ^{-1} across neighboring domains, which is unrealistic. Instead, we can relax the criterion of non-intersection and let spherical domains defined by a cut-off radius around the charge centers to enclose substantial fractions of the respective orbitals, and introduce corrections to avoid multi-valuedness of contributions to δV_i due to overlapping orbitals. The unit cell can then be partitioned into different regions of different numbers of overlapping orbitals. The total charge

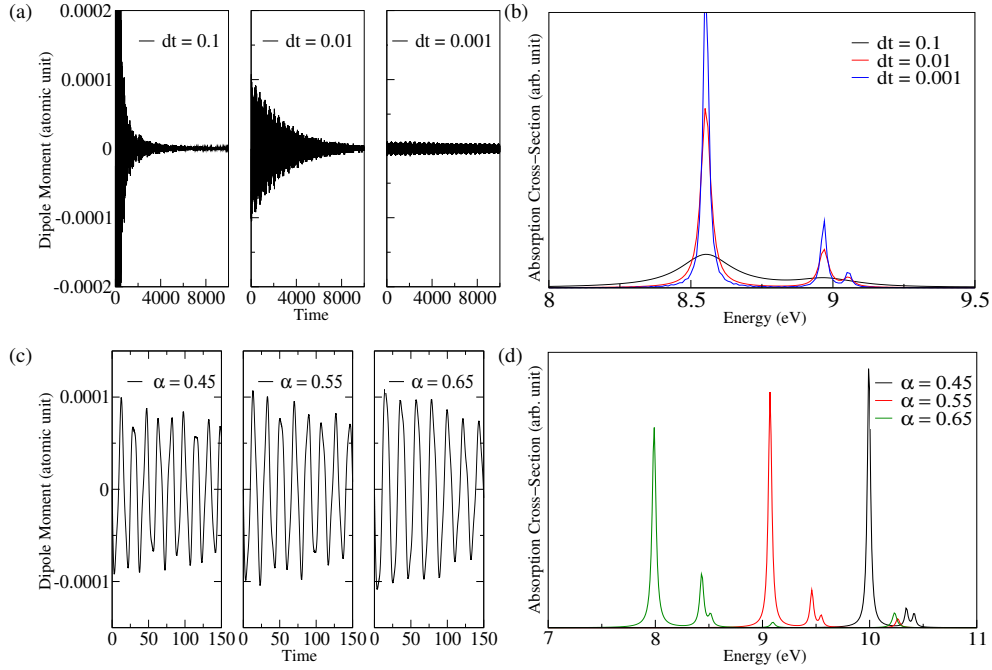Figure 5.2: Nature of anti-causally corrected polarization(a,c) and absorption spectra(b,d) for: (a,b) different time step dt with $\alpha = 0.6$, and (c,d) for different values of α with same time step $dt = 0.01$a.u..
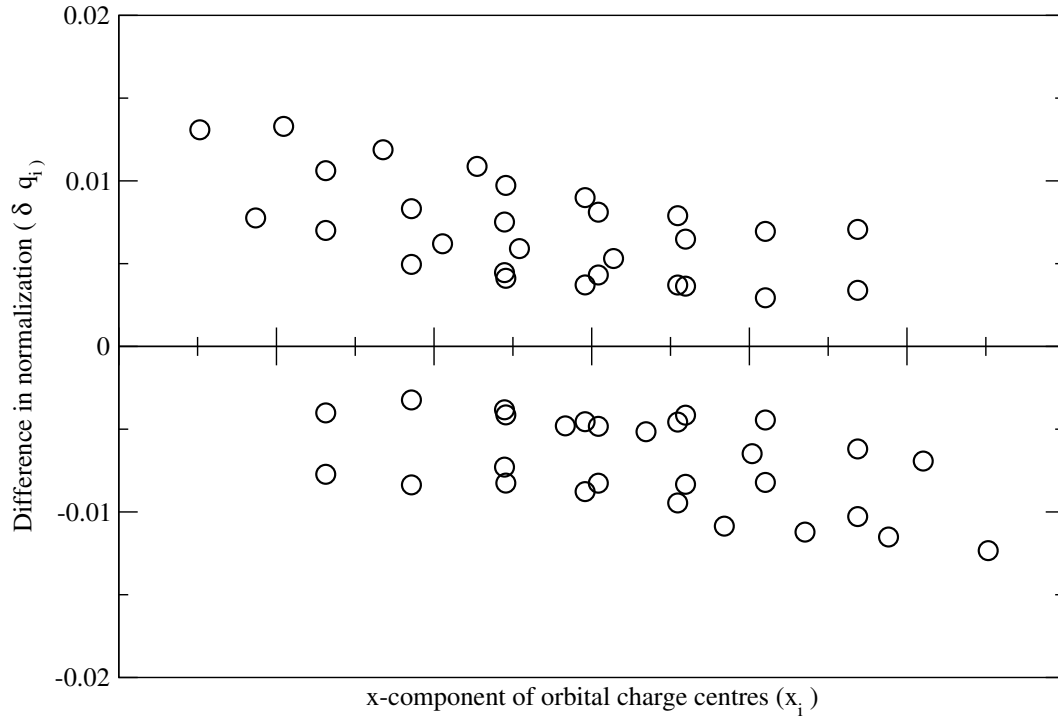

Figure 5.3: Change in charge q_i associated with orbitals due to a static electric field applied to the TB Hamiltonian of adamantane.

of an orbital can be partitioned into such regions as:

$$\rho_i = \rho_{ii} + \sum_{j \neq i} \rho_{ij} + \sum_{(j<k) \neq i} \rho_{ijk} + \sum_{(j<k<l) \neq i} \rho_{ijkl} + \dots \qquad (5.11)$$

where ρ_{ii} is the part of ρ_i which has no overlap with any other orbital, while $\{\rho_{ij,i \neq j}\}$, $\{\rho_{ijk,(j<k) \neq i}\}$ and $\{\rho_{ijkl,(j<k<l) \neq i}\}$ are parts of ρ_i in regions with 2, 3 and 4 overlapping orbitals. Similar partitioning can be done for $\delta \rho_i$ where contributions can be approximately obtained, for example, as:

$$\delta \rho_{ijk} = \delta \rho_i \frac{\rho_{ijk}}{\rho_i}. \qquad (5.12)$$

Values of the contributions would thus depend on the spherical volume considered for each of the orbitals. In this work we find that it is appropriate to consider a spherical region around the charge centers of each orbital such that the sphere encloses about 60% of the total normalization of each orbital.

Adding the contribution from the different regions, we can write:

$$\delta V_I = \sum_{j=1}^{N} \left\{ \delta V_{Ij} + \sum_{k>j}^{N} \left\{ \delta V_{Ijk} + \sum_{l>k>j}^{N} \left\{ \delta V_{Ijkl} + \dots \right\} \right\} \right\}$$

where we have followed the convention of denoting the overlap regions in an ascending order of indexes to avoid over counting. Considering average contributions from each of the regions of overlapping orbitals, we can write as:

$$\delta V_I = \sum_{j=1}^{N} \chi_{Ij}^{-1} \delta \rho_{jj} + \sum_{j=1}^{N} \sum_{k>j}^{N} \frac{1}{2} \left(\chi_{Ij}^{-1} \delta \rho_{jk} + \chi_{Ik}^{-1} \delta \rho_{kj} \right)$$

$$+ \sum_{j=1}^{N} \sum_{k>j}^{N} \sum_{l<k<j}^{N} \frac{1}{3} \left(\chi_{Ij}^{-1} \delta \rho_{jkl} + \chi_{Ik}^{-1} \delta \rho_{klj} + \chi_{Il}^{-1} \delta \rho_{ljk} \right) + \dots$$

$$= \sum_{j=1}^{N} \chi_{Ij}^{-1} \left(\frac{\rho_{jj}}{\rho_j} + \frac{1}{2} \sum_{j<k} \frac{\rho_{jk}}{\rho_j} + \frac{1}{3} \sum_{j<k<l} \frac{\rho_{jkl}}{\rho_j} + \dots \right) \delta \rho_j$$

using Eqn.(5.12), implying:

$$\delta V_I = \sum_{j=1}^{N} \chi_{Ij}^{-1} \alpha_j \delta\rho_j \qquad (5.13)$$

where

$$\alpha_j = \left(\frac{\delta\rho_{jj}}{\rho_j} + \frac{1}{2}\sum_{j<k} \frac{\rho_{jk}}{\rho_j} + \frac{1}{3}\sum \frac{\rho_{jkl}}{\rho_j} + \dots \right) \qquad (5.14)$$

The values of $\{\alpha_j\}$ are therefore a function of cut-off radius to be defined for the orbitals. The role of $\{\alpha_j\}$ is to rescale the contribution $\chi_{Ij}^{-1}\delta\rho_j$ to δV_I due to overlap of $\delta\rho_j$ with that of other orbitals $\delta\rho_{i\neq j}$.

5.3   Computational details

Ground state electronics structure of all the systems considered were calculated using the Quantum Espresso (QE) code,[125] which is a plane wave based implementation of density functional theory (DFT).[9,27] We used norm-conserving pseudo-potentials with the Perdew-Zunger (LDA) exchange-correlation[33] functional and a kinetic energy cut-off of 80 Ry for plane wave basis and four time more for charge density. Self-energy corrections to the single particle levels have been estimated at the non-self-consistent single-shot G_0W_0 level of the GW approximation implemented in the BerkeleyGW code.[127] Generalized plasmon-pole (GPP) model[15] was used to extend the static dielectric function to the finite frequencies. Quasi-particle energies were converged for pentamantane using excess of 4000 empty states. In-house implementations were used to construct HAOs and HAWOs respectively from the KS states of isolated atoms and the given systems. TB parameters in the HAWO basis were obtained using the self-energy corrected single particle levels. Self energy corrected TB parameters were transferred from reference to target systems for nano-diamonds larger than pentamantane through mapping of neighborhood beyond nearest neighbors. The IP level absorption spectra from the density-density response function has been calculated using the Yambo code.[162]

Figure 5.4: ACC-RTD based optical absorption spectra of H passivated C clusters and nano-diamonds for $\alpha = \bar{\alpha} = 0.55$ (used up to propane) and $\alpha = \alpha_H = 0.75$ (used for adamantane and beyond) corresponding to the enclosed normalization of 0.6. The dashed lines are experimental absortion thresholds [18, 19].

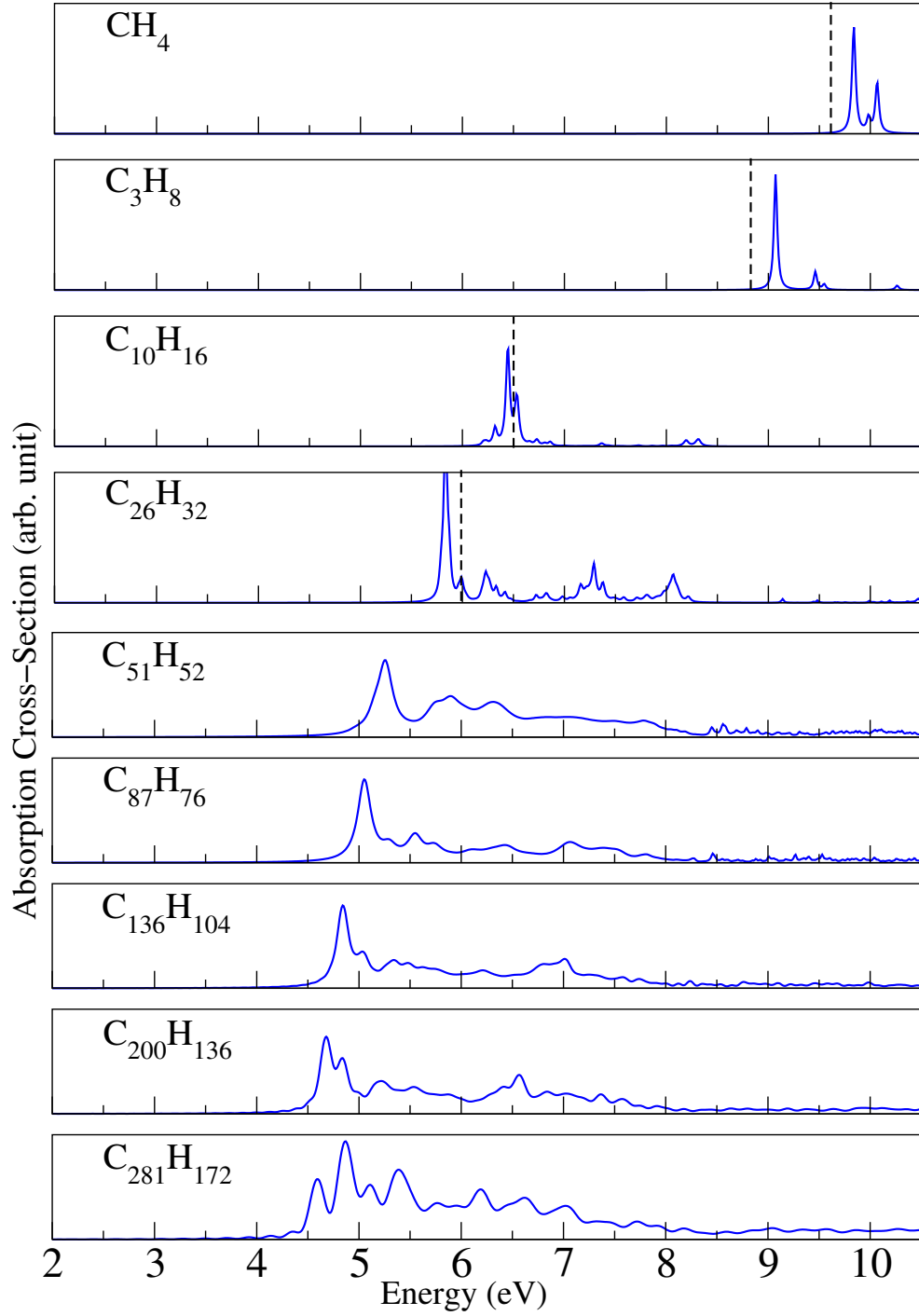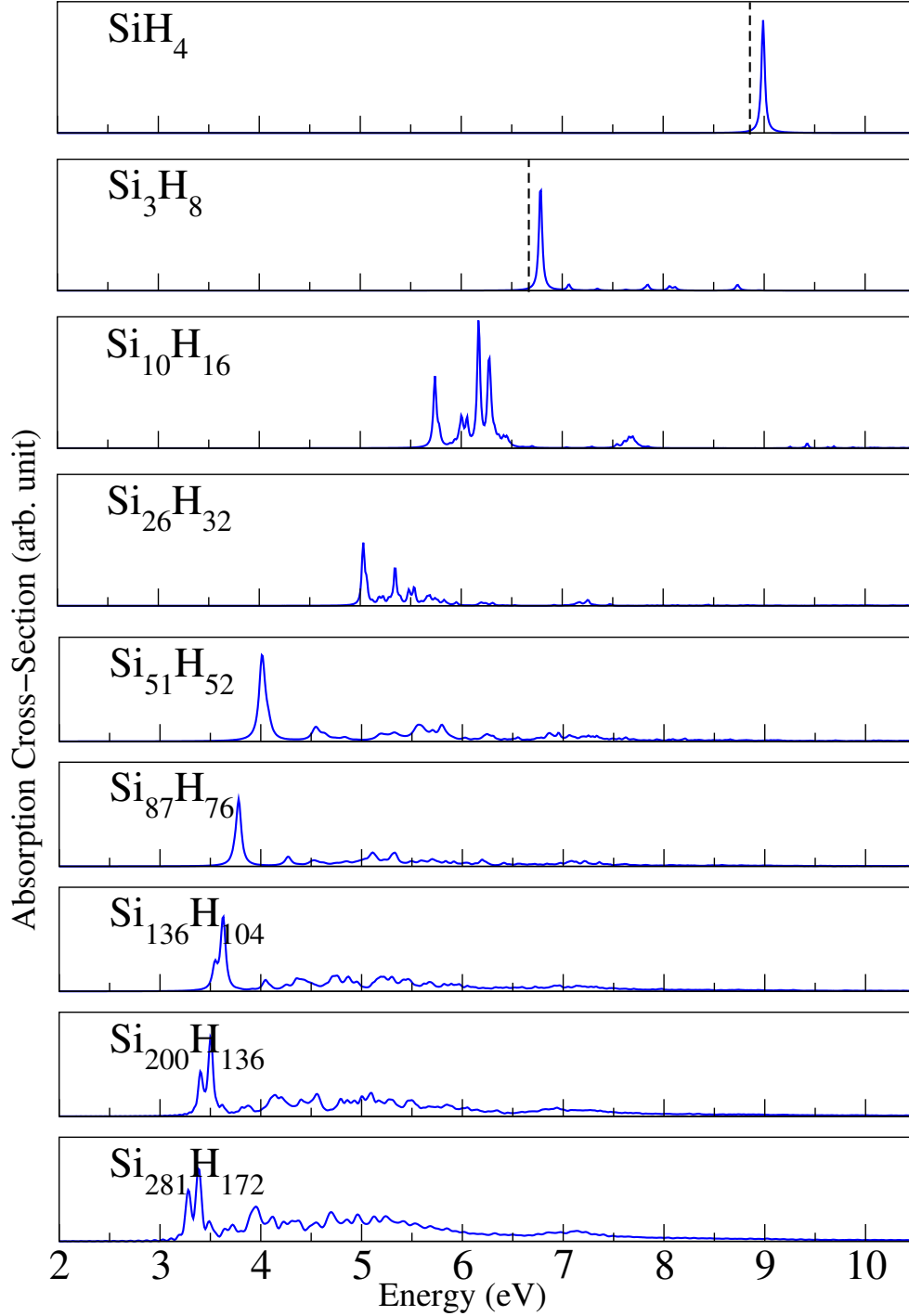Figure 5.5: ACC-RTD based optical absorption spectra of silicon clusters and nano-diamonds for $\alpha = \bar{\alpha} = 0.55$ (used for SiH_4) and $\alpha = \alpha_H = 0.65$ (used for Si_3H_8 onwards) corresponding to the enclosed normalization of 0.6. The dashed lines are lowest experimental absorption peaks approximately estimated from literature [154, 163]

.

5.4   Results and Discussion

To test the efficacy of the RTD approach at the IP level in the directed tight-binding basis within linear response, we compare the spectra obtained using RTD without any anti-causal correction to the spectra computed from the density-density response function evaluated at the IP level[162] using exactly the same KS states used to compute the TB parameters. As suggested by Fig.5.1(a,c,e) polarization fluctuation grows more non-uniform with increasing size of nano-diamonds due different contributions from different regions like vertices, surfaces and ridges.

The agreement of peak positions in two spectra [Fig.5.1(b,d,f)], particularly near the threshold, suggests nominal loss of spectroscopic information due to representation of polarization in terms of charge centers of the HAWO basis orbitals.

In Fig.5.2, we assess the effect of anti-causal correction, and duration of time step (δt), on the evolution of polarization and the consequent absorption spectra. The rate of decay in amplitude of polarization decreases with decreasing δt[Fig.5.2(a)], implying expectedly, lesser perturbation at each step, and thereby lesser mixing of states, leading to their increased life time, causing sharper absorption spectra[Fig.5.2(b)]. Whereas, the red shift of the calculated absorption threshold with increasing α is suggestive of less frequent polarization fluctuation as a result of the anti-causal correction, which is evident in Fig.5.2(c) as we see lesser number of polarization oscillation within same real time as α increases. Estimation of α is thus crucial for accuracy of the absorption threshold rendered by the anti-causally corrected RTD (ACC-RTD) proposed in this work.

As evident from the derivation of Eqn.5.14 the parameter α is essentially a correction factor to approximately account for over counting of charge density due to overlapping of orbitals while associating net charges to orbital charge centers. The approximation is exclusively based on a cutoff radius chosen to define a spherical region around the charge center of each orbital. In fact, instead of fixing the cutoff radius, we find it convenient to fix the normalization enclosed by the spherical region to determine the cutoff radius. Notably, we need not restrict hopping parameters

based on this cutoff radius in our calculation, since we use it only to derive correction
factors to account for dominant overlap of orbitals. For both the C and Si based
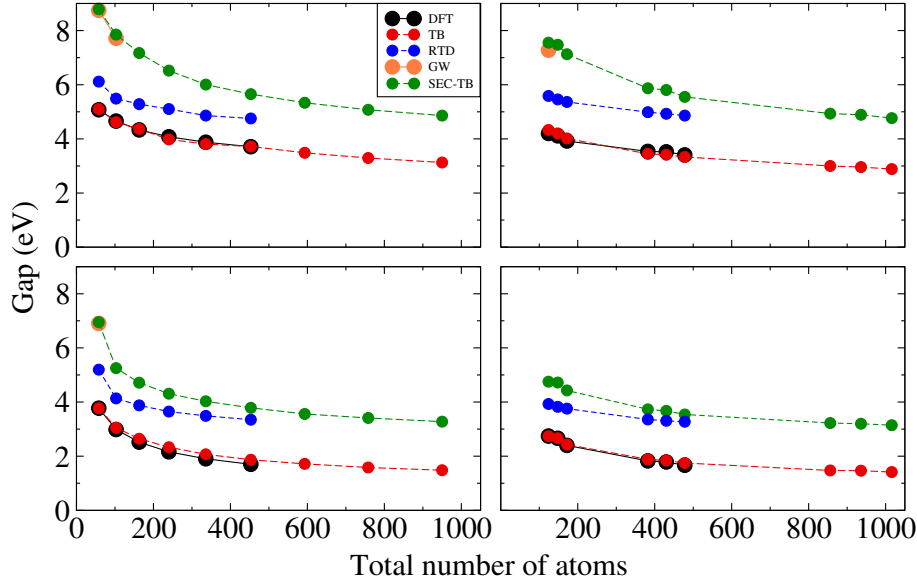
Figure 5.6: Comparison of optical absorption threshold obtained using ACC-RTD
and estimates of HOMO-LOMO gaps with and without self-energy correction, for
pyramidal (a,c) and bi-pyramidal (b,d) systems made of C (a,b) and Si (c,d).

nano-diamonds we find normalization of about 0.6, implying cut-off radius of about
0.8Å 1.22Å and 0.92Å for orbitals of C, Si and H respectively, to render values of
α which match the observed absorption thresholds, well within an error of 0.5 eV.
Similar values of enclosed normalization should therefore work for molecules and
clusters with covalent bonds made of sp^3 orbitals with principle quantum number
starting with 2 in general. Notable that these radius cutoffs are close to the the
covalent radii of C and Si in nano-diamonds and bulks. However, for stability of
the RTD evolution, we need to use a constant α since the unperturbed Hamiltonian
does not have any inhomogeneity other than the on-site terms. The choice of con-
stant α should depend on the orbitals which are the dominant contributors to the
net polarization. With growing system size the key contributions to polarization
increasingly arise from peripheral atoms due to cancellation of contributions from
neighboring atoms in the interior of the systems. This is evident in Fig.5.3, where we
have plotted contribution to polarization from different orbitals across adamantane
due to the uniform static electric field applied in the TB Hamiltonian. In fact, an

effective value of α, between $\bar{\alpha}$ and the α of the peripheral orbitals (α_H in our case), can in principle be derived as:

$$\alpha_{eff} = \frac{\sum_i \delta q_i x_i \alpha_i}{\sum_i \delta q_i x_i} \tag{5.15}$$

where δq_i is a result of a uniform electric field applied in the TB Hamiltonian comparable to that applied in the initial pulse. In this work however we find it sufficient to use a simpler average value ($\bar{\alpha} = \sum_i^N \alpha_i/N$) for the smaller systems. Accordingly, with increasing system size, from methane to adamantane ($C_{10}H_{16}$), we find that the α required to match the experimentally observed[18,19] absorption threshold, or the GW+BSE based estimation[20,21] of the onset of adsorption, evolves from being closer to ($\bar{\alpha}$), to that of the peripheral $1s$ orbitals of H (α_H). This is apparent in Fig.5.4, where the values of α used for methane and propane are that of $\bar{\alpha}$, whereas for adamatane onwards we have used α_H. In-fact, for Si nano-clusters and nano-diamonds[Fig.5.5], which are larger in size than their C based counterparts, α_H renders a satisfactory match with the observed absorption threshold[163] or the same estimated from GW+BSE,[154] for Si_3H_8 itself. It is thus expected that for both, C and Si based larger nano-diamonds, with α_H as per a radius cutoff enclosing about 0.6 normalization, ACC-RTD would render absorption threshold well within an error of 0.5eV, with self-energy corrected TB parameters transferred from pentamantane. In Fig.5.6 we summarize the comparison of the absorption threshold estimated using the ACC-RTD approach for larger nano-diamonds starting with pentamantane, an HOMO-LUMO gaps computed explicitly within DFT as well as DFT+G_0W_0, and the same estimated using TB parameters transferred from pentamantane with and without self-energy correction.

5.5   Conclusion

In this work we present an anti-causally corrected real time dynamics (ACC-RTD) approach within a self-energy corrected minimal tight-binding(TB) framework for computationally inexpensive estimation of primarily the optical absorption threshold for large systems with hundreds of atoms. The anti-causal correction based on the density-density response function computed inexpensively in the minimal TB basis constitutes the key mechanism incorporating the effect of transfer of electron from valence to conduction band. The minimal multi-orbital TB basis is constituted by the hybrid atomic Wannier orbitals(HAWO) which are constructed from the Kohn-Sham single particle states of the system and are directed towards the nearest neighbor coordination by construction. Self-energy corrected TB (SEC-TB) parameters in the HAWO basis are computed within the DFT+G_0W_0 framework for smaller clusters and transferred to large nano-diamonds through mapping of neighborhood. Thus for large systems, with transferred SEC-TB parameters, ACC-RTD parametrized as per the major contributors to dipole-moment, can be expected to render absorption thresholds comparable with GW-BSE based estimates with a small fraction of computational resource required for explicit computation.

5.6   Future Plan

So far in this chapter I have demonstrated the ACC-RTD scheme in system made of sp^3 hybridized four coordinated carbon and silicon. Next I plan to study planer and curved systems made of atoms with sp^2 and intermediate hybridization of valence electrons. Given the unpaired nature of the π-electrons is such system, we expect the values of α differ from that used for sp^3 orbitals. So far I have calculated the optical absorption of C_{60} within the IP level in the TB framework based on non-degenerate HAWOs of sp^{2+} and p_z^+ characters. Next I plan to calculate the
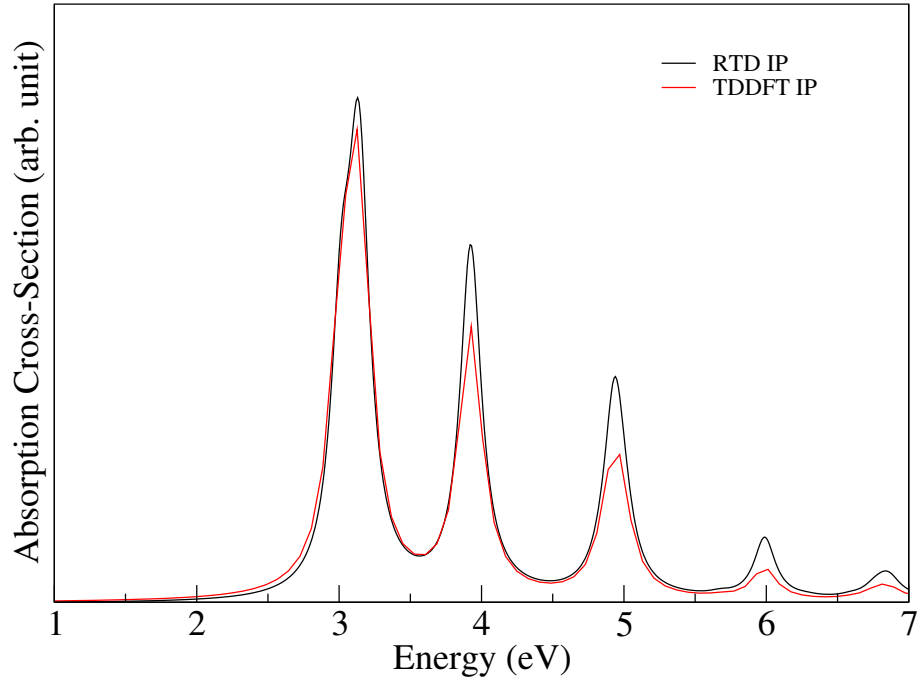
Figure 5.7: RTD based optical absorption spectra of C_{60} within the IP level.

absorption spectra using the proposed ACC-RTD approach to verify the the existing experimental spectra. I plan to also compute absorption spectra of carbon nanotubes and their heterojunctions.

Chapter 6

Optical excitation as a signature of chemical activation

In this chapter we propose to determine the chemical activation of atomic sites in chemically modified substrates through estimation of optical absorption threshold in conformity with Coulson's bond order and local magnetic moment, in agreement with explicit estimation from first principles. We demonstrate the possibility in carbon doped hexagonal boron nitride through correlation of absorption threshold with coulson's bond order(CBO) of the nearest neighbor coordinations around sites synergistically with energetics of adsorption and consolidation of local magnetic moments on active sites. Accordingly, absorption threshold also seems to be an effective indicator of possible catalytic role of such sites in facilitating oxygen reduction reaction.

6.1 Introduction

Non-invasive estimation of level of chemical activation of substrates with possible active sites can be beneficial in determining the catalytic efficiency of the substrate without contaminating it. Estimation and comparison of chemical activation of possible active sites(atoms) have been so far primarily made in terms of the ener-

getics of adsorption of radicals and possible activation barrier,[164,165,166] or the bond dissociation energies accessed experimentally[167,168] or calculated from first principles.[169] In this work we present an alternate approach for easy estimation of the level of activation of sites, and demonstrate the same in a family of low dimensional systems of contemporary interest, namely carbon(C) doped hexagonal boron nitride(hBN).[170,171] These systems have been extensively explored in recent years on account of their tunable electronic, magnetic and chemical functionalities[102,172] rooted at the on-site Coulomb repulsion between electrons of opposite spins. Sites with incomplete sub-shell filling in general are naturally expected to be chemically active since they would energetically prefer formation of covalent bonds with reactants in order to complete sub-shell filling. Often the incompleteness of sub-shell filling is non-uniformly distributed over several sites leading to a variation in degree of chemical activation across sites. Thus the level and distribution of chemical activation varies with shape and size of systems hosting the active sites. Indeed variable degree of chemical activation and catalytic efficiency primarily in the light oxygen reduction reaction(ORR) have been reported for different sizes of hBN-islands[173,174] in graphene, as well as graphene-islands in hBN.[103] For neutral sites, incomplete sub-shell filling would imply retention of unpaired electron in the valence shell with high kinetic energies leading effectively to rise of the valence-band-edge in energy, thus lowering the band gap. Tracking of the absorption threshold thus appears to a possible non-invasive route to identify the degree of chemical activation.

We also chose to use bond order(BO) as an indirect measure of localization, since increase in the average order of all the bonds made by an atom would naturally imply de-localization of the unpaired electron from the host atom to its neighboring sites. We thus calculate *average bond order*(ABO) associated with a site(atom), as a relative measure of its chemical activation and correlative with the optical absorption threshold and strength of local magnetic moment on sites. Coulson's bond order(CBO) computed for the π bond in the basis of p_z orbital obtained from first principles agrees with results available from MO calculations.I have already introduced calculation of CBO in chapter 4. and computation of absorption spectra in

the directed hybrid Wannier orbital basis in chapter 5. In the following first we briefly recap computation of CBOs and define ABO, followed by demonstration of the correlation of ABOs, magnetic moment and absorption threshold in differentiating chemical activation of C atoms in Gr islands embedded in hBN as catalytic host of oxygen reduction reaction(ORR) which constitutes a crucial step in functioning of fuel-cells with acidic electrolyte.

6.2   Methodological details

As define in chapter 4, the traditional or classical definition of BO involving the i-th and j-th atomic orbitals for a given spin is

$$\mathrm{B}_{\vec{R}'\vec{R},ij} = \frac{n^+_{\vec{R}'\vec{R},ij} - n^-_{\vec{R}'\vec{R},ij}}{2},$$

$n^{\pm}_{\vec{R}'\vec{R},ij}$ being the occupation of the bonding(+) and anti-bonding(-) orbitals considered in a suitable localized orbital basis $\{\Phi\}$, which in this chapter are the p_z orbitals of carbon atoms.

Within the subspace of KS states:

$$\mathrm{B}_{\vec{R}'\vec{R},ij} = \mathrm{Re}[\langle \Phi_{\vec{R}',i} \mid \hat{P} \mid \Phi_{\vec{R},j}\rangle]$$
$$= \sum_{\vec{k}}^{BZ} \sum_{l}^{N_{KS}} \frac{f_{\vec{k},l}}{N_k} \mathrm{Re}[e^{i\vec{k}.(\vec{R}'-\vec{R})}U(\vec{k})^*_{li}U(\vec{k})_{lj}] \qquad (6.1)$$

where $\hat{P}$ is the projection operator for a given spin:

$$\hat{P} = \sum_{\vec{k}}^{BZ} \sum_{l}^{N_{KS}} \mid \psi^{KS}_{\vec{k},l}\rangle f_{\vec{k},l}\langle\psi^{KS}_{\vec{k},l} \mid$$

$f_{\vec{k},l}$ being the occupancy of the l-th KS state with wave-vector $\vec{k}$ and $\{U\}$ being the unitary transformation (Eqn.4.9) from the Kohn-Sham single particle states to be p_z orbitals in this chapter. $\mathrm{B}_{\vec{R}'\vec{R},ij}$ in Eqn.(6.1) is the Coulson's bond order(CBO),[146]

used primarily in case of a single orbital per atom, as is the case in this chapter where i and j are effectively the atom indexes.

Average bond order associated with the i-th site is calculated as:

$$ABO_i = \frac{1}{N_{nn}} \sum_{j=1}^{N_{nn}} B_{\vec{R}'\vec{R},ij}, \tag{6.2}$$

where N_{nn} is numbers of nearest-neighboring(nn) around the i-th site.

Local magnetic moment are estimated as :

$$\mu_i = \sum_{\vec{k}}^{BZ} \sum_{l}^{N_{KS}} \frac{f_{\vec{k},l}}{N_k} (|U(\vec{k})_{li,\sigma}|^2 - |U(\vec{k})_{li,\sigma'}|^2) \tag{6.3}$$

Estimation of adsorption energies of ORR intermediates and calculation of ABO are performed with 8×8 super-cells, where as the absorption spectra are computed using the RTD approach for large finite segments of nano-meter length scale.

TB parameters are transferred from smaller reference system to large target systems through mapping neighborhood beyond nearest neighbor as shown in Fig.**??**

In this chapter, we calculate the absorption spectra of large systems only at independent particle level($\alpha = 0$) as described in chapter 5 in the basis of sp^2 and p_z HAWOs with TB parameters evaluated in the DFT levels.

6.3 COMPUTATIONAL DETALIS

First principles calculations have been performed using a plane wave based implementation of DFT,[125] where the screened ionic potentials are approximated by $ultrasoft$[175] pseudo-potentials. Exchange-correlation contribution to total energy is estimated using a gradient corrected Perdew-Burke-Ernzerhof (PBE)[176] functional. Minimum energy configurations of different scenarios of substitutions are obtained in 8×8 super-cell using the BFGS[177] scheme of minimization of total energies, which are converged with plane-wave cutoff 80 Ryd., k-mesh to 5×5 and forces less than

10^{-3} Rydberg/Bohr for all atoms. Adsorption energies are estimated from total energies(E) as $E_{substrate+X} - E_{substrate} - E_X$, where X is the adsorbed species and substrate corresponds to hBN with substitution by C in different configuration as shown in Fig.6.1.

6.4   RESULTS AND DISCUSSION

It has been already shown[103] that substitution by carbon(C) in hBN leads to formation of graphene islands. In this work, we consider substitution by C atoms leading to formation of non-magnetic as well as magnetic islands of graphene respectively, owing to different number of carbon atom in the two sub-lattices in case of the latter, as per Lieb's theorem. In Fig.6.1, we present a map of ABO values in C doped hBN
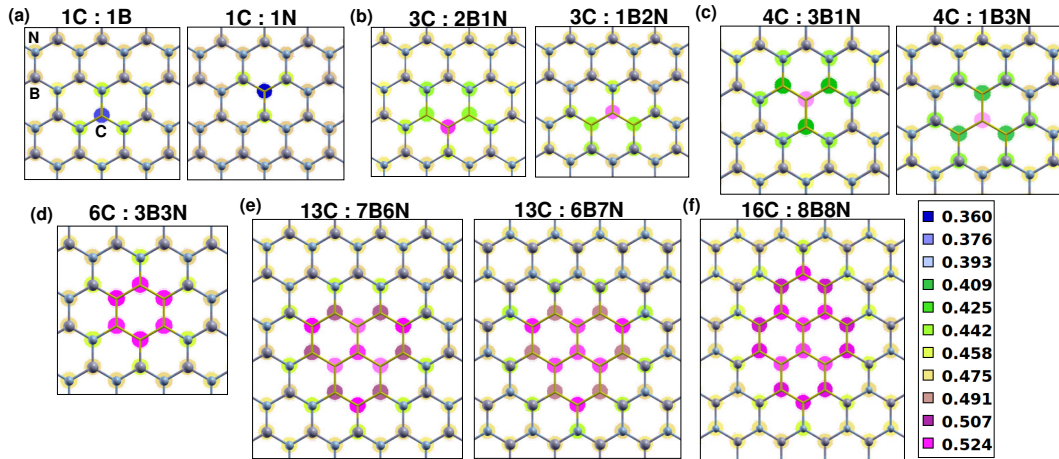
Figure 6.1: Average bond order(ABO) values at different sites for different C-substitution(gray circle) configurations: (a)single C(1C), (b)3C, (c)4C, (e)13C, where red(black)circles represents the N-site rich(B-site rich) substitution, (d)6C and (f)16C containing equal number of sites from both sub-lattices.

with increasing number of substitutions by C. Since we consider only $2p_z$ electrons, the BOs and subsequently the ABOs reported here are one less than their respective total values on account of the absence of σ orbitals. As evident from the contour plots, ABOs vary from peripheral sites to the inner sites based on shape and sizes of the island. Since a lower value of ABO of a site corresponds to higher localization of p_z electron on the site, and thereby a higher level of chemical activation, sites

at the periphery are thus relatively more chemically active than those within the magnetic islands. Such variation is much weaker in the non-magnetic islands like 8B8N and completely absent in 3B3N which is arguably the least active akin to pristine graphene. With increasing size of islands, ABOs of C-atoms at the periphery increases systematically leading to modest activation crucial for catalysis, whereas, expectedly the ABO values C-atoms deep inside the islands become increasingly similar to that in infinite graphene.

In Fig.6.2 we present the correlation of ABO to magnetic moments localized on C atoms due to localization of p_z electrons. The expected correlation reinforces the effectiveness of ABO as a measure of localization of p_z electrons in magnetic islands.

Figure 6.2: Variation of magnetic moment(absolute value) per site with ABOs for magneic and non-magnetic C-island. Non- magnetic C-islands(3B3N, 8B8N) are represented with fill symbols. Legend as per Fig.6.1.

Next we present a detailed demonstration of correlation of ABO to chemical activation estimated in terms of the energetics of adsorption of ORR intermediates. Complete reduction of O_2 to $2H_2O$ starting with O_2 adsorbed on an active site proceeds in general in the following pathway [Eqn. 6.4−6.8].

$$* + O_2 = O_2^*$$

(6.4)

$$O_2^* + H^+ + e^- = OOH^* \tag{6.5}$$

$$OOH^* + H^+ + e^- = O^* + H_2O \tag{6.6}$$

$$O^* + H^+ + e^- = OH^* \tag{6.7}$$

$$OH^* + H^+ + e^- = H_2O \tag{6.8}$$

where "$*$" denotes the substrate and X^* denotes the chemisorbed X: O_2, OOH, O, and OH. Adsorption of O_2 being generally weak, the major rate limiting steps are the reduction of the intermediates OOH^* and OH^*. We therefore study adsorption of these intermediates in comparison with that of atomic H. As evident in Fig.6.3, a modest level of adsorption favorable[103] for effective catalysis is found for ABO around 0.5. Comparing with magnetic moments of the active sites, it is clear that higher the magnetic moment, higher the level of chemical activation and lower the value of ABO.
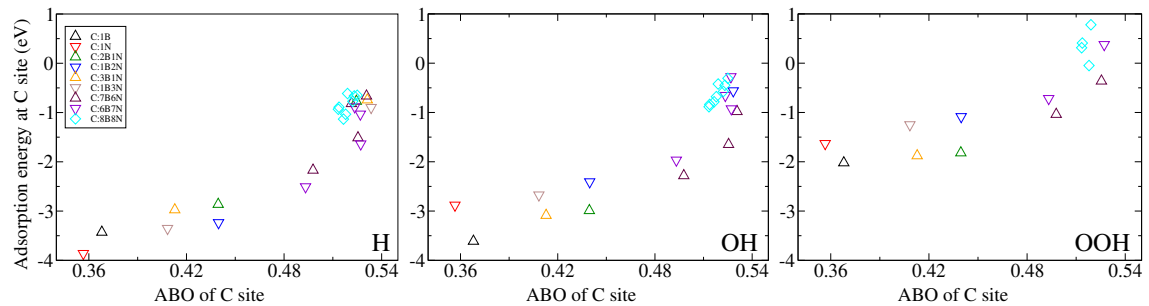

Figure 6.3: Adsorption energies of H, OH and OOH (as mentioned in the inset) on inequivalent C atoms with respect to ABO of those sites, for both B-rich(up-triangle) and N-rich (down -triangle) C-islands embedded in hBN. Non-magnetic island(8B8N) represented by diamond symbol. Legend as per Fig.6.1.

Next we correlate the chemical activation of sites to their spectral signature. We have calculated the IP level absorption spectra of realistically large segments of hBN with substitution by C using the RTD approach with TB parameters in the $sp^2 + p_z$ HAWO basis transferred from smaller reference systems. To test the efficacy of RTD approach in magnetic system, in Fig.6.4, we compare the IP level TDDFT spectra with the same obtained with the RTD without the anti-causal correction

proposed in chapter5, for a reference system with a magnetic moment of $2\mu_b$ due to substitution by four C atoms.
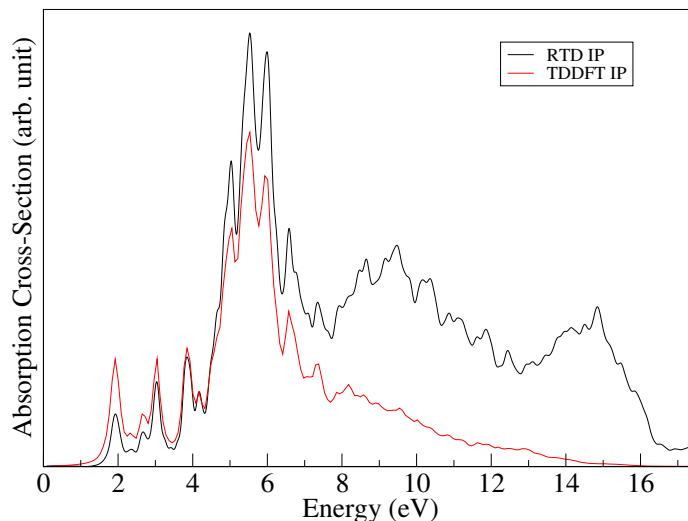

Figure 6.4: Conformity test of RTD spectra of 4C@1B3N with respect to TDDFT spectra at the IP level.

Finally in Fig.6.5, we plot the absorption thresholds of the different substitution configurations. Fig.6.5 clearly suggests a lower absorption threshold for the chemically active magnetic islands than those of the non-magnetic islands, in agreement with the trends suggested by the ABO values as well as the magnetic moments. Among the non-magnetic islands, absorption threshold of 8B8N is lower than that of smaller non-magnetic islands which is also consistent with the trend of chemical activation among the non-magnetic islands, as also suggested by the ABO values.

6.5   CONCLUSION

In this work, we propose average of Coulson's bond order of nearest neighbor coordinations around a site, calculated in a minimal tight binding basis to be an effective measure of chemical activation leading to possible oxygen reduction reaction catalysis hosted by carbon doped hexagonal boron nitride surface. We also demonstrate the absorption threshold to be an effective non-invasive probe to asses the level of chemical activation of such systems. This application demonstrates the effective-
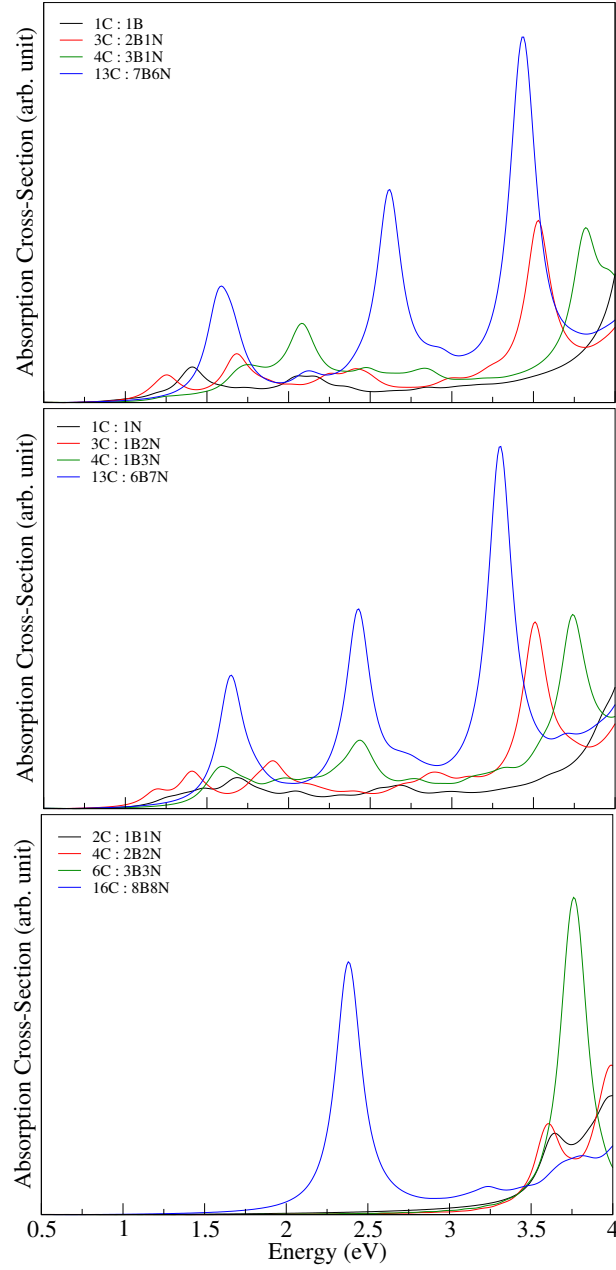
Figure 6.5: Absorption spectra of the different substitution configurations. Legend as per Fig.6.1.

ness of the tight binding based real time dynamics approach as an easy tool to asses applicability of experimentally realizable nano-structures consisting of thousands of atoms, for different technological applications.

References

[1] Erich Runge and Eberhard KU Gross, *Physical review letters*, **52**, 997 (1984).

[2] EKU Gross and W Kohn. *inAdvances in Quantum Chemistry, vol. 21: Density Functional Theory of Many-Fermion Systems, edited by SB Trickey*. 1990.

[3] A Zangwill and Paul Soven, *Physical Review A*, **21**, 1561 (1980).

[4] Alexander L Fetter and John Dirk Walecka. *Quantum theory of many-particle systems*. Courier Corporation, 2012.

[5] Lars Hedin and Stig Lundqvist. "Effects of electron-electron and electron-phonon interactions on the one-electron states of solids". In: *Solid state physics*. Vol. 23. Elsevier, 1970, 1–181.

[6] Edwin E Salpeter and Hans Albrecht Bethe, *Physical Review*, **84**, 1232 (1951).

[7] Michael Rohlfing and Steven G Louie, *Physical Review B*, **62**, 4927 (2000).

[8] Gregory H Wannier, *Physical Review*, **52**, 191 (1937).

[9] P. Hohenberg and W. Kohn, *Phys. Rev.*, **136**, B864–B871 (1964).

[10] Manoar Hossain, Joydev De, and Joydeep Bhattacharjee, *The Journal of Physical Chemistry A*, **125**, 6805–6817 (2021).

[11] Joydev De et al., *Physical Chemistry Chemical Physics*, (2023).

[12] I Mayer, *Chemical Physics Letters*, **117**, 396–396 (1985).

[13] I Mayer, *International journal of quantum chemistry*, **29**, 73–84 (1986).

[14] Kenneth B Wiberg, *Tetrahedron*, **24**, 1083–1096 (1968).

[15] Mark S Hybertsen and Steven G Louie, *Physical Review B*, **34**, 5390 (1986).

[16] Xiaofeng Qian et al., *Physical Review B*, **73**, 035408 (2006).

[17] Harshani Ovamini Wijewardane and Carsten A Ullrich, *Physical review letters*, **100**, 056404 (2008).

[18] Lasse Landt et al., *Physical review letters*, **103**, 047402 (2009).

[19] Ernst-Eckhard Koch and d M Skibowski, *Chemical Physics Letters*, **9**, 429–432 (1971).

[20] Tamás Demján et al., *The Journal of chemical physics*, **141**, 064308 (2014).

[21] Huabing Yin et al., *The Journal of Chemical Physics*, **140**, 214315 (2014).

[22] M. Born and R. Oppenheimer, *Annalen der Physik*, **389**, 457–484 (1927).

[23] J. C. Slater, *Phys. Rev.*, **34**, 1293–1322 (1929).

[24] Richard M. Stevens and William N. Lipscomb, *The Journal of Chemical Physics*, **40**, 2238–2247 (1964).

[25] Llewellyn H Thomas. "The calculation of atomic fields". In: *Mathematical proceedings of the Cambridge philosophical society*. Vol. 23. 5. Cambridge University Press. 1927, 542–548.

[26] Enrico Fermi, *Zeitschrift für Physik*, **48**, 73–79 (1928).

[27] Walter Kohn and Lu Jeu Sham, *Physical review*, **140**, A1133 (1965).

[28] John P. Perdew and Karla Schmidt, *AIP Conference Proceedings*, **577**, 1–20 (2001).

[29] Robert G. Parr and Weitao Yang. *Density-Functional Theory of Atoms and Molecules (International Series of Monographs on Chemistry)*. Oxford University Press, USA, 1994. ISBN: 0195092767.

[30] E. Engel and R.M. Dreizler. *Density Functional Theory: An Advanced Course.* Theoretical and Mathematical Physics. Springer Berlin Heidelberg, 2011. ISBN: 9783642140907.

[31] D. M. Ceperley and B. J. Alder, *Phys. Rev. Lett.*, **45**, 566–569 (1980).

[32] S. H. Vosko, L. Wilk, and M. Nusair, *Canadian Journal of Physics*, **58**, 1200–1211 (1980).

[33] J. P. Perdew and Alex Zunger, *Phys. Rev. B*, **23**, 5048–5079 (1981).

[34] John P. Perdew and Yue Wang, *Phys. Rev. B*, **45**, 13244–13249 (1992).

[35] O. Gunnarsson and B. I. Lundqvist, *Phys. Rev. B*, **13**, 4274–4298 (1976).

[36] Kieron Burke, John P. Perdew, and Matthias Ernzerhof, *The Journal of Chemical Physics*, **109**, 3760–3771 (1998).

[37] John P. Perdew, Kieron Burke, and Matthias Ernzerhof, *Phys. Rev. Lett.*, **77**, 3865–3868 (1996).

[38] Kieron Burke, John P. Perdew, and Yue Wang. "Derivation of a Generalized Gradient Approximation: The PW91 Density Functional". In: *Electronic Density Functional Theory: Recent Progress and New Directions*. Ed. by John F. Dobson, Giovanni Vignale, and Mukunda P. Das. Boston, MA: Springer US, 1998, 81–111. ISBN: 978-1-4899-0316-7.

[39] Chengteh Lee, Weitao Yang, and Robert G. Parr, *Phys. Rev. B*, **37**, 785–789 (1988).

[40] R. Armiento and A. E. Mattsson, *Phys. Rev. B*, **72**, 085108 (2005).

[41] Jorge Kohanoff. *Electronic Structure Calculations for Solids and Molecules: Theory and Computational Methods*. Cambridge University Press, 2006.

[42] Axel D Becke, *The Journal of chemical physics*, **98**, 1372–1377 (1993).

[43] Axel D. Becke, *The Journal of Chemical Physics*, **98**, 5648–5652 (1993).

[44] A. D. Becke, *Phys. Rev. A*, **38**, 3098–3100 (1988).

[45] Carlo Adamo, Gustavo E. Scuseria, and Vincenzo Barone, *The Journal of Chemical Physics*, **111**, 2889–2899 (1999).

[46] John P. Perdew, Matthias Ernzerhof, and Kieron Burke, *The Journal of Chemical Physics*, **105**, 9982–9985 (1996).

[47] Yan Zhao and Donald G. Truhlar, *Journal of Chemical Theory and Computation*, **2**, 1009–1018 (2006).

[48] Yan Zhao and Donald G. Truhlar, *The Journal of Physical Chemistry A*, **109**, 5656–5667 (2005).

[49] Hisayoshi Iikura et al., *The Journal of Chemical Physics*, **115**, 3540–3544 (2001).

[50] Jochen Heyd, Gustavo E Scuseria, and Matthias Ernzerhof, *The Journal of chemical physics*, **118**, 8207–8215 (2003).

[51] Oleg A Vydrov and Gustavo E Scuseria, *The Journal of chemical physics*, **125**, 234109 (2006).

[52] Mary A Rohrdanz, Katie M Martins, and John M Herbert, *The Journal of chemical physics*, **130**, 054112 (2009).

[53] Viktor N. Staroverov et al., *Phys. Rev. B*, **69**, 075102 (2004).

[54] Susi Lehtola et al., *SoftwareX*, **7**, 1 –5 (2018).

[55] Richard M Martin. *Electronic structure: basic theory and practical methods.* Cambridge university press, 2020.

[56] URL: https://en.wikipedia.org/wiki/Pseudopotential.

[57] DR Hamann, M Schlüter, and C Chiang, *Physical Review Letters*, **43**, 1494 (1979).

[58] David Vanderbilt, *Physical review B*, **41**, 7892 (1990).

[59] Giovanni Onida, Lucia Reining, and Angel Rubio, *Reviews of modern physics*, **74**, 601 (2002).

[60] Henrik Bruus and Karsten Flensberg. *Many-body quantum theory in condensed matter physics: an introduction.* Oxford university press, 2004.

[61] Lars Hedin, *Physical Review*, **139**, A796 (1965).

[62] Neil W Ashcroft, N David Mermin, et al. *Solid state physics.* 1976.

[63] Manoar Hossain and Joydeep Bhattacharjee. "Self energy corrected tight-binding framework in directed hybrid orbital basis from first principles". PhD thesis. School of Physical Sciences, NISER, Bhubaneswar, 2022.

[64] G Strinati, *Physical Review Letters*, **49**, 1519 (1982).

[65] Linus Pauling, *Journal of the American Chemical Society*, **53**, 1367–1400 (1931).

[66] John C Slater, *Physical Review*, **37**, 481 (1931).

[67] G Doggett, *Proceedings of the Physical Society*, **86**, 393 (1965).

[68] Giuseppe Del Re, *Theoretica chimica acta*, **1**, 188–197 (1963).

[69] Rev McWeeny, *Reviews of Modern Physics*, **32**, 335 (1960).

[70] G Del Re, U Esposito, and M Carpentieri, *Theoretica chimica acta*, **6**, 36–44 (1966).

[71] Alan E Reed, Larry A Curtiss, and Frank Weinhold, *Chemical Reviews*, **88**, 899–926 (1988).

[72] R McWeeny and G Del Re, *Theoretica chimica acta*, **10**, 13–22 (1968).

[73] JN Murrell, *The Journal of Chemical Physics*, **32**, 767–770 (1960).

[74] I Mayer, *The Journal of Physical Chemistry*, **100**, 6249–6257 (1996).

[75] I Mayer, *Chemical physics letters*, **242**, 499–506 (1995).

[76] JP Foster and F Weinhold, *Journal of the American Chemical Society*, **102**, 7211–7218 (1980).

[77] John C Slater, *Physical Review*, **36**, 57 (1930).

[78] Warren J Hehre, Robert F Stewart, and John A Pople, *The Journal of Chemical Physics*, **51**, 2657–2664 (1969).

[79] Thom H Dunning Jr, *The Journal of chemical physics*, **90**, 1007–1023 (1989).

[80] Chang-Guo Zhan and Zhen-Min Hu, *Theoretica chimica acta*, **84**, 511–520 (1993).

[81] Aaron C West et al., *The Journal of chemical physics*, **139**, 234107 (2013).

[82] Michel Dupuis and Meghana Nallapu, *Journal of computational chemistry*, **40**, 39–50 (2019).

[83] AB Rives and F Weinhold, *International Journal of Quantum Chemistry*, **18**, 201–209 (1980).

[84] MS Gopinathan, *Journal of Molecular Structure: THEOCHEM*, **169**, 379–388 (1988).

[85] Carol A Baxter and David B Cook, *International journal of quantum chemistry*, **60**, 173–183 (1996).

[86] EF Kirkwood and DB Cook, *Theoretica chimica acta*, **44**, 139–149 (1977).

[87] Jiali Gao et al., *The Journal of Physical Chemistry A*, **102**, 4714–4721 (1998).

[88] Jingzhi Pu, Jiali Gao, and Donald G Truhlar, *The Journal of Physical Chemistry A*, **108**, 632–650 (2004).

[89] IV Popov, AL Tchougreeff, and R Dronskowski, *Low Temperature Physics*, **46**, 655–670 (2020).

[90] Michael Victor Berry, *Proceedings of the Royal Society of London. A. Mathematical and Physical Sciences*, **392**, 45–57 (1984).

[91] Raffaele Resta, *Reviews of modern physics*, **66**, 899 (1994).

[92] RD King-Smith and David Vanderbilt, *Physical Review B*, **47**, 1651 (1993).

[93] Nicola Marzari and David Vanderbilt, *Physical review B*, **56**, 12847 (1997).

[94] Joydeep Bhattacharjee and Umesh V Waghmare, *Physical Review B*, **73**, 121102 (2006).

[95] Jean-François Cardoso and Antoine Souloumiac, *SIAM journal on matrix analysis and applications*, **17**, 161–164 (1996).

[96] Herman H Goldstine, Francis J Murray, and John Von Neumann, *Journal of the ACM (JACM)*, **6**, 59–96 (1959).

[97] JM Foster and SFi Boys, *Reviews of Modern Physics*, **32**, 300 (1960).

[98] Hiroshi Tatewaki and Sigeru Huzinaga, *The Journal of Chemical Physics*, **71**, 4339–4348 (1979).

[99] R Bruce King, *Coordination Chemistry Reviews*, **197**, 141–168 (2000).

[100] Denis Rafael Nacbar, Allan Victor Ribeiro, and Alexys Bruno-Alfonso, *Materials Research*, **17**, 1474–1476 (2014).

[101] DM David Jeba Singh et al., *The Journal of Physical Chemistry A*, **109**, 7339–7342 (2005).

[102] Joydeep Bhattacharjee, *The journal of physical chemistry letters*, **6**, 1653–1660 (2015).

[103] Rita Maji and Joydeep Bhattacharjee, *The Journal of Physical Chemistry C*, **123**, 16731–16740 (2019).

[104] Per-Olov Löwdin, *The Journal of Chemical Physics*, **18**, 365–375 (1950).

[105] Michael W Schmidt, Emily A Hull, and Theresa L Windus, *The Journal of Physical Chemistry A*, **119**, 10408–10427 (2015).

[106] Nicola Marzari et al., *Reviews of Modern Physics*, **84**, 1419 (2012).

[107] Young-Su Lee, Marco Buongiorno Nardelli, and Nicola Marzari, *Physical review letters*, **95**, 076804 (2005).

[108] Dominik Gresch et al., *Physical Review Materials*, **2**, 103805 (2018).

[109] Arrigo Calzolari et al., *Physical Review B*, **69**, 035108 (2004).

[110] CESARE Franchini et al., *Journal of Physics: Condensed Matter*, **24**, 235602 (2012).

[111] Jeil Jung and Allan H MacDonald, *Physical Review B*, **87**, 195450 (2013).

[112] Xiaofeng Qian et al., *Physical Review B*, **78**, 245112 (2008).

[113] Xiaofeng Qian, Ju Li, and Sidney Yip, *Physical Review B*, **82**, 195442 (2010).

[114] Pino D'Amico et al., *Physical Review B*, **94**, 165166 (2016).

[115] Luis A Agapito et al., *Physical Review B*, **93**, 125137 (2016).

[116] Sheng-Ying Yue et al., *Physical Review B*, **95**, 085207 (2017).

[117] Ilya V Popov et al., *Physical Chemistry Chemical Physics*, **21**, 18138–18148 (2019).

[118] Kenneth B Wiberg, *Accounts of chemical research*, **29**, 229–234 (1996).

[119] Alexander N Rudenko and Mikhail I Katsnelson, *Physical Review B*, **89**, 201408 (2014).

[120] Irene Aguilera, Christoph Friedrich, and Stefan Blügel, *Physical Review B*, **100**, 155147 (2019).

[121] Jin Yu, Mikhail I Katsnelson, and Shengjun Yuan, *Physical Review B*, **98**, 115117 (2018).

[122] Alexander Grüneis et al., *Physical Review B*, **78**, 205425 (2008).

[123] Yeongsu Cho and Timothy C Berkelbach, *The Journal of Physical Chemistry Letters*, **10**, 6189–6196 (2019).

[124] Akitaka Sawamura et al., *Journal of Applied Physics*, **121**, 235704 (2017).

[125] Paolo Giannozzi et al., *Journal of physics: Condensed matter*, **21**, 395502 (2009).

[126] John P Perdew and Alex Zunger, *Physical Review B*, **23**, 5048 (1981).

[127] Jack Deslippe et al., *Computer Physics Communications*, **183**, 1269–1289 (2012).

[128] Li Yang et al., *Physical Review Letters*, **99**, 186801 (2007).

[129] Jean-Yves Raty and G Galli, *Journal of Electroanalytical Chemistry*, **584**, 9–12 (2005).

[130] Jean-Yves Raty et al., *Physical review letters*, **90**, 037401 (2003).

[131] ND Drummond et al., *Physical review letters*, **95**, 096801 (2005).

[132] Takao Sasagawa and Zhi-xun Shen, *Journal of applied physics*, **104**, 073704 (2008).

[133] WC Lu et al., *The Journal of chemical physics*, **120**, 2629–2637 (2004).

[134] I Mayer, *Journal of computational chemistry*, **28**, 204–221 (2007).

[135] Arash A Mostofi et al., *Computer physics communications*, **178**, 685–699 (2008).

[136] François Gygi, Jean-Luc Fattebert, and Eric Schwegler, *Computer physics communications*, **155**, 1–6 (2003).

[137] Aaron C West et al., *The Journal of Physical Chemistry A*, **119**, 10368–10375 (2015).

[138] I. Mayer, *Chemical Physics Letters*, **117**, 396 (1985).

[139] K.B. Wiberg, *Tetrahedron*, **24**, 1083–1096 (1968).

[140] AB Sannigrahi and Tapas Kar, *Journal of Chemical Education*, **65**, 674 (1988).

[141] Tapas Kar and AB Sannigrahi, *Journal of Molecular Structure: THEOCHEM*, **165**, 47–54 (1988).

[142] LS Yadav and JS Yadav, *Journal of Molecular Structure: THEOCHEM*, **165**, 289–295 (1988).

[143] Adam J Bridgeman et al., *Journal of the Chemical Society, Dalton Transactions*, 2095–2108 (2001).

[144] James Stevenson et al., *Chemistry of Materials*, **29**, 2435–2444 (2017).

[145] Pier Luigi Silvestrelli, *The Journal of Chemical Physics*, **146**, 244315 (2017).

[146] Charles Alfred Coulson, *Proceedings of the Royal Society of London. Series A. Mathematical and Physical Sciences*, **169**, 413–428 (1939).

[147] RS Mulliken, *The Journal of Chemical Physics*, **23**, 2338–2342 (1955).

[148] John P Perdew, Kieron Burke, and Matthias Ernzerhof, *Phys Rev Lett*, **77**, 3865 (1996).

[149] T Van Buuren et al., *Physical Review Letters*, **80**, 3803 (1998).

[150] Louis E Brus, *The Journal of chemical physics*, **80**, 4403–4409 (1984).

[151] C Bostedt et al., *Applied physics letters*, **84**, 4056–4058 (2004).

[152] A Paul Alivisatos, *The Journal of Physical Chemistry*, **100**, 13226–13239 (1996).

[153] Jean-Yves Raty and Giulia Galli, *Computer physics communications*, **169**, 14–19 (2005).

[154] Murilo L Tiago and James R Chelikowsky, *Physical Review B*, **73**, 205334 (2006).

[155] Lars Hedin and Bengt I Lundqvist, *Journal of Physics C: Solid state physics*, **4**, 2064 (1971).

[156] CY Wang et al., *Journal of Physics: Condensed Matter*, **31**, 214002 (2019).

[157] Silvana Botti et al., *Physical Review B*, **69**, 155112 (2004).

[158] Manoar Hossain and Joydeep Bhattacharjee, *The Journal of Chemical Physics*, **153**, 144103 (2020).

[159] Lars Hedin, *Solid State Physics*, **23**, 1 (1969).

[160] Richard S Varga. *Matrix iterative methods*. Prentice Hall Incorporated, 1962.

[161] K Yabana et al., *physica status solidi (b)*, **243**, 1121–1138 (2006).

[162] Andrea Marini et al., *Computer Physics Communications*, **180**, 1392–1403 (2009).

[163] Uichi Itoh et al., *The Journal of chemical physics*, **85**, 4867–4872 (1986).

[164] O Leenaerts, B Partoens, and FM Peeters, *Physical Review B*, **77**, 125416 (2008).

[165] Kwanyong Seo et al., *Journal of the American Chemical Society*, **127**, 15724–15729 (2005).

[166] Christopher L Muhich et al., *The Journal of Physical Chemistry C*, **117**, 10523–10535 (2013).

[167] Geunsik Lee et al., *The Journal of Physical Chemistry C*, **113**, 14225–14229 (2009).

[168] Stephen J Blanksby and G Barney Ellison, *Accounts of chemical research*, **36**, 255–263 (2003).

[169] Yong Feng et al., *Journal of chemical information and computer sciences*, **43**, 2005–2013 (2003).

[170] Rita Maji and Joydeep Bhattacharjee, *Physical Review B*, **99**, 125409 (2019).

[171] Xianlong Wei et al., *ACS nano*, **5**, 2916–2922 (2011).

[172] Oleg V Yazyev, *Reports on Progress in Physics*, **73**, 056501 (2010).

[173] Changshui Huang et al., *Chemical reviews*, **118**, 7744–7803 (2018).

[174] Nurten Akman and Cem Özdoğan, *Journal of Physics and Chemistry of Solids*, **115**, 187–198 (2018).

[175] David Vanderbilt,

[176] John P Perdew et al., *Proceedings of the national academy of sciences*, **114**, 2801–2806 (2017).

[177] R Fletcher. *Sums of Squares and Nonlinear Equations, Practical Methods of Optimization*. 1987.